The use of loop mirrors and chirped fibre Bragg gratings in actively-modelocked fibre lasers

John Whiteford David Gray

Doctor of Philosophy

Aston University

June 1998

Aston University

The use of loop mirrors and chirped fibre Bragg gratings in actively-modelocked fibre lasers

John Whiteford David Gray

Doctor of Philosophy

1998

Abstract

The development of an all-optical communications infrastructure requires appropriate optical switching devices and supporting hardware. This thesis presents several novel fibre lasers which are useful pulse sources for high speed optical data processing and communications. They share several attributes in common: flexibility, stability and low-jitter output. They all produce short (picosecond) and are suitable as sources for soliton systems.

The lasers are all-fibre systems using erbium-doped fibre for gain, and are actively-modelocked using a dual-wavelength nonlinear optical loop mirror (NOLM) as a modulator. Control over the operating wavelength and intra-cavity dispersion is obtained using a chirped in-fibre Bragg grating.

Systems operating both at 76MHz and gigahertz frequencies are presented, the latter using a semiconductor laser amplifier to enhance nonlinear action in the loop mirror. A novel dual-wavelength system in which two linear cavities share a common modulator is presented with results which show that the jitter between the two wavelengths is low enough for use in switching experiments with data rates of up to 130Gbit/s.

Keywords: Erbium-doped fibre laser; Nonlinear-optical loop mirror; soliton sources

Acknowledgments

Firstly, I would like to thank Professor Nick Doran, my supervisor, for his advice, support and constructive criticism throughout the duration of my research, and especially for his encouragement during the writing of this thesis.

On the practical front, Peter Kean helped me through the transition from theoretician to experimentalist and was a constant source of advice, background information and practical know-how. Later, Andrew Gloag assumed this role and discussions with him were invaluable in the experimental work on semiconductor amplifiers.

Lin Zhang and Kate Sugden manufactured the gratings used in this thesis, and efficiently translated initial specifications into useful devices. Allister Pattison provided the motivation for the dual-wavelength system, and many interesting discussions. In fact, there are too many people within the Photonics Research Group to thank individually.

Finally, I'd like to thank my parents and Karen for their support and patience.

Statement on Collaborative Work

The experimental work in Chapter 4 was performed in collaboration with Peter Kean, that in Chapter 5 with Allister Pattison, and the work of Chapter 6 with Andrew Gloag.

This research was supported by a studentship from the Engineering and Physical Sciences Research Council.

To my parents, my brothers Alan and Laurence, and my wife Karen.

Contents

List of Figures

Chapter 1

Introduction

Modern society is increasingly dependent on information, rather than physical resources; in the same way as the industrial revolution drove the development of improvements in transport, the so-called "information revolution" is driving changes in communications technology.

This century has already seen the widespread development of radio, television and the telephone. These technologies had the effect of shortening the time taken to get a message from one part of the world to another, though their applications were significantly different.

Much of the development of these systems has occurred through incremental improvements —altering the design of copper cables to maximise their bandwidth for transatlantic applications, increasing picture definition on television systems, and providing colour, stereo sound and so on.

There have been two major exceptions to this. The first, which will not be covered further, is satellite communications. Originally intended for transatlantic communications (both video and audio) satellite communications are becoming predominant for use with mobile base stations —however, they suffer from long round-trip delay, are expensive to install and maintain, have poor fidelity and are readily intercepted.

The second technology, which relates to the subject of this thesis, is optical fibre-based communications. While optical communication is not new (semaphore

and signal lamps are old concepts), free-space optical communication is limited by weather, atmospheric conditions and obstructions. For high-performance, reliable systems over tens or hundreds of kilometres, guided-wave systems are preferable.

The first proposals to use optical waveguides were made in 1966 [1, 2]; at first, optical fibres had high attenuation ($\approx$ 1000dB/km) compared to coaxial cables ($\approx 5 - 10$dB/km) and were substantially more difficult to join without significant loss. Over time, however, these problems have been overcome and optical fibres manufactured from silica glass are now close to the loss limit imposed by silica.

The other development which has affected optical communications is the development of the laser in the early 1960s [3]. One of the previous limitations of freespace optical communications had been the light sources available. The laser offered a high-power, narrow, collimated beam, though obviously free-space communication still suffered from the problems of obstruction and atmospheric effects. However, lasers were ideal test sources for optical components, including optical fibres.

Over the last twenty years or so, optical fibre systems have matured —there are now thousands of kilometres of fibre installed worldwide, and much of the related equipment is readily available commercially. Optical fibres are very much a mainstream technology.

However, the increasing use of computer networks and the demands for higher quality delivery of telephone service (and more recent usage for delivery of video —both in a traditional broadcast system and for more interactive services, such as "video-on-demand") have continued to drive the development of optical fibre communications systems towards higher bandwidth systems. Current systems are still some way from the fundamental limit of the optical carrier frequency.

Systems development has been concerned with other aspects than the transmission medium alone: there has been a trend towards moving the generation, regeneration and processing of signals into the optical domain. Optical processing is potentially faster than electrical processing, and the most significant restriction on current fibre-based systems is the lack of suitable electronics. As an example, a link carrying 40Gbit/s has been possible for several years [4, 5], but the elec-

tronics required to process a signal at this rate are expensive and complex. Higher transmission rates will only exacerbate this problem.

All-optical processing is still a new field; the methods are not as mature as for electronic processing. However, the history of the microprocessor suggests that over time, the processing power available in a small device increases rapidly. Obviously, much optical processing will be performed in solid-state integrated waveguide devices in the future, but the testbed for many of the new processing techniques remains fibre.

This thesis is not itself concerned with optical data processing or transmission systems, but a necessary adjunct to them —the generation of stable clock signals for that processing. The aim has not been to push for the highest possible speeds, but to demonstrate principles and integrate novel components to form a practical source; for example, the dual-wavelength laser system described in Chapter 5 was successfully used as the clock source for data processing experiments.

1.1 Design parameters for high-bitrate sources

This thesis describes several high repetition-rate optical sources. In order to assess their utility, this section will outline the significant desirable or essential features of a pulse source for communications or all-optical data processing. These characteristics can be read as a desired specification for the sources described.

Operating wavelength The laser should operate in the 1.5μm telecommunications window —this is the preferred operating region for modern telecommunications systems. It should be possible to design the system to operate at a very specific wavelength required by a particular application.

Pulse profile The pulses produced should be solitons (see Section 2.5), as this is a format of choice for many communications and processing applications[6].

Pulse width The pulse widths should be in the picosecond regime for use with high-bitrate systems. (Even if the pulse source operates at a low repetition-

rate, it may be used with high-bitrate systems which require that pulses are short enough to leave a suitable interval between pulses to avoid interference).

Jitter The timing jitter (*i.e.* variation in interpulse spacing) should be minimised, for the reasons given above —jitter can result in interpulse interactions which lead to corruption of data. Amplitude and wavelength jitter have similar effects in dispersive, nonlinear systems and should be minimised.

Power The power output capability of the source should be sufficient to allow the generation of a full pulse train of N=1 solitons. The amplitude of the output pulses should be as consistent as possible *i.e.* jitter and patterning should be minimised.

Stability The characteristics of the output from the system should not change over time. Minimal intervention should be required to start up the system and keep it running normally.

Reliability Dependence on environmental conditions should be minimised. The system should be robust, easy to construct and flexible to allow alterations to its operating parameters.

This thesis addresses these issues, and describes laser systems with readily-selectable wavelengths and picosecond soliton output. The output has low jitter and excellent long-term stability. These sources are therefore good candidates for optical data processing and communications. One system, the dual wavelength system in Chapter 5 is particularly suitable for use in demanding optical switching applications.

1.2 Thesis Overview

A Note on Terminology: This thesis refers frequently to linear cavities; this is a description of the physical layout of the cavity and not of the processes or components in the cavity. The lasers in this thesis produce soliton output, so there are clearly nonlinear *processes* involved!

This thesis is concerned with the development of actively mode-locked fibre lasers for use in high-speed optical data communications and processing applications. While the emphasis is on linear cavities, some alternative constructions are discussed. The systems presented use chirped fibre Bragg gratings and loop mirrors as the end reflectors of the cavities. By changing the characteristics of these devices, significant differences in operation can be achieved.

Chapter 2 outlines the properties of silica optical fibre —dispersion, loss and nonlinearity —which are most relevant to the work in this thesis. It describes solitons, nonlinear optical loop mirrors and Bragg gratings, all of which are used in the lasers described in this thesis.

Chapter 3 considers the theory of mode-locked laser operation and describes several configurations of laser cavity. Techniques for determining the intracavity dispersion of a laser system are also presented.

Chapter 4 presents a simple, linear cavity fibre laser and discusses some of the design techniques employed and results obtained.

Chapter 5 develops the laser system of Chapter 4 into a system consisting of two lasers operating at different wavelengths but very closely synchronised. This system has been successfully used in all-optical switching experiments.

Chapter 6 presents a modification of the simple linear cavity laser described above, in which the loop mirror is replaced with a loop mirror containing a semiconductor laser amplifier.

Chapter 7 considers some of the design issues raised by the systems earlier in the thesis, considers how these systems compare with other possible sources, and looks at some possible directions for future development of the systems outlined.

This includes the possibility of manufacturing gratings with profiles tailored to particular applications, and some novel applications of the systems described. Finally, it summarises the principal aspects of the thesis, and considers the place of these lasers in context.

Chapter 2

The properties of optical fibre

Silica optical fibre is the basic medium out of which all the laser systems described later were constructed; its properties are responsible for the existence of soliton behaviour, and the limitations on soliton communications systems. It is therefore appropriate to consider the basic properties of the medium before discussing in more detail its application to the fibre lasers described in this thesis.

2.1 Loss

While it is possible to construct optical fibre from a variety of media ([7, section 3.7]), silica glass remains the preferred material: it is in plentiful supply and can be made pure enough (*i.e.* the transmission loss can be reduced sufficiently) for useful deployment in single span systems of several hundred kilometres in length. Careful control of fibre materials allows a loss of $\approx$ 0.2dB/km at 1.55μm to be obtained; this is fundamentally limited by the intrinsic properties of the glass used.

The loss characteristic of typical silica optical fibre is shown in Figure 2.1. It is clear that short-wavelength performance is limited by Rayleigh scattering (which varies as λ^{-4}). The large feature at $\approx 1.37\mu$m and the smaller one at $\approx 1.23\mu$m are harmonics of the fundamental OH^- absorption peak at $\approx 2.73\mu$m. This profile differs from that of bulk silica, as the silica used for optical fibre manufacture is doped with other chemicals (such as germania, GeO_2) in order to produce the refractive

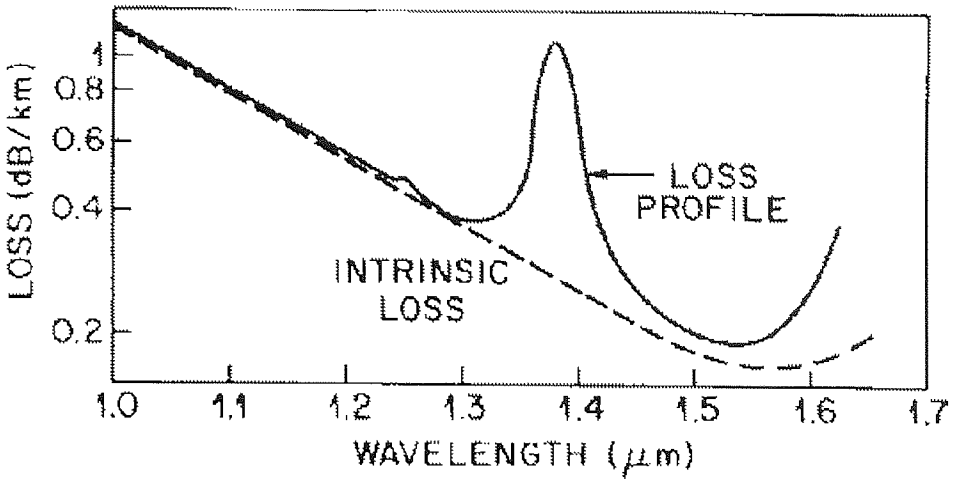

Figure 2.1: Loss profile of single-mode optical fibre

index difference necessary to form a fibre waveguide.

From the loss profile, it is clear that the minimum loss occurs at $\approx 1.55\mu$m. This wavelength is the preferred wavelength for modern, long-haul systems. Earlier systems, however, operated at $\approx 1.3\mu$m, where there is another low loss window (the operating regions at $\approx 1.3\mu$m and $\approx 1.55\mu$m are referred to as the second and third telecommunications windows; the first is at $\approx 0.85\mu$m and is not relevant to this thesis). The original choice of 1.3μm operation was a consequence of the dispersive properties of silica fibre.

2.2 Chromatic Dispersion

All materials exhibit a variation in refractive index with wavelength; this is a consequence of resonant interactions between radiation and the electronic structure of the material. At frequencies distant from the resonant frequencies, the relationship is a smooth curve. (In silica, the resonances are in the ultraviolet and far infrared).

For communications applications this is expressed in the variation of the propagation constant (this discussion assumes just one propagation mode *i.e.* that a single mode fibre is being used; in a multimode fibre, there would be slightly differ-

ent dispersion curves for each mode),

$$\beta = \frac{2\pi}{\lambda} n(\omega) \tag{2.1}$$

For a smooth curve, it is reasonable to expand this using a Taylor expansion around ω_0, where ω_0 is the mean frequency of the optical carrier of interest[8]:

$$\beta(\omega) = \beta_0 + \beta_1(\omega - \omega_0) + \frac{1}{2}\beta_2(\omega - \omega_0)^2 + \frac{1}{6}\beta_3(\omega - \omega_0)^3 + \cdots \tag{2.2}$$

where

$$\beta_m = \left| \frac{d^m \beta}{d\omega^m} \right|_{\omega=\omega_0} \quad (m = 0, 1, 2, \ldots) \tag{2.3}$$

For a pulse, the envelope moves at the group velocity $v_g = d\omega/d\beta = 1/\beta_1$. This dictates the velocity with which energy, and thus information, is transferred. (By contrast, the phase velocity indicates the rate at which the phase profile of the underlying carrier moves, and is not of interest for communications applications. β_2, in the second term of Equation 2.2, is the derivative of the group velocity, and is thus described as group-velocity dispersion (GVD):

$$\beta_2 = \frac{d}{d\omega}\frac{1}{v_g} = -\frac{1}{v_g^2}\frac{dv_g}{d\omega} \text{ps}^2 \text{ km}^{-1} \tag{2.4}$$

For practical purposes, it is more convenient to express GVD in wavelength and delay terms:

$$D = -\frac{2\pi c \beta_2}{\lambda^2} \text{ps/(nm.km)} \tag{2.5}$$

This is described as group delay dispersion (GDD), and is the most common way to express the dispersion of a fibre device, as delay and wavelength are readily measured in a practical situation. In the units used above, the dispersion of standard telecommunications fibre is $D \approx +16$ ps/(nm.km) at 1.5μm. Figure 2.2 shows the relationship between group delay and wavelength.

Note that there are two components; the material dispersion component is contributed by the fundamental properties of silica, while the waveguide dispersion is a consequence of the different properties of the core and cladding, and varies as the power distribution of the signal varies with wavelength.

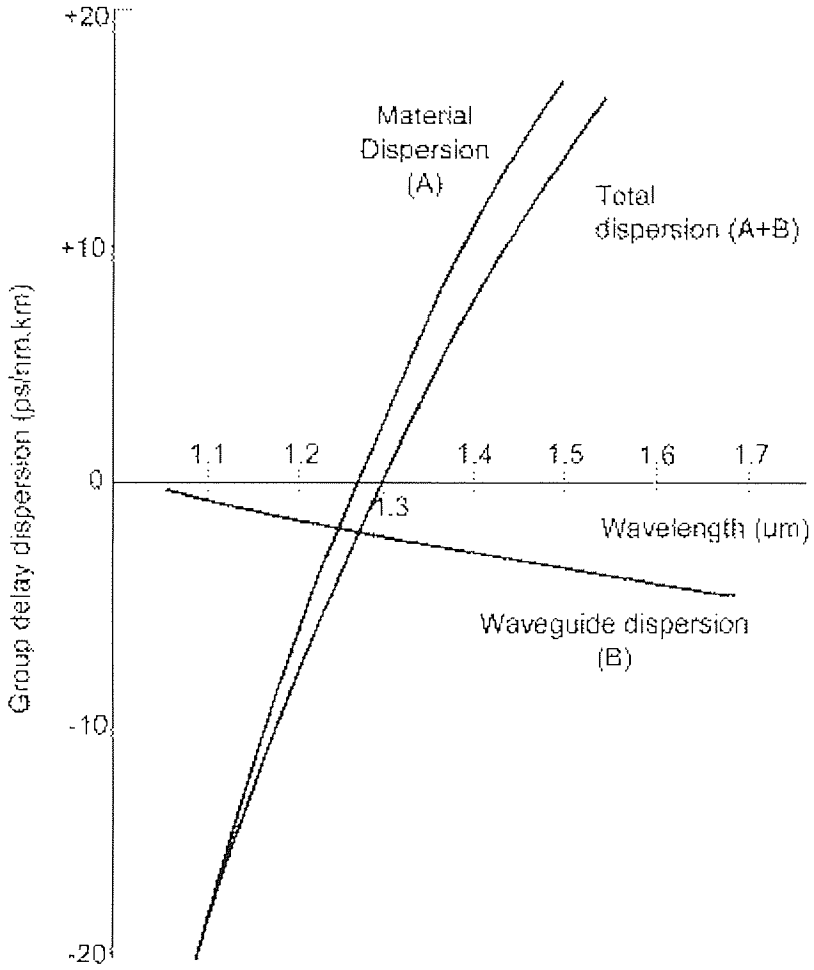

Figure 2.2: Variation of D with wavelength for a standard silica fibre. Note that the material dispersion is zero for $\lambda \approx 1.27\mu m$*, and the total dispersion is zero at* $\approx 1.32\mu m$.

DL, the GDD multiplied by the propagation distance is the property that will normally be referred to by the term "dispersion" in this thesis: it is one of the defining properties of the laser cavities and fibre gratings used in this thesis. In practice, the fibre gratings are described in terms of the value of DL (in ps/nm) without any separate measurement of D and L.

In propagation studies, the effect of the dispersion on a pulse is frequently quantified by defining the "dispersion length" L_D as the fibre length over which dispersive effects become significant. This is related to the half-width of the pulse at the $(1/e)$ point, T_0 and the fibre GVD by the relation:

$$L_D = \frac{T_0^2}{|\beta_2|} \tag{2.6}$$

Note that this thesis will generally refer to full-width at half-maximum (FWHM) pulse widths; τ(FWHM)= AT_0 where A is dependent on the pulse shape, and is $\approx$ 1.763 for sech^2 profiles and $\approx$ 1.665 for gaussian pulses. Note that all of the results presented in this thesis use τ for the FWHM pulse width.

In communications systems, it is the GVD which is responsible for the dispersive broadening of pulses. Any pulse has a spectral width which is inversely proportional to its pulsewidth, where the constant of proportionality is a function of the pulse shape, and can be determined from Fourier analysis of the temporal form of the pulse. Generally, the spectral width $\Delta\omega$ can be approximated by $2/\tau$. This range of wavelengths within a pulse results in a broadening of the pulse within a dispersive environment, as different wavelength components travel at different speeds (this assumes that the spectral components are evenly distributed throughout the temporal envelope of the pulse —pulses which are chirped *i.e.* which have the short wavelengths at one edge of the pulse envelope and long wavelengths at another may be compressed in a dispersive environment, depending on the sign of the dispersion and the direction of the chirp).

In a high bit-rate communications system, where the interpulse interval is small, temporal broadening of pulses will lead to intersymbol interference —this limits

either the transmission length or the maximum bit-rate. It was therefore a requirement of the first generation of long-haul singlemode fibre systems that dispersion was minimised.

Operation at the so-called dispersion zero ($\beta_2 = 0$) minimised pulse broadening, but it could not be completely eliminated as the value of β_3 ("third-order dispersion") becomes significant. The effect of third-order dispersion in laser systems has been analysed [9].

Figure 2.2 shows that D is zero at $\approx 1.3\mu$m. This corresponds to the low-loss window described above. This was therefore the operating region chosen for first-generation systems. In the region where β_2 is positive (and D is negative), long wavelengths travel faster than short wavelengths —this region is described as the normal dispersion region; the region where β_2 is negative is described as the anomalous dispersion regime, where shorter wavelengths travel faster. Note that the sign of GDD is the opposite of the sign of GVD, so the GDD is positive in the anomalous dispersion regime.

In order to exploit the lowest-loss window at 1.55μm (which has around half the loss of the 1.3μm window) it is necessary to overcome the higher dispersion of $D = +16$ps/(nm.km) at these wavelengths.

Two techniques have been used for the purpose. Firstly, the dispersion of a fibre waveguide differs from that of bulk silica: partly due to the doping mentioned above and also because of waveguide dispersion, which is determined by the refractive index profile of the core. It is possible to use these two effects to shift the dispersion zero, λ_D, to the 1.55μm region. Fibre altered in this way is commercially available (described as dispersion-shifted fibre) and has been considered for both transmission and processing applications.

The second approach is to use nonlinear effects in the fibre to balance the dispersive broadening; this will be described below.

2.3 Birefringence

As a consequence of the manufacturing process, silica fibre has essentially random birefringence. A signal launched into a length of fibre on a specific polarisation will be emitted from the other end with an unpredictable polarisation. It is possible to enforce polarisation preservation by deliberately making the fibre possess a high birefringence (either through making the core elliptical, or by stressing it using additional stress members in the fibre) or by careful control over the manufacturing process. However, these approaches increase the cost of the system and the difficulty in splicing fibre together.

One of the consequences of the random polarisation state of the fibre is that where fibre needs to be coupled to polarisation sensitive devices, transformation of the polarisation state is required. This can be performed by stressing the fibre in a predictable way.

This can be achieved by winding the fibre onto a cylinder and clamping the ends —rotating the cylinder will rotate the polarisation state. Using an appropriate sized cylinder and number of turns of fibre, the behaviour of a waveplate can be emulated. In order to produce a λ/m waveplate, the radius R of the cylinder required is [10]:

$$R = \frac{2\pi a r^2}{\lambda} Nm \tag{2.7}$$

Where $a = 0.133$ (which contains photoelastic and Poisson ratio constants for silica), r is the outer radius of the fibre (*i.e.* 125μm for standard fibre), N is the number of turns of fibre on the cylinder and λ is the operating wavelength. In practice, obtaining an exact match is difficult because the number of turns is small and must be a whole number. However, only an approximate match is required for useful operation.

Conversion from one arbitrary polarisation state to another requires three waveplates, two quarter-wave plates with a half-wave plate between them. Consequently, polarisation controllers consist of 3 cylinders in a row around which fibre is wound; the cylinders can be rotated independently, but the fibre is clamped between the

cylinders.

2.4 Nonlinear effects

Materials and EM radiation interact through the oscillation of bound electrons; for low levels of incident radiation, the oscillation can be well-approximated by simple harmonic motion. However, for higher intensities, nonlinearity arises.

The response of the medium is expressed in the polarisation, which is described as[8]:

$$P = \varepsilon_0(\chi^{(1)}E + \chi^{(2)}E^2 + \chi^{(3)}E^3 + \cdots) \tag{2.8}$$

ε_0 is the vacuum permittivity, E is the incident field and P is the resultant polarisation. The polarisation is dominated by the linear susceptibility $\chi^{(1)}$, which contains components relating to the refractive index n and the fibre loss. $\chi^{(2)}$ is responsible for second-harmonic generation and sum/difference frequency generation. However $\chi^{(2)}$ is zero for silica as it possesses inversion symmetry.

As a consequence, the largest nonlinearities in silica are $\chi^{(3)}$ effects. These are four-photon effects (*i.e.* they involve four interacting signals) and include third-harmonic generation and four-wave mixing. However, these effects require phase-matching between the signals involved, and as the signals are at different wavelengths this is unlikely to occur.

More significant are the degenerate cases of four-wave mixing, in which more than one signal is at the same wavelength. The case where all the signals have the same wavelength and the case where two are at λ_1 and two are at λ_2 are inherently phase-matched. These cases are self-phase modulation (SPM) and cross-phase modulation (XPM) respectively which are described below. They can together be classed as nonlinear refraction as they result in an intensity-dependent change in refractive index. This in turn imparts a phase shift of:

$$\phi_{NL} = \frac{\omega z}{c}\Delta n \tag{2.9}$$

The polarisation change resulting from all the $\chi^{(3)}$ effects is proportional to $|E|^3$ and consequently results in a refractive index term proportional to $|E|^2$. As $|E|^2$ is the optical intensity, the nonlinear refraction may be written as:

$$n(I,\omega) = n_0(\omega) + n_2 I \tag{2.10}$$

(the nonlinear refractive index is only very weakly dependent on frequency at visible and infrared frequencies).

2.4.1 SPM and XPM

SPM and XPM are degenerate cases of four-wave mixing.

Analysis of the possible permutations of sum and difference combinations with two different frequencies involved shows that there are nine permutations, of which three involve only one frequency (and contribute to SPM) and six involve two frequencies (and contribute to XPM). As a consequence of this, XPM is a larger effect by a factor of two. (XPM also affects signals at the same wavelength in orthogonal polarisation states, but has only 2/3 of the strength of SPM in this case because of the degeneracy of the signal wavelengths. For an elliptical polarisation state, this has the effect of inducing a nonlinear polarisation rotation. However, its effect will be ignored in this chapter).

The effect of SPM and XPM on two co-propagating signals can be expressed as:

$$\phi_1^{NL} = \frac{2\pi n_2 L}{\lambda}[|E_1|^2 + 2|E_2|^2] \tag{2.11}$$

$$\phi_2^{NL} = \frac{2\pi n_2 L}{\lambda}[|E_2|^2 + 2|E_1|^2] \tag{2.12}$$

where L is the propagation distance and n_2 is the nonlinear refractive index (or Kerr coefficient) and has a value of $n_2 = 2.5 \times 10^{-12}\mathrm{m}^2/\mathrm{W}$ for silica. Although this is a small value in comparison to some other materials, the small effective area of the core of a singlemode fibre results in a high intensity. This coupled with the guiding of the fibre (and its low loss) allows long interaction lengths to be used. As a consequence, optical fibre is a useful medium for studying the effect of nonlinear interactions.

In this thesis, cross-phase modulation is used to produce an all-optical modulator. More significantly, perhaps, self-phase modulation is a critical part of the formation of soliton pulses.

2.5 Soliton propagation

A soliton-like pulse was first observed in 1838 by John Scott Russell, in the Union Canal near Edinburgh [11] although it was over a century until the theory of solitons was related to optical fibres[12]. Briefly, a soliton is a pulse which, in a lossless environment free from perturbations, propagates indefinitely without change of shape.

The effects of nonlinearity and dispersion can be incorporated into a propagation equation[13, 8]:

$$i\frac{\partial A}{\partial z} = -\frac{i}{2}\alpha A + \frac{1}{2}\beta_2\frac{\partial^2 A}{\partial T^2} - \gamma|A|^2 A \tag{2.13}$$

where $A(z,T)$ is the pulse envelope amplitude, z and T are the propagation distance and time, α is the absorption coefficient, β_2 is the GVD and γ is the nonlinear coefficient.

For simplicity, this equation can be rewritten in a normalised form, by making the substitutions

$$u = N\frac{A}{\sqrt{P_0}}, \tag{2.14}$$

$$\xi = \frac{z}{L_D}, \tag{2.15}$$

$$\tau = \frac{T}{T_0} \tag{2.16}$$

P_0 is the peak power, T_0 is the pulsewidth, and L_D is the dispersion length.

N is a parameter defined by

$$N^2 = \frac{\gamma P_0 T_0^2}{|\beta_2|} \tag{2.17}$$

This gives a normalised propagation equation of the form:

$$i\frac{\partial u}{\partial \xi} + \frac{1}{2}\frac{\partial^2 u}{\partial \tau^2} + |u|^2 u = 0 \tag{2.18}$$

This equation can be solved using an inverse scattering technique; the form of solution of most interest for this thesis is the so-called soliton solution:

$$u(\xi, \tau) = e^{\frac{1}{2}i\xi}\mathrm{sech}\tau \tag{2.19}$$

This is the case for which the nonlinear contributions from the SPM and GVD balance overall (they are out of phase, however, which leads to the distinctive evolution of the soliton envelope). There are an infinite number of solutions, with discrete power values, and these solutions are distinguished by the parameter N.

For communications purposes, only $N = 1$ solitons are useful; higher-order solitons split into multiple low order solitons when propagated. The behaviour of solitons in transmission systems has been widely published [14, 13]

The production of soliton pulses does not require a great deal of design: if there is sufficient power available in an environment with anomalous dispersion and nonlinearity, they will evolve from existing pulses by shedding excess radiation. The anomalous dispersion regime of silica fibre is such an environment, and it is therefore relatively straightforward to build a soliton laser from silica fibre.

Because the soliton solution is stable, small perturbations only result in the reshaping of the pulse. However, the effect of periodic perturbations is somewhat more complex, and leads to the generation of coherent dispersive radiation. While this is relevant to propagation systems, it is also significant in fibre lasers, and is discussed in Section 3.6.2.

2.6 The Nonlinear-Optical Loop Mirror

The nonlinear-optical loop mirror, first described by Doran & Wood [15] has since been developed as a versatile device for many optical switching applications. As an all-optical device, it does not suffer from the bandwidth limitations of electronics; its simple design makes it practical to build and operate. Finally, the loop

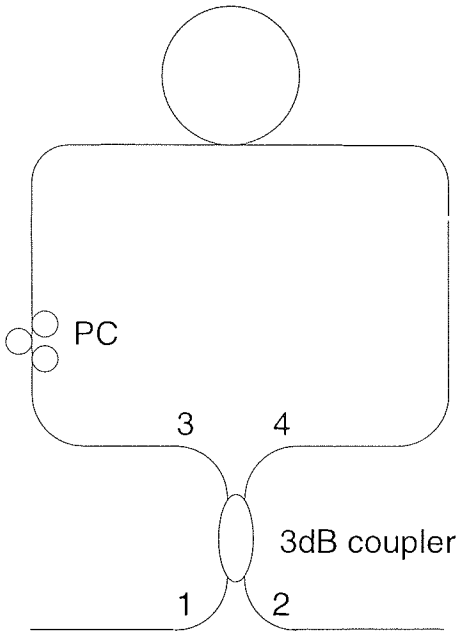

Figure 2.3: Fibre loop mirror. PC: polarisation controller. The numbering on the ports of the 3dB coupler corresponds to the description in the text.

configuration allows it to work interferometrically without the sensitivity to environmental variations which is a problem with linear interferometer structures such as the Mach-Zender interferometer which it most closely resembles.

The loop mirror has already been applied to all-optical switching and demultiplexing —several novel devices are based around a loop mirror architecture, such as the TOAD [16] and parametric loop mirror, using four-wave mixing [17, 18].

2.6.1 Linear Fibre Loop Mirror

The design of a fibre loop mirror is shown in Figure 2.3. It consists of a coupler, two ports of which have been joined with a loop of fibre. An incoming signal is split by the coupler and propagates in both directions round the loop: it then recombines interferometrically at the coupler. This recombination results in the signal being "reflected" (*i.e.* it exits the coupler via the port it entered on). This behaviour is a consequence of the $\frac{\pi}{2}$ phase shift in a signal when it crosses between the cores of a fused-fibre coupler.

To illustrate this, consider a signal entering port 1; it will be split into two equal

components by the coupler. One will travel clockwise round the loop, with no net phase shift, while the other will travel counterclockwise after crossing the coupler and acquiring a $\frac{\pi}{2}$ phase shift. When they return to the coupler ports, the clockwise propagating signal will cross the coupler attaining a $\frac{\pi}{2}$ shift (equal to that of the counterclockwise signal) and the two will constructively interfere. Consequently, they will exit on port 1.

The signal cannot exit on port 2, to do so would require the counterclockwise signal to cross the coupler a second time, so that it had a net phase shift of π; it would destructively interfere with the clockwise signal which had no phase shift. It follows that if the coupler is equally balanced, there is no output from port 2.

The utility of the fibre loop mirror, however, lies in changing the relative phase of one of the propagating signals: this can be performed using a polarisation controller asymmetrically placed in the loop.

If this controller produces a differential phase of π between two signals counter-propagating through it, the reflectivity will be changed from 100% (no difference in phase through controller) to 0% (π difference in phase). This relies on rotating the polarisation of the signal passing through the polarisation such that the signal in one direction travels for longer along the fast axis of the fibre. A NOLM, however, exploits the nonlinear properties of fibre to introduce a differential phase shift via SPM (or XPM, as discussed below).

In a nonlinear loop mirror, the coupler is deliberately unbalanced; this means that the clockwise and counterclockwise signals have different amplitudes; at low intensities (as described above) this difference will only be manifest as a decrease in the contrast of the loop mirror (some energy will always be transmitted and some always reflected). At higher intensities, the higher-intensity signal will acquire a larger nonlinear phase shift than the lower-intensity signal. This differential phase shift will transform the loop from a reflector to a transmitter.

This can be described analytically. The coupling equations for a coupler with an intensity coupling ratio of $\alpha : 1 - \alpha$ are:

$$E_3 = \sqrt{\alpha}E_1 + i\sqrt{1-\alpha}E_2 \quad (2.20)$$

$$E_4 = i\sqrt{1-\alpha}E_1 + \sqrt{\alpha}E_2 \quad (2.21)$$

If we initially consider the case of a signal of wavelength λ where $E_2 = 0$; the signals E_3 and E_4 after propagation around the loop of length L become:

$$E_3^* = \sqrt{\alpha}E_1 \exp(i\frac{2\pi n_2 L}{\lambda}\alpha|E_1|^2) \quad (2.22)$$

$$E_4^* = i\sqrt{1-\alpha}E_1 \exp[i\frac{2\pi n_2 L}{\lambda}(1-\alpha)|E_1|^2] \quad (2.23)$$

Note the presence of the extra phase change from SPM, as in Equation 2.11 with E_2 zero. These signals can be recombined using the equation describing the coupler and the resultant transmission of the NOLM is:

$$|E_2|^2 = |E_1|^2(1 - 2\alpha(1-\alpha)(1 + cos((1-2\alpha)|E_1|^2\frac{2\pi n_2 L}{\lambda}))) \quad (2.24)$$

A graph of $|E_2|^2$ (transmitted power) against $|E_1|^2$ (input power) is shown in Figure 2.4. Note that for a coupler closer to being balanced, the switching power (*i.e.* the input power corresponding to the first transmission peak) is higher; for an unbalanced coupler, the switching power is lower, but the contrast ratio (*i.e.* the maximum change in transmission) is also reduced.

Note that the transmission minima occur at

$$|E_1|^2 = \frac{m\lambda}{(1-2\alpha)n_2 L} \quad (2.25)$$

where m is integer, and the maxima for m= $1/2, 3/2, 5/2$ etc. This switching curve is the basis of the transmission plots in Figure 3.1.

This dependence of reflectivity upon intensity allows the NOLM to function as a fast saturable absorber for a laser: with appropriate biasing, high-intensity pulses can be transmitted, while low intensity cw (continuous wave *i.e.* non-pulsed) background can be reflected. This is the basis of the figure-of-eight laser. The use of a NOLM in a laser cavity is discussed by Duling *et al* [19].

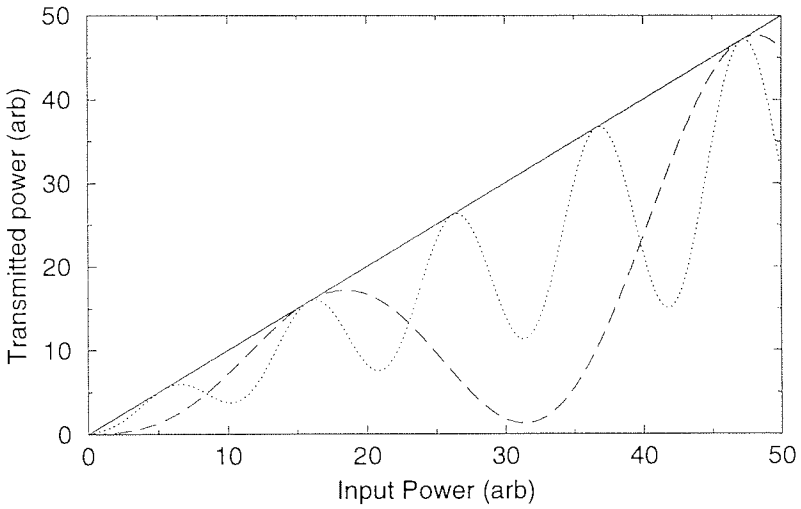

Figure 2.4: Plot of transmitted power against input power for $\alpha = 0.4$ (dashed line) and $\alpha = 0.2$ (dotted line). The solid line indicates a linear relationship between input and output power for comparison.

One further variation on the NOLM is the inclusion of an amplifier in the loop mirror [20]. This has been used in figure-of-eight laser configurations and to suppress relaxation oscillations in a cw laser [21].

2.6.2 Dual-wavelength loop mirror

The nonlinear phase shift need not be produced by SPM; one of the practical switching applications of the NOLM is to use a signal at a different wavelength: the induced cross-phase modulation (XPM) has a similar effect to the SPM above. Figure 2.5 illustrates a dual-wavelength NOLM. There are several major differences:

- The coupler can have an exact 50/50 splitting ratio; the control (λ_2) only co-propagates with one component of the signal (λ_1). This means that one component acquires a phase shift through XPM while the other does not. The device will therefore act as a switch dependent on the control pulse power only.

- The signal (λ_1) need not be a high-intensity signal; the acquired phase shift from XPM is dependent on the control pulse power, and this can be increased so that a low-amplitude signal can be switched.

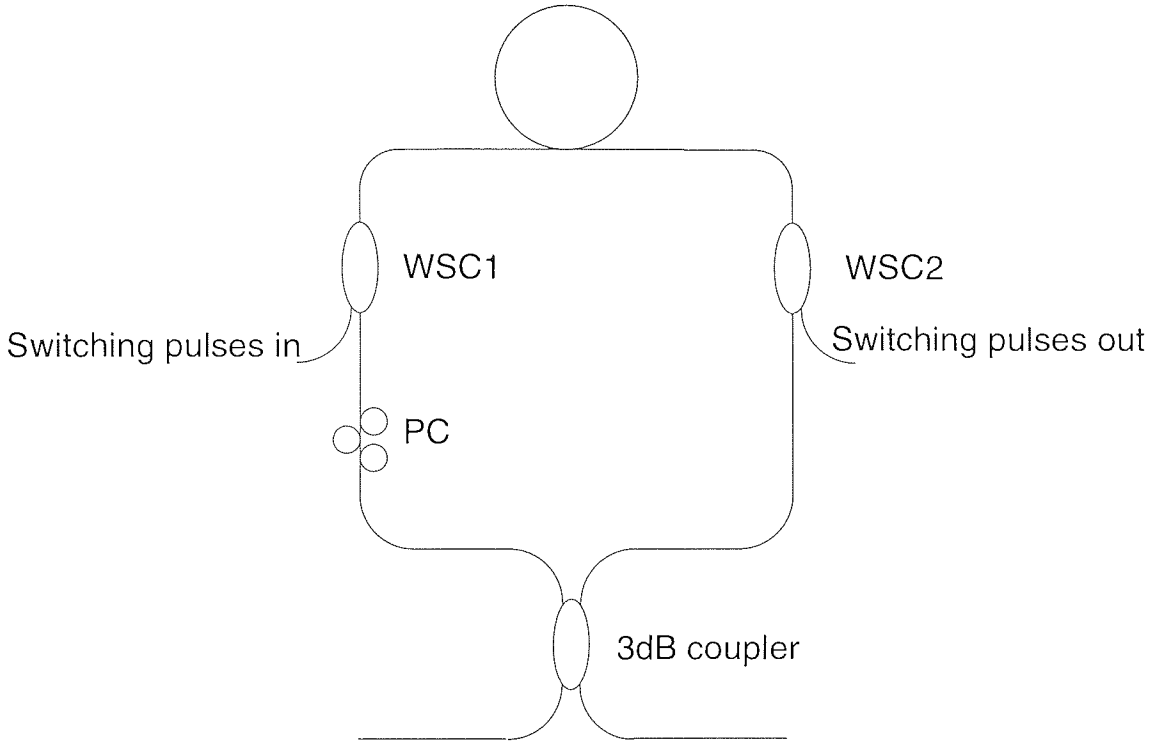

Figure 2.5: Schematic of a dual-wavelength loop mirror. WSC 1 and 2: wavelength selective couplers, PC: polarisation controller

- If the signal and control copropagate for a long distance, or if their wavelengths differ substantially, dispersion will introduce a relative delay between them; this is significant if pulses are being switched, as the dispersion will cause a walk-off between the signal and control pulses. The effect of this is to widen the switching window of the loop mirror [22]. Several analyses of switching window characteristics of dual-wavelength NOLMs have been performed [23, 24]

This device obviously has applications in high-speed switching, by allowing data from one wavelength to be transferred to another wavelength[25]. If data streams are used at both inputs the device can be biased to function in a manner equivalent to an AND gate[26]. Variations on this geometry can be used, for example, to provide an XOR gate, and thus pattern matching[27]. This can be used as the basis for an all-optical switching system. Combined with clock recovery, it can be used for all-optical regeneration[28].

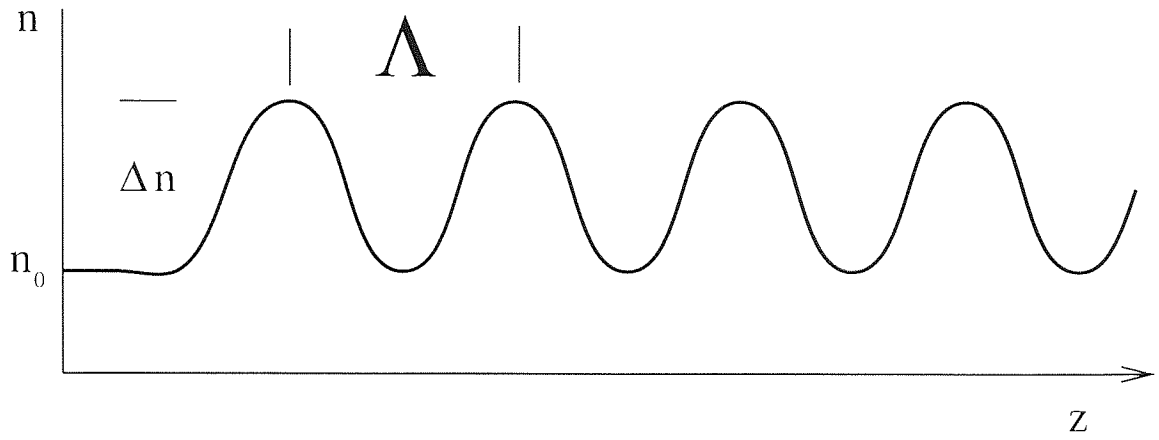

Figure 2.6: Refractive index profile of a fibre Bragg grating. The z-axis lies along the length of the fibre. Λ is the grating period, and Δn the amplitude of the refractive index variation. n_0 is the unmodified dispersion of the fibre core.

2.7 Chirped fibre gratings

The distinctive feature of the laser systems described in this thesis is that they all use chirped fibre Bragg gratings (CFBG) as principal components. This section will consider the theory of operation of Bragg gratings and discuss their characteristics, particularly with reference to their use in fibre laser systems.

The theory of operation of linear Bragg gratings forms the basis on which chirped gratings operate, so the theory and fabrication of linear gratings will be considered first.

2.7.1 Theory of linear Bragg gratings

A linear diffraction grating consists of a constant-period refractive index modulation in the core of an optical fibre. Each period in the refractive index variation gives rise to a reflection (the perturbation in the refractive index results in a coupling between modes). However, as the magnitude of each interaction is small, many hundreds of interactions are necessary to produce a significant total reflected signal. In general, however, the reflected signals will be out of phase with one another, unless the wavelength satisfies the so-called "Bragg condition" namely that

$$m\lambda = 2n\Lambda \tag{2.26}$$

Where λ is the free space wavelength, n is the effective refractive index, $m = 1, 2, \cdots$ and Λ is the period of the refractive index variation. The reflected signal is not subject to further reflections because, having experienced a $\pi/2$ phase shift on its first reflection, a second reflection would result in it being out of phase with (and thus destructively interfering with) the forward signal.

Obviously there will be some coupling even if the wavelength does not exactly satisfy the Bragg condition, and this leads to any linear grating having a finite bandwidth. Using coupled mode theory[29, 30] the properties of a linear Bragg grating can be determined analytically.

Firstly, it is assumed that there exist forward and backward travelling waves:

$$\mathbf{E_F}(x, y, z) = \mathbf{E_F}(x, y)e^{-j\beta z} \tag{2.27}$$

$$\mathbf{E_B}(x, y, z) = \mathbf{E_B}(x, y)e^{j\beta z} \tag{2.28}$$

which are solutions to a standard wave equation, and that the refractive index change is small compared to the refractive index *i.e.* that the grating can be treated as a perturbation.

Qualitatively, a solution to the perturbed wave equation consisting of the superposition of a forward and backward mode is expected, where A_F and A_B are the amplitudes of the forward and backward signals respectively, which have a dependence on z as light is coupled from one mode to the other. The exponent for the backward signal contains $\beta - K$ ($K = 2\pi/\Lambda$, the wavevector representing the grating) which is equivalent to $-\beta$ when the Bragg condition is satisfied *i.e.* when $K = 2\beta$.

$$\mathbf{E} = A_F(z)\mathbf{E}(x, y)e^{-j\beta z} + A_B(z)\mathbf{E}(x, y)e^{-j(\beta - K)z} \tag{2.29}$$

By substituting this into the perturbed equation and simplifying (second-order derivatives of A_F and A_B are neglected, and components relating to the spatial

mode are removed as they satisfy the unperturbed wave equation. Higher-order diffraction is also neglected) a pair of coupled differential equations is obtained. These equations are straightforward coupled-mode equations, where κ is a coupling coefficient proportional to the index modulation Δn and the overlap of the refractive index modulation with the power distribution of the guided mode:

$$\frac{dA_F}{dz} + j\kappa A_B = 0 \tag{2.30}$$

$$\frac{dA_B}{dz} - j2\Delta\beta A_B - j\kappa A_F = 0 \tag{2.31}$$

The solution of these equations gives the reflectivity of the grating:

$$R = \frac{\kappa^2 \sinh^2(SL)}{\Delta\beta^2 \sinh^2(SL) + S^2 \cosh^2(SL)} \quad \text{for } \kappa^2 > \Delta\beta^2 \tag{2.32}$$

$$R = \frac{\kappa^2 \sin^2(QL)}{\Delta\beta^2 - \kappa^2 \cos^2(QL)} \quad \text{for } \kappa^2 < \Delta\beta^2 \tag{2.33}$$

$$\tag{2.34}$$

where

$$S = \sqrt{\kappa^2 - \Delta\beta^2}$$

$$Q = \sqrt{\Delta\beta^2 - \kappa^2}$$

and L is the length of the grating. This function is illustrated in Figure 2.7 for three values of κL. It is clear that as the coupling strength or grating length increase, the reflectivity also increases. At the same time, greater coupling strength leads to stronger sidelobes and a greater bandwidth.

2.7.2 Photorefractive effects in silica fibre

The grating model described above depends on the ability to modulate the refractive index of the fibre in a periodic manner. The means by which this is accomplished is discussed below, but the physical origin of the refractive index change is discussed first. Several mechanisms have been proposed, and these have been reviewed[31, 32].

The refractive index shift appears to be a consequence of the creation of defects in the crystal structure of the fibre, induced by the absorption of ultraviolet light.

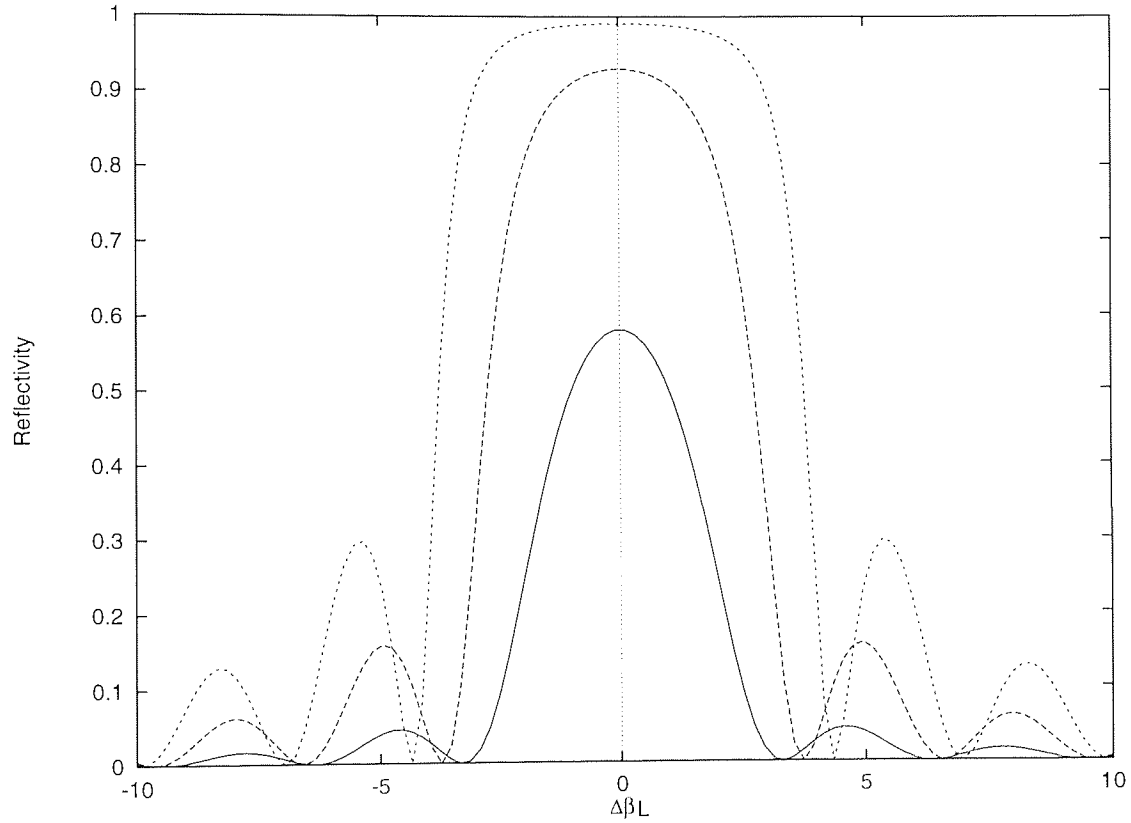

Figure 2.7: Reflectivity of a linear grating. $\Delta\beta$ is the offset of the incident wavevector from the Bragg condition, L is the grating length. κ is the coupling coefficient; the solid line indicates $\kappa L = 1$, the long-dashed line $\kappa L = 2$ and the short-dashed line $\kappa L = 3$.

These defects result in UV absorption and a refractive index shift, but do not significantly change the absorption at longer wavelengths —this is important for the practical use of fibre gratings. In fact, the excess loss from a high-reflectivity Bragg grating is typically as low as 0.01dB [32].

The mechanism accepted as the major contributor to the change in refractive index is the ionisation of a GeO defect, leading to the formation of a colour centre. The strong resonant absorption which results from this affects the refractive index of the fibre[33]. Various dopants can be used to accentuate this process, most commonly boron[34]. Additionally, hydrogen can be diffused into the fibre under high pressure and this significantly increases the photosensitivity[35, 36]. However, the hydrogen diffuses out of the fibre again, and prompt exposure is necessary to obtain the benefit of the enhanced photosensitivity. Furthermore, the dynamics of the hydrogen diffusion result in a longer term drift in the Bragg wavelength[37].

2.7.3 Fabrication of linear gratings

Linear fibre gratings were first fabricated using a standing-wave technique [38, 39]. This involved two counterpropagating 488nm beams (from an argon-ion laser) in the fibre; the points of maximum intensity in the standing-wave profile resulted in the greatest index change. This technique, however, can only be used to write gratings which reflect at the original reflection wavelength.

More recently, a holographic process was proposed [40] where two coherent beams were applied to the side of the fibre, such that their interference pattern induced the refractive index change. A schematic of this arrangement is shown in Figure 2.8. The reflection wavelength of the grating can be readily changed by altering the angle (θ) between the two beams. Typically, the beams used for holographic writing are in the ultraviolet, either from an excimer laser, a doubled argon-ion laser or a quadrupled Nd^{3+}:YAG.

Finally, it is possible to fabricate gratings using a phase mask. A phase mask is an optical flat with an etched corrugation. This corrugation results in an interference

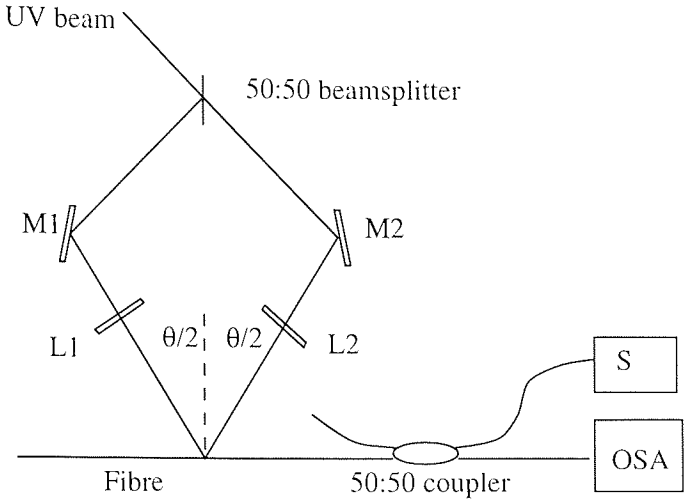

Figure 2.8: System for holographic fabrication of gratings. M1 and M2 are mirrors, L1 and L2 are identical cylindrical lenses with their axes in the same plane as the axis of the fibre. The source, S, is a broadband light source and allows the profile of the grating to be viewed on an optical spectrum analyser (OSA) as it develops.

pattern being produced on a fibre behind the mask. The phase mask itself is etched using electron-beam lithography. However, this method used alone can only produce gratings matching the period of the phase mask. However, temperature or stress during the writing of the grating may allow a shift in wavelength of up to 2.5nm[41].

2.7.4 Chirped Bragg gratings

A chirped Bragg grating is a grating in which the period of the refractive index modulation changes along the length of the grating; different parts of the grating have different Bragg wavelengths. This allows the production of gratings with a larger reflection bandwidth than that obtainable with a linear grating.

In addition, a chirped grating is a dispersive element *i.e.* incident signals at different wavelengths experience different round trip delays on reflection. The variation in the period of the refractive index variation in a chirped grating makes the grating less amenable to exact analysis, but numerical techniques can instead be employed[42].

Holographic writing

In order to produce a non-uniform period using the holographic writing system described above, the fibre must either be bent on a mandrel[43] so that the angle of incidence of the fringes varies along the fibre, or cylindrical lenses of different focal lengths can be used to the same effect[44] by inducing different amounts of curvature in the sets of interfering wavefronts. Obviously, the latter is easier to control and less likely to result in fibre damage. The majority of gratings used in this thesis were manufactured by this method. Very large grating bandwidths can be obtained using this technique [45].

Phase masks

As described for linear gratings, phase masks can also be used for the fabrication of chirped gratings; as the phase mask acts as a "template" for a grating, an arbitrary modulation pattern can be produced, allowing the manufacture of chirped gratings. Each phase mask, however, is only useful for a fairly small wavelength range; a set of gratings can be concatenated to form a longer grating [46, 47].

A further enhancement of this process allows the manufacture of arbitrary grating profiles using a two-pass approach[48]. Figure 2.9 shows the experimental setup used for this technique.

The ultraviolet beam (from a frequency-doubled Ar^+ laser) is reduced to a diameter of around 0.5mm and focused onto the fibre core using a cylindrical lens. The mirror and lens are set on a translation stage allowing the beam to be scanned along the fibre. An acousto-optic modulator provides for control of the amplitude of the beam. The phase-mask used has a uniform period *i.e.* is unchirped.

On the first pass, the writing beam passes through the phase mask and writes an unchirped grating into the fibre. The modulator is used to alter the intensity of the writing beam —this allows the production of an apodised grating. On the second pass, the phase mask is removed, and the beam is scanned along the fibre at a varying speed. This alters the overall refractive index of the fibre and adds a

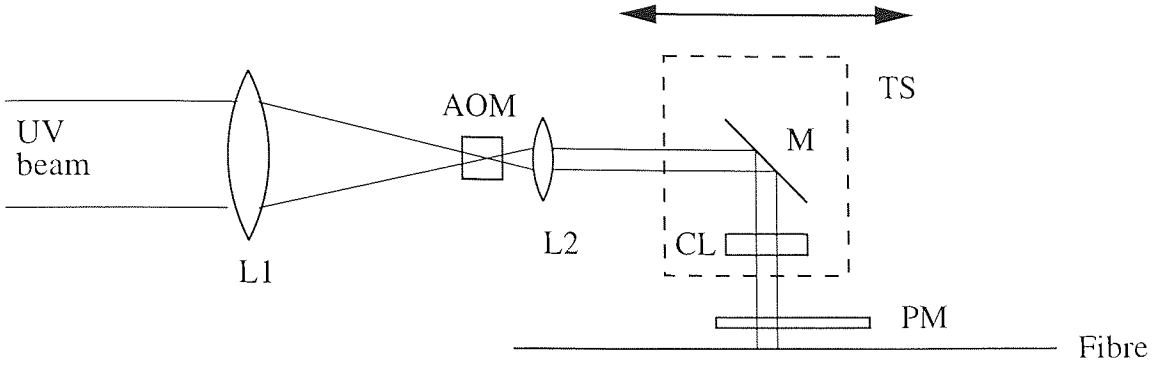

Figure 2.9: Schematic of two-pass grating fabrication system. L1 and L2 form a beam reducer; AOM: acousto-optic modulator for beam intensity control; M: folding mirror, CL: cylindrical lens, both mounted on TS: motorised translation stage under computer control; PM: phase mask

chirp to the grating. The profile of scanning speed against displacement along the grating can be arbitrary, and can be calculated from the desired grating parameters. The entire process can be computer-controlled, allowing the production of complex dispersion profiles and the ability to introduce an ideal apodisation function.

Apodisation

The ripple on the reflection profile arises because the reflection profile is proportional to the Fourier transform of the envelope of the refractive index modulation[49]. As a consequence it will contain high frequency components if the edge of the grating is close to a step function. To remove these components, it is necessary to use a function for the grating envelope whose transform does not contain high frequency terms. In practice, this requires the amplitude of the grating to be decreased towards its edges.

2.7.5 Properties and characterisation of gratings

This section will outline some of the principle features of in-fibre Bragg gratings which are relevant to their use in this thesis.

Long term stability

For Bragg gratings to be useful in a deployed commercial system, they must have good long-term stability, of the order of tens of years. A drift in centre wavelength or change in reflectivity will obviously affect the performance of the system.

Generally speaking, the reflectivity of Bragg gratings undergoes a temperature-dependent decay over time[33]. This consists of an initial rapid decay, followed by a longer term decay whose rate decreases with time. This decay process has been modelled[50] and this suggests that annealing of a grating at a high temperature will induce the initial rapid decay, leaving a grating with good long-term stability.

In addition to the change in reflectivity, a wavelength change has also been observed[51]. As with the reflectivity change, annealing induces the initial shift and leads to longer-term stability.

Short wavelength loss

One important feature of strong gratings is that they are not entirely lossless — wavelengths shorter than the grating wavelength are coupled to radiation modes by the strong perturbation of the grating, and this is visible on the transmission profile of the grating. In practice, the loss appears as a sequence of sharp notches in the transmission spectrum, though this is a consequence of the radiation modes from the fibre core being coupled into the cladding[49].

Characterisation of gratings

It is clear that the reflection and dispersion properties of chirped gratings are both significant in their application to optical fibre systems. As a consequence, a technique for measuring these properties is necessary. Figure 2.10 shows the experimental setup used for this purpose for several of these measurements in this thesis.

This system operates by measuring the reflected power and round-trip phase change from a grating as the wavelength varies. The source involved is a narrow-linewidth tunable laser with a linewidth of $\approx$ 50kHz. This is obviously broadened

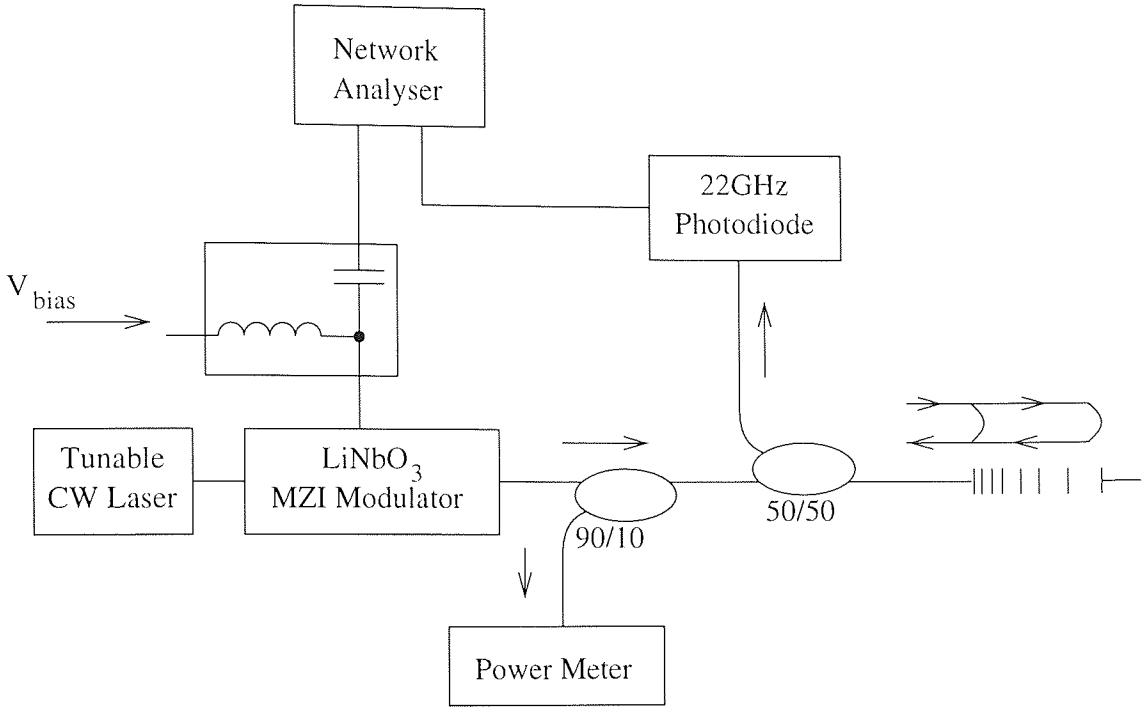

Figure 2.10: System used for measuring the reflectivity and delay profile of a chirped grating. The network analyser measures the delay relationship between the outward and reflected signal, and the power meter measures the reflected power

by modulating it with a radio-frequency signal.

Figure 2.12 shows a sample grating profile produced from this method. It is clear that the profile differs from the ideal shown in Figure 2.11. Most noticeably, there is a periodic modulation on the delay profile of the grating, and significant variation along the reflection profile. Both of these features have an impact on a laser system. The variation in reflectivity results in irregular dispersion tuning (see Section 3.5) and the variation on the delay profile results in a variable dispersion across the grating. As the GDD is the first derivative of delay with respect to wavelength, the ideal case where the delay profile is linear corresponds to a constant dispersion across the grating. Several observed effects in the lasers of this thesis are believed to relate to the nonuniformity of the gratings. Apodisation (see above) is a straightforward way to reduce the periodic delay and reflectivity modulation.

Although many different gratings were used experimentally in this thesis, a comparatively small number were found to work effectively in the systems constructed;

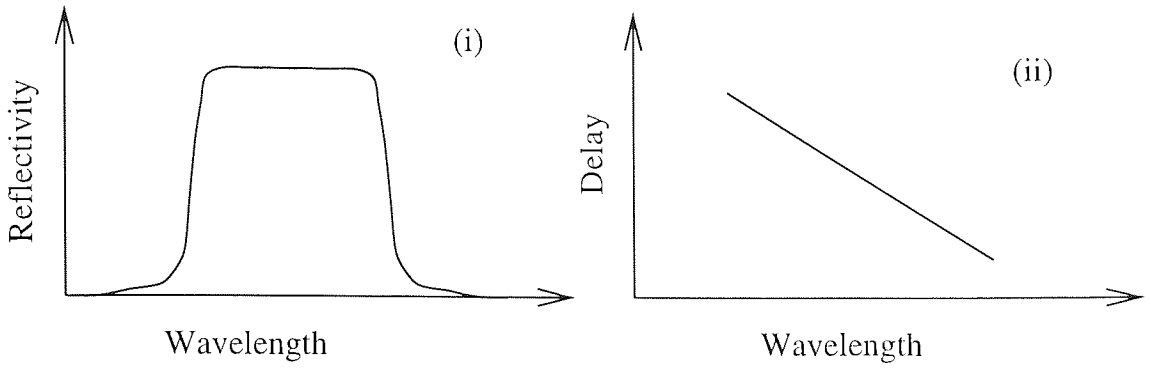

*Figure 2.11: Ideal profile of a chirped grating: (i) Reflectivity: note constant reflectivity across central part of grating. (ii) Delay: linear relationship (*i.e. *constant dispersion) across central region of grating*

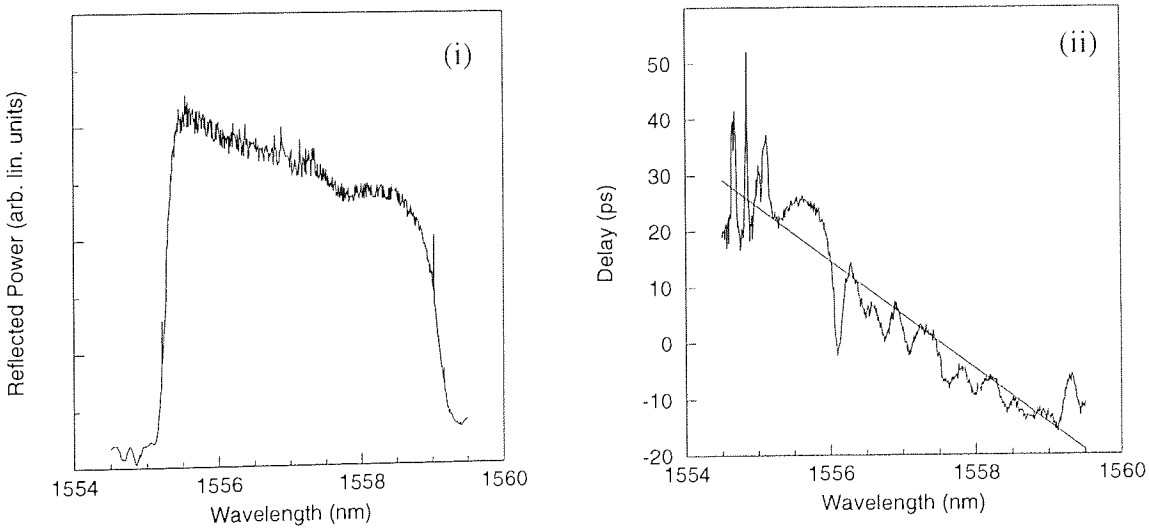

Figure 2.12: Sample of a grating profile produced using the setup of Figure 2.10. (i) is the reflection profile of the grating and (ii) is the phase profile. Note that there is significant modulation along the delay profile.

Number	Type	λ_c(nm)	$\Delta\lambda$(nm)	R	Length (nm)	Dispersion (ps/nm)
115	C	1550	20	50%	4	2
179	C	1557	4	100%	4	10
L138	C	1551	10	100%	4	4
L140	C	1542	24	100%	4	1.67
L160	C	1558	2	100%	6	20

Table 2.1: Table showing properties of principal fibre gratings used in experimental work. The numbers in the first column are the serial numbers of the gratings, and are referred to in results and discussion later. λ_c and $\Delta\lambda$ are the central wavelength and FWHM bandwidth. R is the approximate reflectivity and the length refers to the physical length of the grating. The bandwidth and length combined allow the calculation of an approximate dispersion value.

a summary of the properties of these is shown in Table 2.1. The dispersion values for the gratings are approximate values calculated using the relation:

$$D = \frac{2nL}{c\Delta\lambda} \tag{2.35}$$

where D is the dispersion in ps/nm, n is the effective refractive index, c is the speed of light *in vacuo* and $\Delta\lambda$ is the bandwidth of the grating.

2.7.6 Applications of Bragg gratings

The use of fibre Bragg gratings as laser reflectors is covered in the following chapters of this thesis, but they have also been applied to numerous other applications [33].

Bragg gratings are commonly used as sensors; the spectral profile of gratings is affected by factors such as strain [52, 53] and temperature[54]. These systems rely on a change in the reflection wavelength as a consequence of strain or temperature changes. It is possible also to produce a long chain of gratings in the same fibre with different reflection wavelengths and use a tunable source to address them. This

can provide a cost-effective distributed sensor architecture, particularly suitable for embedding into composite materials[55].

Furthermore, the ability to produce an arbitrary delay and reflection profile has made fibre Bragg gratings a popular choice for pulse compression [56, 57, 58] gain-flattening of amplifiers[59] and dispersion compensation in transmission systems[60, 61]. This can be simple dispersion compensation using gratings with linear chirp[62], or cubic and quadratic compensation using gratings with more sophisticated profiles[63]. The ability to produce customised dispersion profiles has also been used to provide variable time delays for phased-array radar systems[64].

Chapter 3

Fibre Laser Systems

This chapter considers the principles of operation of fibre lasers, with a particular emphasis on modelocking techniques. It starts, however, with a brief review of doped-fibre amplifiers as they are a central feature of fibre lasers.

3.1 Erbium-doped fibre amplifiers

An appropriate source of optical gain is a prerequisite for a fibre laser. While other techniques, such as amplification via stimulated Raman scattering [65], are possible, semiconductor or doped-fibre amplifiers are the gain media of choice for the majority of systems. (Semiconductor laser amplifiers will be covered in a different context in Chapter 6. Although they have been used as gain media for lasers, they have low saturation powers and, as bulk devices, are not as readily integrated into a laser cavity as doped-fibre amplifiers.)

A doped-fibre amplifier is simply a length of fibre which contains rare-earth dopant ions in its core. These ions have an energy level structure which is conducive to lasing: Neodymium has been used for many years in the Nd^{3+}:YAG laser system and in some fibre laser systems[66]; erbium is now widely used in fibre-based systems, because it can provide high gain and can be efficiently pumped using readily available sources. Other rare-earth dopants include thulium[67] and ytterbium-erbium co-doping[68, 69].

The pumping process in a doped-fibre amplifier involves propagating the pump down the doped fibre as well as the signal. The pump may be coupled in using a wavelength-selective coupler, or through a dichroic mirror or Bragg grating in the case of a linear cavity. The systems in this thesis all use a wavelength-selective couplerapproach and erbium-doped fibre amplifiers.

Erbium has several pump absorption bands including 532nm, 670nm, 807nm, 980nm and 1480nm. However, several of these wavelengths have poor efficiency due to excited state absorption (ESA) [70, 71], and most current systems use 980nm or 1480nm pumping with semiconductor laser diodes though earlier systems used 532nm which corresponds to frequency-doubled Nd^{3+}:YAG [72, 73]. Amplifiers pumped simultaneously at both theses wavelengths have also been proposed for long-haul communications systems[74]. A trend towards integration has led to the production of integrated fibre amplifier modules which require only a power supply and have a single control for the pump power.

The theory and gain dynamics of erbium-doped fibre amplifiers are outwith the scope of this thesis, but substantial literature exists [75, 76]. In addition to the normal fibre parameters, the doping concentration[77], amplifier length[78] and exact pump wavelength[79] may need to be adjusted to optimise the operation of the amplifier.

3.2 General operating features of laser systems

A laser system, at its simplest, consists of an optical amplifier with feedback. If the gain along one complete pass of the system is greater than the loss, laser action will occur.

As stimulated emission produces coherent radiation, the output of the laser will be coherent. Furthermore, the laser cavity is a resonant cavity and therefore has a set of frequency modes. These modes are "axial" modes i.e. they are resonant along the length of the cavity and are distinct from the radial modes of (for example) an optical fibre. The modes are present on the laser output spectrum, though they

are very closely spaced for larger laser systems (the difference in optical frequency between modes is the resonant frequency of the cavity, which will often be in the megahertz regime. As a consequence, the mode structure is not normally visible on the output spectrum).

For closely spaced modes, the output of the laser will readily switch between different modes due to environmental disturbances, and this may result in extra amplitude noise on the output (the phase relationship between different modes is not fixed).

Mode-locking is the process of producing pulsed output from a laser cavity by locking the phase of multiple cavity modes. The only stable solution where many of these modes are locked consists of a pulse or pulses circulating in the laser cavity. Techniques used for mode-locking can be described in two broad categories, active and passive. In an actively-modelocked system, an external signal applied to the cavity is responsible for the laser generating pulsed output. By contrast, a passively-modelocked system generates pulses as a consequence of the design of the cavity and the intrinsic properties of its components; no external signal is required.

These two approaches will now be described in more detail.

3.3 Active mode-locking

Active mode-locking is accomplished by the introduction of a modulator into a laser cavity. This affects the cavity either through amplitude modulation (the cavity gain/loss is modulated by the external signal) or frequency modulation (the cavity round-trip delay or phase is modulated by the external signal). However, it is necessary that the frequency of the modulation matches the fundamental frequency of the cavity, or a multiple of it.

A thorough description of the theory of active modelocking has been published by Siegman and Kuizenga [80]. The operation of mode-locking can be visualised either in terms of the time-domain or the frequency domain. In the time domain, a temporal energy distribution (a pulse) travels around the cavity, passing through

the modulator on each occasion; the effect of the modulation is thus enhanced by multiple passes around the cavity, particularly in the case where the modulation frequency is a multiple of the cavity mode spacing.

In the frequency domain, the mode spectrum of the system (a collection of independent oscillating axial modes) is altered; the modulation adds sidebands to all the axial modes of the laser. If the modulation frequency is equal to $c/2nL$ (or a harmonic), the sidebands on one mode will overlap with other modes and will interfere; the consequence of this is that the independent oscillation of the modes is suppressed.

3.3.1 Amplitude modulation

The operation of amplitude modulation is straightforward. In the time domain, a pulse which passes through the modulator at maximum transmission will pass through the modulator when it is again at maximum transmission. When this effect is accumulated from several passes around the cavity, this will result in suppressing pulses other than those synchronised with the external signal. The behaviour of an amplitude-modulated system with a slightly detuned external signal is dependent on the intracavity dispersion and is described in Section 3.5.

3.3.2 Frequency modulation

The operation of frequency modulation is more complex. The modulator imparts a phase change onto the intracavity signal. As this is rapidly varying, it results in a Doppler shift proportional to the rate of phase change *i.e.* $\frac{d\phi}{dt}$. This will be zero at the extremes of the phase modulation profile: stable pulses can form at these points. The circulating energy at other positions will acquire successive Doppler shifts until it is shifted out of the gain band of the laser. The phase profile around the region of the pulse can be approximated as a quadratic curve, and this has the consequence of adding a linear frequency shift across the pulse. As a consequence, the output pulses from an FM-mode-locked laser are chirped.

3.4 Passive mode-locking

Passive mode-locking requires that pulses circulating in the cavity experience a lower loss than continuous wave (cw) radiation. This is achieved through the design of the cavity and its components.

Although some passively modelocked systems have used linear cavities [81], many have been based around ring or figure-of-eight cavities. In linear cavity systems, spatial hole burning can occur in the gain medium and this frustrates self-starting of the laser and interferes with the operation of saturable absorbers —this is due to the appearance of maximum and minimum amplitude points in the cavity, while operating in a cw mode. If a cw maxima overlaps with a saturable absorber and partially saturates it, its effect on a pulse will be reduced. Additionally, spatial hole burning results in a fluctuating balance of modes in action in the cavity, reducing the stability of the output and adversely affecting mode coherence.

A ring or figure-of-eight configuration avoids some of the difficulties of a double-pass, linear system; the pulse evolution around the ring is more straightforward, and the evolution of polarisation, for example, can be controlled and exploited more readily in a ring topology. Some of the systems based on these effects are discussed in Section 3.7.2.

A wide range of passive modelocking techniques are in use, but all rely on making a pulsed mode of operation experience a lower loss than a cw one. This can be accomplished in several ways. Firstly, a saturable absorber (typically either a chemical or multiple quantum well device[81]) can be used [82]. This is a component which "bleaches" under higher intensity and thus has a lower loss for a high-intensity signal. For use in modelocking applications, the device obviously needs a fast response.

Another device with similar characteristics is the NOLM (see Section 2.6) and this forms the basis of the Figure-of-eight laser (see Section 3.7.3). Finally, a ring laser with a polarising element can be used; this relies on nonlinear polarisation rotation (NPR).

The final significant concern with passively modelocked systems is that they

may not "self-start" *i.e.* the system may initially be stable in a cw mode and not modelock without a perturbation being applied. Krausz *et al* [83] consider that the threshold for self-starting is dependent on the cavity length and the coherence time of laser modes. Haus *et al* [84] report that the major factor opposing self-starting is interferometric effects from spurious intracavity reflections. In practice it would appear more straightforward to reduce these in a ring cavity. Both papers suggest that a shorter cavity round-trip time encourages self-starting, and a linear cavity will generally have a longer round trip time than a ring cavity. Hybrid systems involving a mixture of passive and active components, such as [85] have been proposed as a solution that has the benefits of passively-modelocked systems (short pulses) and has a low threshold for self-starting.

3.5 Dispersion tuning

In the case of an actively mode-locked laser locked using an amplitude modulator, a change in length of the cavity will result in a change of the operating wavelength [86]. Consider a switching window as shown in Figure 3.1(ii), where the central line is the centre of the window (which is repeated with a period T_0) and the cavity has a length of L.

In the case of a laser operating at λ_0, the round-trip time of the cavity will be that which leads to maximum reflection (*i.e.* minimum loss) from the loop mirror. A pulse in the cavity will therefore always make one round trip in T_0 seconds.

If the length of fibre in the cavity is increased, adding a delay of ΔT then after one round trip, a pulse at λ_0 will reach the reference point of the loop mirror after the reflection peak, at the point indicated by the dashed line. On a second pass it will be further still from the centre of the reflection profile.

This can be expressed as a reduction in the intracavity gain for that wavelength, while a wavelength λ where :

$$\lambda - \lambda_0 = \frac{n\Delta L}{cDL} \tag{3.1}$$

will instead experience maximum transmission. As a consequence, assuming an

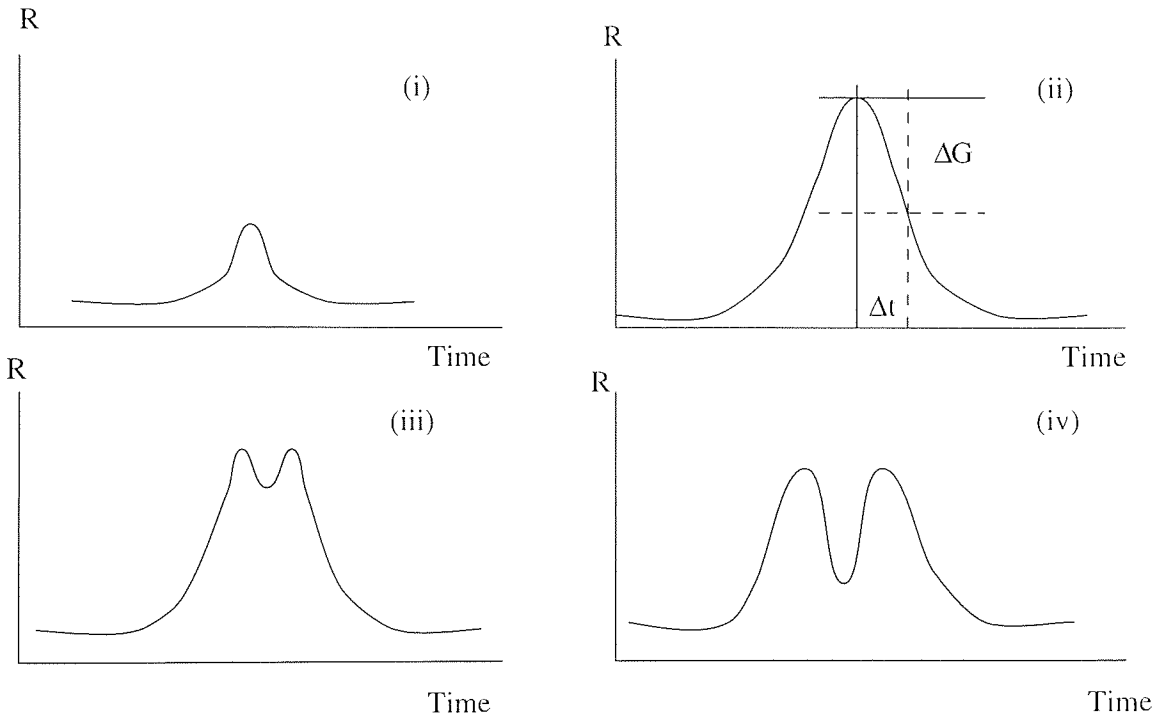

Figure 3.1: Illustration of dual-wavelength loop mirror reflection characteristics for increasing switching power from (i) to (iv). Horizontal axis is time, and vertical axis is reflectivity; these curves can be derived by transforming the pulse envelope through Equation 2.24. The loop mirror reflection profile used in practice was similar to (ii). The vertical and horizontal lines on (ii) illustrate the operation of dispersion tuning.

otherwise flat gain spectrum, the output wavelength will change. If, however, the operating wavelength is in a region of varying gain, the laser will operate preferentially at the point of highest gain. Effective dispersion tuning will rely on strong modulation; insufficient modulation may "pull" the operating wavelength but will not result in full dispersion tuning. The effect of this "pulling" will be most noticeable in systems with filtering or other strong gain variations.

3.6 Dispersion measurement

While it is, in theory, possible to calculate the dispersion within a cavity by summing the dispersion contributions from its constituent parts, this is impractical for many systems. Firstly, it is possible that the dispersion of some components may be complex; and secondly, for a real system, the effect of "gain pulling" and other behaviour of the system is best observed with the system operating. This section will therefore present two methods for the determination of intracavity dispersion measurement.

However. both of these techniques will generally produce average values of dispersion (averaged over the spectral width of the pulse); more accurate determination of the dispersion of components can only be obtained using narrow-linewidth cw sources. This approach is used to determine the dispersion characteristics of chirped fibre gratings in Section 2.7.5.

3.6.1 Dispersion tuning as a measurement technique

Dispersion tuning, as described in Section 3.5 above, is capable of determining intracavity dispersion with reasonable resolution; a plot of wavelength change against the change in cavity length (and thus delay) is straightforward to obtain, and the reciprocal of the gradient of such a graph is a measure of the cavity dispersion: this will tend to average any features in the dispersion profile.

3.6.2 Soliton sidebands

A perturbation, such as a loss or gain, will cause a soliton to shed coherent radiation. After amplification, for example, the pulse may not have the optimum envelope shape, and will shed energy to attain this shape.

As the soliton is a stable solution (see Section 2.5), perturbations such as gain or loss result in the shedding of radiation so that the pulse is again a stable solution within the new environment. The radiation shed after a lumped amplifier is coherent like the original soliton, and in a periodic system in which energy is shed at each amplification, interference effects occur.

These effects manifest themselves as sidebands on the optical spectrum of the soliton, and their positions can be readily related to the parameters of the transmission or laser system[87, 88, 89].

The fibre dispersion around the soliton central angular frequency $\Delta\omega_0$ can be expressed as a Taylor expansion (from Equation 2.2, with $\Delta\omega \equiv \omega - \omega_0$:

$$\beta(\omega) = \beta_0 + \beta_1\Delta\omega + \frac{1}{2}\beta_2\Delta\omega^2 + \frac{1}{6}\beta_3\Delta\omega^3 + \cdots \tag{3.2}$$

Using this expansion (as far as the third-order term) as the propagation constant of the dispersive wave component (β_d), and the same expression (neglecting third- and higher-order dispersion terms for simplicity) as the propagation constant of the soliton (β_s). The phase difference between the soliton and the dispersive wave as they propagate is therefore:

$$\phi_s - \phi_d = L(\beta_s - \beta_d) \tag{3.3}$$

This phase difference must be an integer multiple of 2π to form a sideband peak. As $\Delta\omega^2 = \tau_0^{-2}$, the soliton propagation constant β_s can be written as:

$$\beta_s = \beta_0 + \beta_1\Delta\omega - \frac{1}{2}\beta_2\tau_0^{-2} \tag{3.4}$$

Including the phase-matching condition, the sideband positions $\Delta\omega_N$ are described by

$$2\pi N = -\frac{1}{2}\beta_2 L(\tau_0^{-2} - \Delta\omega^2) - \frac{1}{6}\beta_3 L\Delta\omega^3 \quad (3.5)$$

$$N = -\frac{1}{4\pi}\beta_2 L\tau_0^{-2} - \frac{1}{4\pi}\beta_2 L\Delta\omega_N^2 - \frac{1}{12\pi}\beta_3 L\Delta\omega_N^3 \quad (3.6)$$

This equation can be compared to a standard cubic:

$$N(\Delta\omega) = A + B\Delta\omega + C\Delta\omega^2 + D\Delta\omega^3 \quad (3.7)$$

Consequently, if a cubic is fitted to a plot of N against $\Delta\omega_N$, the values of A, B, C and D determined from the fit can be related to various parameters of the laser system.

$$\beta_2 L = -4\pi C \quad (3.8)$$

$$\beta_3 L = -12\pi D \quad (3.9)$$

$$\tau_0^2 = \frac{A}{C} \quad (3.10)$$

It is therefore possible to determine the intracavity dispersion and pulsewidth from the positions of the sidebands. The sideband amplitudes are larger for shorter pulses, but are not related to system parameters in a straightforward way[89], save that the overall power in the sidebands is an indication of the extent of perturbation in the system.

This technique is used in Section 4.3.2 —see, for example Figures 4.10 and 4.12 for an example.

3.7 Fibre laser configurations

This section will outline several different configurations of fibre laser which have been used to produce soliton output. There are many variations on the basic schemes outlined here. The three cavity types are linear, ring and figure-of-eight (F8L). While the figure-of-eight is a particular case of a ring laser, it is widely used for short pulse generation and merits separate discussion.

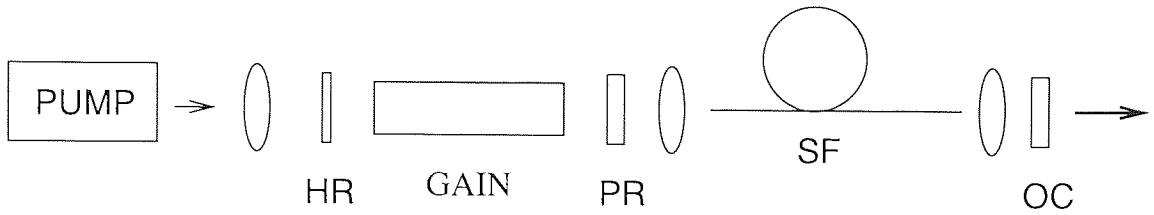

Figure 3.2: Synchronously-pumped coupled-cavity laser. EDF: erbium-doped fibre, HR: high reflector, PR: partial reflector, OC: output coupler, PC: polarisation controller, SF: standard fibre,

Finally, it should be noted that there are hybrid cavities such as the "sigma" cavity in which part of the cavity is double-pass (*i.e.* similar to a linear cavity) and another part is single-pass (*i.e.* similar to a ring cavity). This has been used to implement rapid cw tunability[90] and allows passive, polarisation rotation effects (discussed below) to shorten actively-modelocked pulses [91].

3.7.1 Linear cavity lasers

In this sense, the word linear relates to the physical layout of the cavity rather than to the optical behaviour of its constituent elements (all the cavities used in this thesis make use of nonlinear optical effects). The linear configuration was that used for the first laser, and it is the format which most commercial lasers use (In bulk optics, the alignment of a linear cavity is more straightforward than that of a ring cavity).

Early systems which produced soliton output (including the first "soliton laser" [92]) used a synchronously-pumped linear cavity coupled to an external nonlinear cavity which causes pulse compression. An example of such a system is shown in Figure 3.2.

The pulse compression in such a laser is a consequence of the nonlinear external cavity chirping the pulse; when this is added to the original pulse, the result is a compressed pulse. In the soliton laser above, the main cavity was a solid-state cavity, and only the nonlinear cavity was constructed in fibre. Phase modulation (rather than gain modulation) is described by Stock *et al* [86]. Several designs of coupled

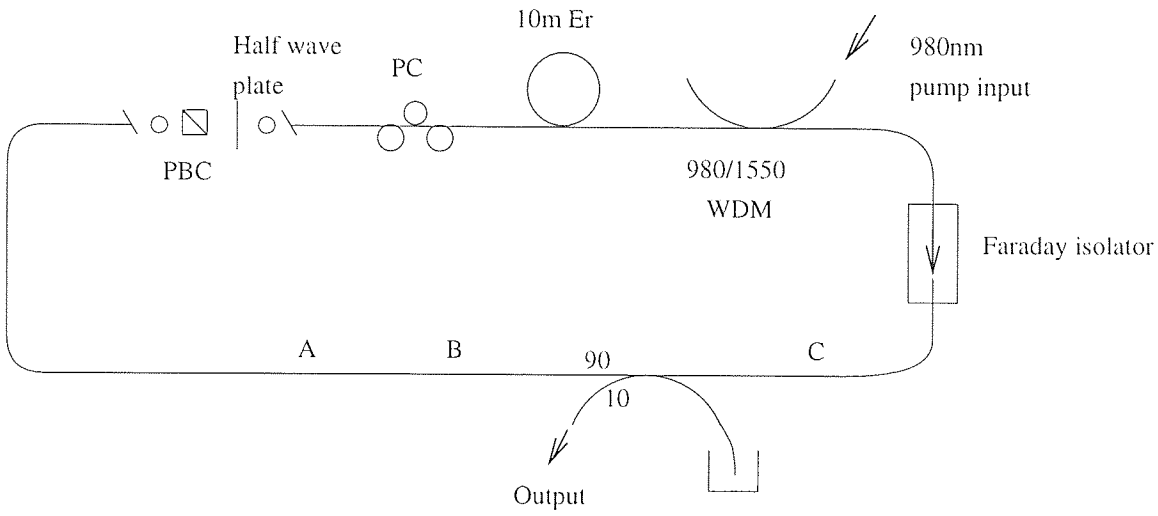

Figure 3.3: Ring laser using nonlinear polarisation rotation

cavity have been proposed: These use bulk mirrors [93] or fibre Bragg gratings [94] between cavities. The theory underlying these cavities has been studied [95].

The availability of erbium-doped fibre simplified the construction of soliton lasers in fibre. Earlier lasers used many bulk components alongside the amplifier [96, 97]. Further rationalisation removed many of the bulk components from laser systems. This has led to the development of all-fibre lasers, which are clearly to be preferred on grounds of stability and ease of construction: in a system designed for use in the real world, any freespace optics have to be very rigorously packaged.

Stability, however, remains a significant concern; both acoustic noise and thermal fluctuations lead to variations in the optical length of laser cavities. In this respect, the performance of actively and passively modelocked lasers differs. Various schemes have been proposed, particularly for ring lasers, to address the problems of thermal drift and acoustic noise.

3.7.2 Ring lasers

While ring lasers have been used as the basis for fibre gyroscopes[98] and narrow linewidth or widely tunable cw sources[99, 100, 101], this section will concentrate on their use as pulse sources.

Ring lasers, for example that shown in Figure 3.3, can be constructed using nonlinear polarisation rotation (first used as an effect in fibre by Stolen *et al* [102], and later used for modelocking fibre lasers[103, 104, 105]). Pulses as short as 77fs have been produced by these systems [106], and output wavelength ranges up to 82nm [107] have been reported. Tuning mechanisms involving birefringent plates [108] and varying the power of an optical pump [69] have been presented.

Nonlinear polarisation rotation is a consequence of nonlinear refractive index; a high-intensity signal at an angle to the fast axis of the fibre will result in a change in the refractive index along the fast axis, which results in the polarisation state rotating towards the fast axis. A cw signal will experience no such phase shift and as a consequence will not be rotated. A polariser can therefore be used to introduce a differential loss between the states, and the system will function as a fast saturable absorber, resulting in passive mode-locking.

However, as such ring lasers depend on polarisation changes for their operation, the polarisation sensitivity inherent in their operation may be a source of instability —thermal or acoustic effects typically alter polarisation (the random birefringence of standard telecommunications fibre exacerbates these effects).

A resonant ring may be used (in a manner similar to a coupled cavity) to stabilise the repetition rate of a passively-modelocked ring laser [109, 110]; this assumes that stabilising a comparatively short ring is easier than stabilising the entire cavity.

Ring lasers may also be actively modelocked; active modelocking using both phase modulation and amplitude modulation[111] has been reported. A solid-state [112] or all-optical phase modulator is inserted into the ring and this can be used as a modelocking signal. Such a system is commonly used for clock recovery [28]. While NPR is usually used in passive systems, it has also been used as an active modelocking technique [113] and for simple modulation[114].

The nature of many passively-modelocked systems is such that they may produce random trains of pulses, and with careful adjustment yield pulse trains with a fixed period. This particular concern is less relevant to actively modelocked systems, in which environmental fluctuations are likely to result in amplitude or wavelength

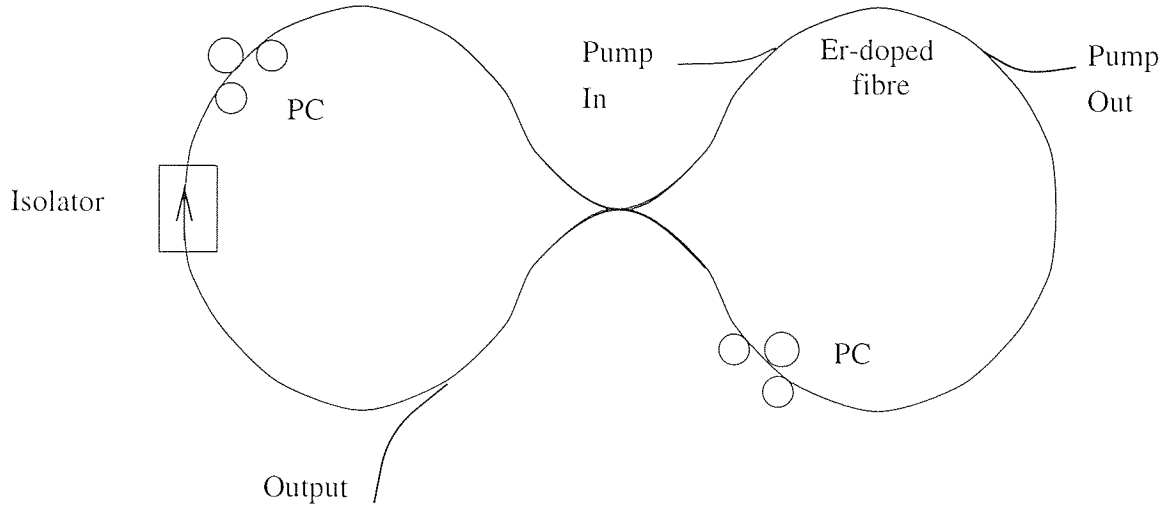

Figure 3.4: Figure-of-eight laser

changes, depending on the construction of the cavity.

The stability of a ring laser can be improved by including it as part of a phase-locked loop [115, 116] or using a regenerative mode-locking technique [117, 118]. [119] uses the change in output noise at two separate frequencies to monitor cavity length drifts.

A further technique employed with ring lasers is the sliding-frequency laser [120], in which an acousto-optic tunable filter (AOTF) is swept across a wavelength range. Soliton pulses will reform at the new central wavelength after each pass through the filter, while spontaneous emission, or a cw signal, will be suppressed by the filter. This is analogous to the use of sliding filters in transmission systems (though in a long linear system, fixed filters are used instead of the tunable filters required for a ring system).

3.7.3 Figure-of-eight lasers

A figure-of-eight laser [121] is a ring laser containing a fibre loop mirror (most commonly a nonlinear amplifying loop mirror[20] which functions as a saturable absorber) and a unidirectional section containing an isolator[122, 123, 124]. Other designs of figure-of-eight have been reported, including dispersion decreasing (ta-

pered) fibre [125] and hybrid active/passive devices [85]. A clock recovery system employing a figure-of-eight has been reported[126].

3.8 Harmonic modelocking and clock division

The discussion so far has assumed that the output repetition rate of the laser is the same as the frequency of the modelocking signal. However, this is not always the case.

If the input control pulse frequency is detuned from an exact multiple of the cavity resonant frequency, it is possible to obtain harmonic generation [127, 128]. Broadly speaking, if the cavity fundamental frequency *i.e.* the mode spacing is Δf, and the normal modulation frequency is $p\Delta f$, then detuning of the modulation frequency by $\Delta f/n$ will produce $np+1$ pulses in the cavity; this corresponds to an output rate of $(np+1)\Delta f$. A detuning of $\Delta f/2$ produces frequency doubling, for example. This process has been used to produce 200GHz pulse trains [128]. Using semiconductor laser amplifiers, it is also possible to obtain clock division [129].

An alternative approach to the production of high-frequency pulse trains is dual-frequency beat generation in which two cw signals at very similar wavelengths generate a beat frequency according to their wavelength difference [130, 131, 132]. This method has the disadvantage that it can *only* generate repetition rates in the high GHz to THz regimes, and requires that the two wavelengths be closely matched.

Chapter 4

Linear Cavity Laser with a Chirped Grating

This chapter presents a simple linear laser system and examines its operation. The effect of the fibre grating on the performance of the laser is also considered.

The design of this particular system consists of a linear, standing-wave cavity. A linear cavity of similar design to that described here was investigated by Nelson, Smith and Blow [133]. The significant differences are that they use a much longer (6.4km) loop mirror and a linear fibre grating. The longer loop mirror permits the use of lower-powered control pulses, but increases the intracavity dispersion and the length of fibre which is subject to acoustic and thermal influence.

The linear grating in [133] has a bandwidth of 0.5nm, and the cavity described produced Gaussian pulses. The system to be described in this chapter is capable of producing both sech^2 and Gaussian pulses by exploiting the dispersion modification potential of a chirped grating.

Both of these systems are simple standing-wave laser cavities, and they allow the use of fibre Bragg gratings as end mirrors. This is more significant where the FBG is chirped and is to be used for dispersion control; it must be used in reflection and this is easiest to accomplish with a linear cavity. Passively-modelocked systems using chirped gratings have been described by Fermann *et al* [134, 135]

It is possible to use a circulator or coupler in a ring cavity to include a grating

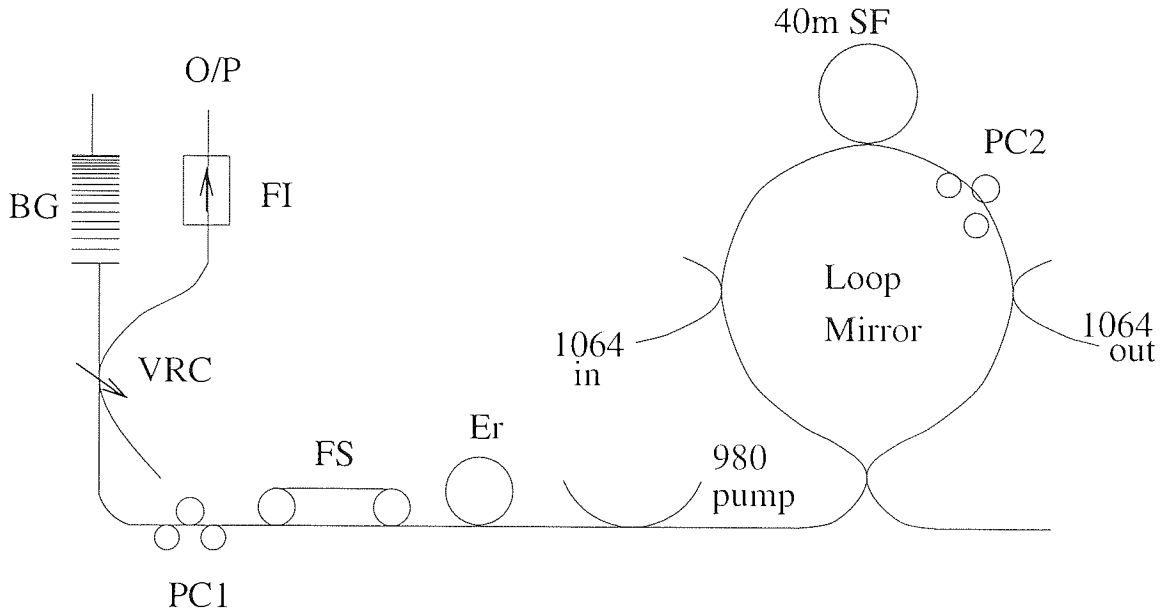

Figure 4.1: Schematic of linear-cavity laser. FS: fibre stretcher; ISO: Isolator; PC: polarisation controller; SF: standard fibre; WSC1,2: 1064nm/1550nm wavelength-selective couplers; WSC3: 980nm/1550nm wavelength-selective coupler.

[136, 137], but this is less straightforward than using the grating as the end reflector on a linear cavity, and involves some additional loss.

The use of chirped gratings is the particularly novel feature of this system; it is only in recent years that chirped fibre Bragg gratings have become more widely available, allowing both the operating wavelength and dispersion of the system to be set with a single device. This chapter will examine the design of a system using a chirped fibre Bragg Grating and NOLM, and discuss the effect that different gratings have upon its operation.

4.1 Design and construction of laser system

Figure 4.1 shows the layout of the cavity.

The dual-wavelength loop mirror functions as one end reflector, and contains approximately 40m of standard fibre between two wavelength-selective couplers(WSC1 and WSC2). These are used to couple a 1064nm pulse stream into the 40m length of fibre so that it co-propagates with the intracavity signal before being extracted.

The control pulses at 1064nm are provided by a mode-locked Nd^{3+}:YAG laser operating at (nominally) 76MHz and with a pulse duration of $\approx$ 90ps (FWHM). The loop mirror contains a polarisation controller to allow the loop to be biased into reflection or transmission without a control signal present (see Section 2.6).

The central part of the cavity consists of an erbium-doped fibre amplifier (EDFA) consisting of approximately 10m of erbium-doped fibre, and a coupler (WSC3) to couple in pump light at 980nm. The pump energy was provided by a Ti^{+}:Al_2O_3 laser.

The cavity also contains a fibre stretcher for matching the cavity length to a multiple of the the period of the control pulses (see Section 4.1.2 below) and a polarisation controller to allow the intracavity polarisation to be adjusted. The output is provided through a variable-ratio coupler and an isolator. The reflector at the opposite end from the loop mirror is a chirped in-fibre Bragg grating (CFBG) which sets both the operating wavelength and dominates the intracavity dispersion.

As discussed in Section 3.3, the modulation frequency must be a harmonic of the cavity fundamental frequency. In this system, the modulation frequency was fixed, and the cavity round trip time (*i.e.* length) had to be altered to match the modulation frequency. The design of the fibre stretcher allows a maximum length change of around $\pm$2.5cm, so the manual addition or removal of fibre was necessary before the fibre stretcher could be used.

In order to make this adjustment, the laser was operated in a cw mode and the mode beat noise harmonics observed. These appear on the radio-frequency spectrum of the cavity output at intervals of the cavity fundamental frequency. For the laser to operate, one of these harmonics must coincide with the modulation signal at $\approx$ 76MHz. By measuring the difference between the cavity noise signal and the Nd^{3+}:YAG frequency, $\Delta\nu_N$, the length change required in the cavity could be calculated and the appropriate length of fibre to add or remove determined as:

$$\Delta L = -\frac{cN}{2n}\frac{\Delta\nu_N}{\nu_N^2} \tag{4.1}$$

where ΔL is the necessary length change, N is the number of the harmonic being observed, c is the speed of light *in vacuo*, n is the refractive index of the fibre (≈ 1.452), $\Delta\nu_N$ is the difference between the frequency of the Nth harmonic and the Nd^{3+}:YAG frequency and ν_N is the frequency of the Nth harmonic.

4.1.1 Loop mirror design

The choice of control pulses (1064nm, 76MHz) was dictated by the availability of a Nd^{3+}:YAG laser as a stable, high power, pulse source. The length (40m) of the fibre in the loop mirror between the wavelength-selective couplerswas determined from the walk-off distance of a 90ps pulse at 1064nm with a $\approx$ 10ps pulse at 1550nm. Because the intracavity pulse is much shorter than the switching pulse, its length can be ignored, and the walk-off length is the length of fibre required to produce a delay difference of 90ps between a pulse at 1064nm and 1550nm.

The delay difference d_{12} (ps/m) between two pulses at wavelengths λ_1 and λ_2 is given by:

$$d_{12} = \frac{1}{v_g(\lambda_1)} - \frac{1}{v_g(\lambda_2)} \tag{4.2}$$

and the walk-off length is $L_w = \frac{\tau}{d_{12}}$ for a pulse duration of τ.

For $\lambda_1 = 1064$nm and $\lambda_2 = 1550$nm, the two values of v_g are 2.050×10^8m/s and 2.052×10^8m/s respectively. (Because the dispersion zero of standard fibre is at $\approx 1.3\mu$m, these two wavelengths lie either side.)

This gives $d_{12} = 3.37$ps/m, and a walk-off length for a 90ps pulse of 26.7m. In practice, a slightly longer length of 40m was used, as a small amount of extra walk-off would only have the effect of broadening the switching window slightly.

4.1.2 Calibration of fibre stretcher

The fibre stretcher consisted of standard fibre wound around two metal drums about 30cm apart, one of which was attached to a micrometer-driven translation stage. The total length of fibre on the fibre stretcher was about 10m. Instead of estimating the

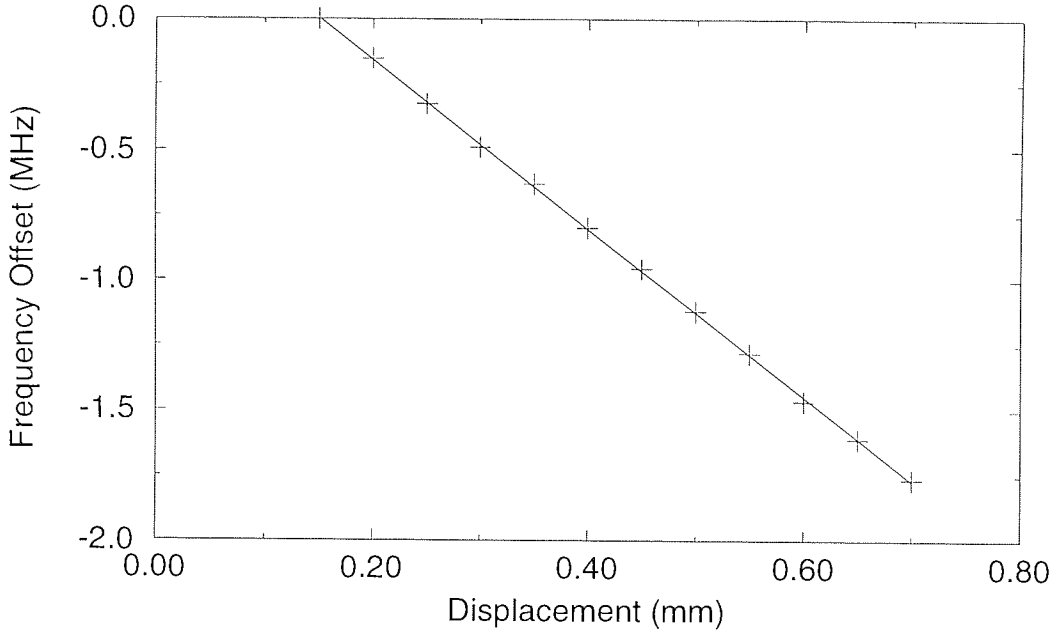

Figure 4.2: Calibration curve of fibre stretcher. Solid line is least squares fit of a straight line

length change from the number of turns on the stretcher, it is more reliable to measure the actual characteristics. The fibre stretcher was calibrated by incorporating it into the cavity and observing the displacement of a high harmonic ($N = 50$) of the cavity resonant frequency as the fibre was stretched.

The results of this are shown in Figure 4.2. The straight-line fit corresponds to a length change of 19.28mm in the cavity round trip length for every 1mm of change indicated on the micrometer. This value (or its time equivalent, 1mm indicated $\equiv$ 186.4ps) can be used to calibrate the results of dispersion tuning experiments.

4.1.3 Loop Mirror switching performance

In order to determine the modulation depth of the loop mirror, a simple continuous wave erbium-fibre laser was coupled, via an isolator to one port of the loop mirror. The transmitted signal was observed on a 30GHz digital sampling scope (the duty cycle of the control pulses, and therefore of the output signal is so high that the switching will result in an average power change of only around 0.5%.) The switching depth at an optimum control pulse average power of $\approx$ 95mW was 79%. The

switching window had a width of 117ps with these settings: an increase in the switching power had the effect of increasing the window width further. The periodic nature of the nonlinearity was visible at higher powers, as the modulation depth at the centre of the window started to decrease again.

The loop mirror is longer than the walk-off length calculated in Section 4.1.1 and the effect of this is to widen the switching window [22].

The system was tolerant of variation in the power of the switching pulses, and average powers of as low as 65mW could be used successfully, though this resulted in an increase in the noise and jitter visible on the output pulses. This corresponds with the work of von der Linde [138] who observed an increase in jitter when the modulator drive amplitude of a laser system was reduced. All the work in this chapter was performed with the switching pulse power optimised.

An increase in the control pulse power beyond $\approx$ 120mW led to a gradual onset of instability. There are two possible causes of this. The first is the alteration of the switching window shape; the dispersion tuning/mode-locking process described in Section 3.5 will only be effective for a simple switching window; if the window has a central feature (see Figure 3.1) then the stability of the output will be reduced by the availability of two apparent windows in the switching profile. Alternatively, the instability may be caused by the onset of stimulated Raman scattering [22].

4.2 Pulse output characteristics

In this section a selection of results will be presented for the system described above, using the three different gratings described above. A typical autocorrelation (i) and spectrum (ii) of an output pulse from this laser system is shown in Figure 4.3

The central wavelength of the pulse is 1553.76nm (point A on Figure 4.8 (i)) and the FWHM spectral width is 0.38nm. Assuming a sech^2 pulse envelope the real width of the pulse is 4.64ps, and this would yield a time-bandwidth product of 0.22. This may be due to a cw peak at the centre of the spectrum altering the measured spectral width.

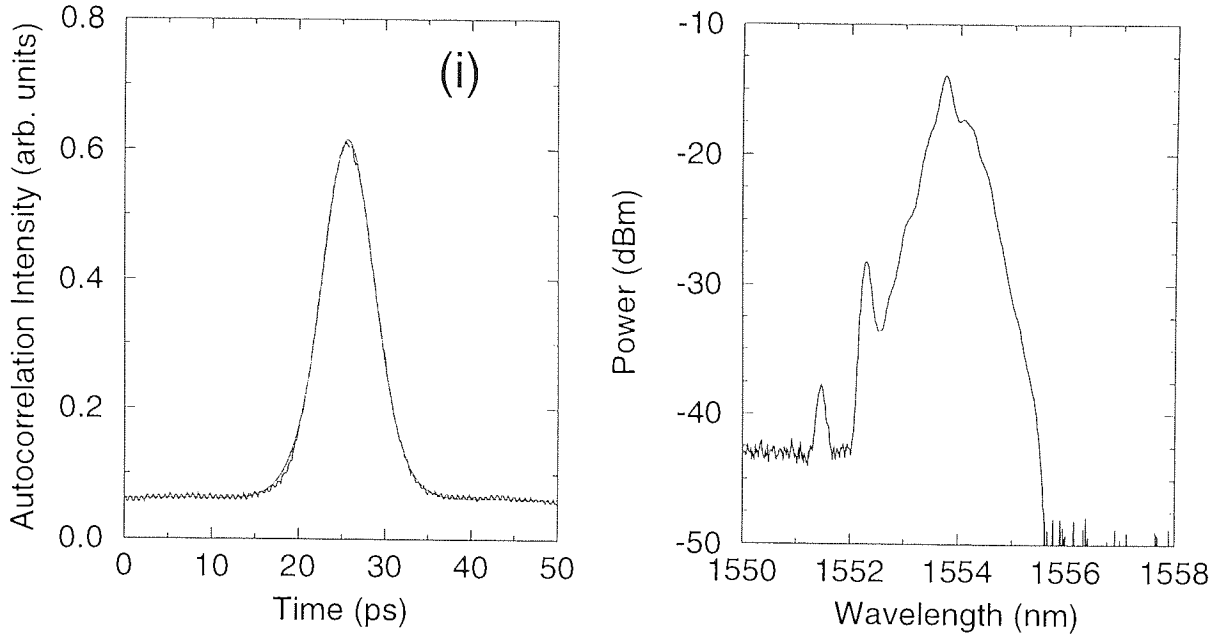

Figure 4.3: Autocorrelation (i) and spectrum (ii) of pulse, using grating L138. Dashed line on (i) is best fit to autocorrelation of sech^2*, with autocorrelation width of* $7.2ps$*.*

For short pulses, however, the cavity did not support a complete pulse train; this was obtained with pulses of $\approx$ 6ps and longer. This is probably due to insufficient intracavity power.

Figure 4.4 shows another pulse train obtained at a different operating point (λ = 1549.1nm, B on Figure 4.8). This pulse has a pulse width of 6.8ps (assuming a sech^2 pulse shape) and a spectral width of 0.21nm. This yields a time-bandwidth product of 0.18, possibly for the same reasons given above.

Figure 4.5 shows an autocorrelation and corresponding spectrum for a different operating point on the grating. The pulse width is 8.7ps and the spectral width is 0.53nm. This gives a time-bandwidth product of 0.58, significantly greater than the bandwidth limit of 0.316. This suggests that the output pulse is chirped.

In areas of the grating where the dispersion was higher (*e.g.* regions C and D in Figure 4.8) the pulses were substantially longer. An example is shown in Figure 4.6, in which the pulse width is 26.8ps and the spectral width is 0.20nm. Consequently, the time-bandwidth product is 0.67, substantially broader than the bandwidth limit

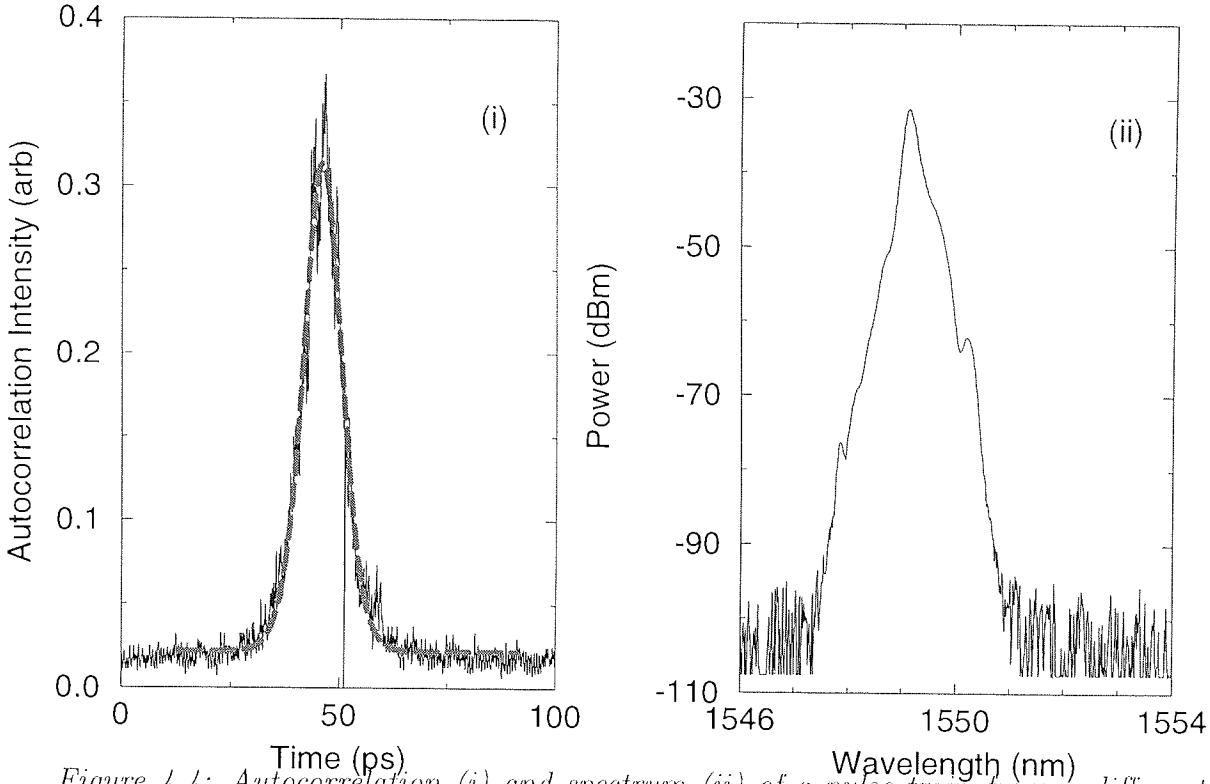

Figure 4.4: Autocorrelation (i) and spectrum (ii) of a pulse train from a different grating operating point from that used in Figure 4.3. Solid line on (i) is best fit to sech^2, *τ(FWHM)=6.8ps.*

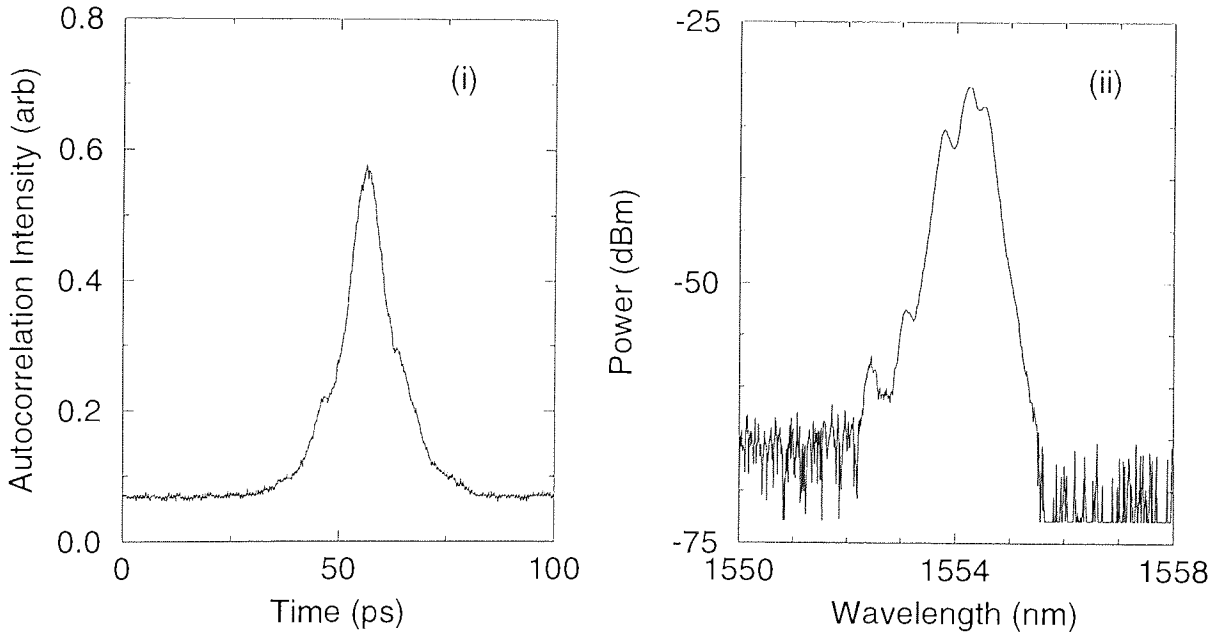

Figure 4.5: Autocorrelation (i) and spectrum (ii) of a pulse train, using grating L138. τ(FWHM)=8.7ps

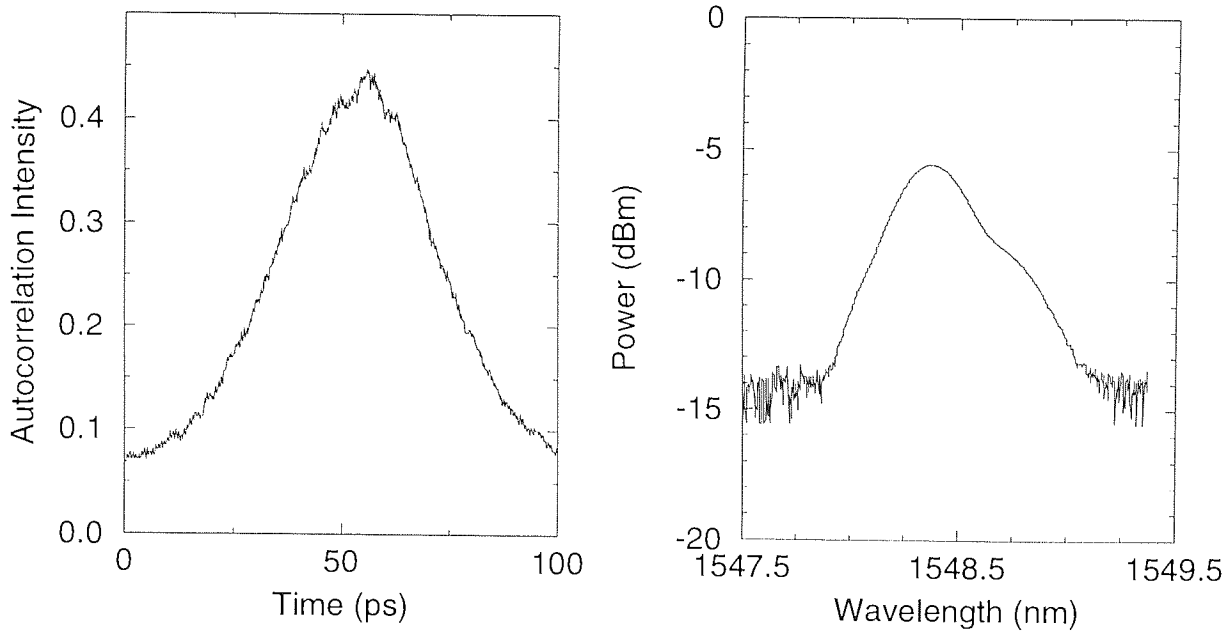

Figure 4.6: Pulses obtained in a higher-dispersion region of the grating (around point C). Note that the pulse is significantly broader (26.3ps) than those from other operating points.

—this suggests some degree of chirp on the pulse.

However, there was an insufficient number of operating points to satisfactorily test the relationship between dispersion and pulse width. Additionally, accurate determination of the grating dispersion on a local scale is difficult, though Figures 4.8 and 4.9 offer two views of the grating dispersion.

By reversing the direction of the grating, the sign of the cavity dispersion could be reversed (the magnitude of the total dispersion may not remain the same because of the intrinsic dispersion of the cavity). An example of an output pulse and spectrum produced from this mode of operation (though using a different grating, L160) is shown in Figure 4.7. The spectral width of this pulse is 0.23nm and the temporal width is 20.1ps, giving a time-bandwidth product of 0.58. This is slightly greater than the bandwidth limit of 0.441 which suggests that the pulse is slightly chirped. However, not all of the gratings produced stable output when reversed, and the grating used in Figure 4.7 did not produce stable output when used in the anomalous dispersion regime. However, this is most likely a property of the gratings used, and

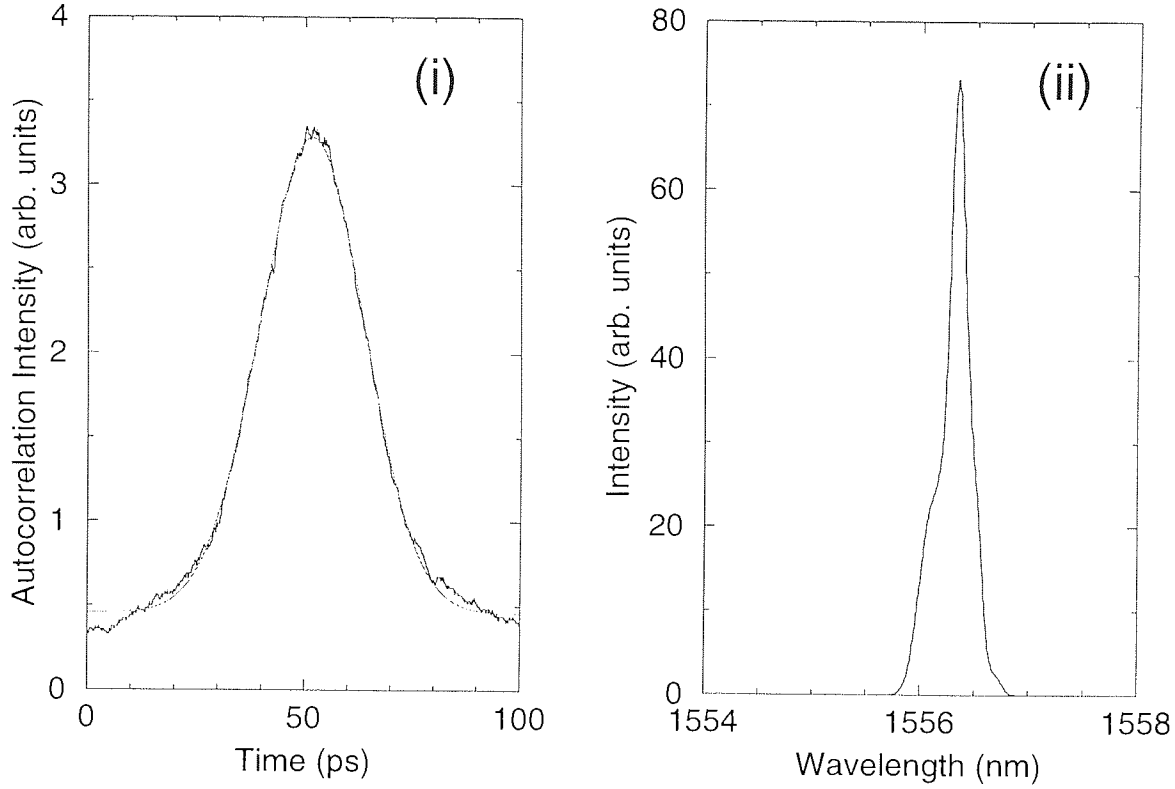

Figure 4.7: Autocorrelation (i) and spectrum (ii) for a system with overall normal dispersion. Solid line on (i) indicates best Gaussian fit: $\tau(FWHM)$=20.1ps.

not a general feature of the cavity.

4.3 Dispersion measurement and tuning

The intracavity dispersion determines the dispersion tuning of the cavity, and also affects the pulse width [139]. This section will describe some of the techniques used for measuring the intracavity dispersion.

4.3.1 Dispersion tuning of laser cavity

As the length of the cavity is altered, the operating wavelength will shift, as described in Section 3.5. The magnitude of the shift is proportional to the length change and inversely proportional to the intracavity dispersion. The intracavity dispersion can be determined by plotting the wavelength against the round-trip delay change. The

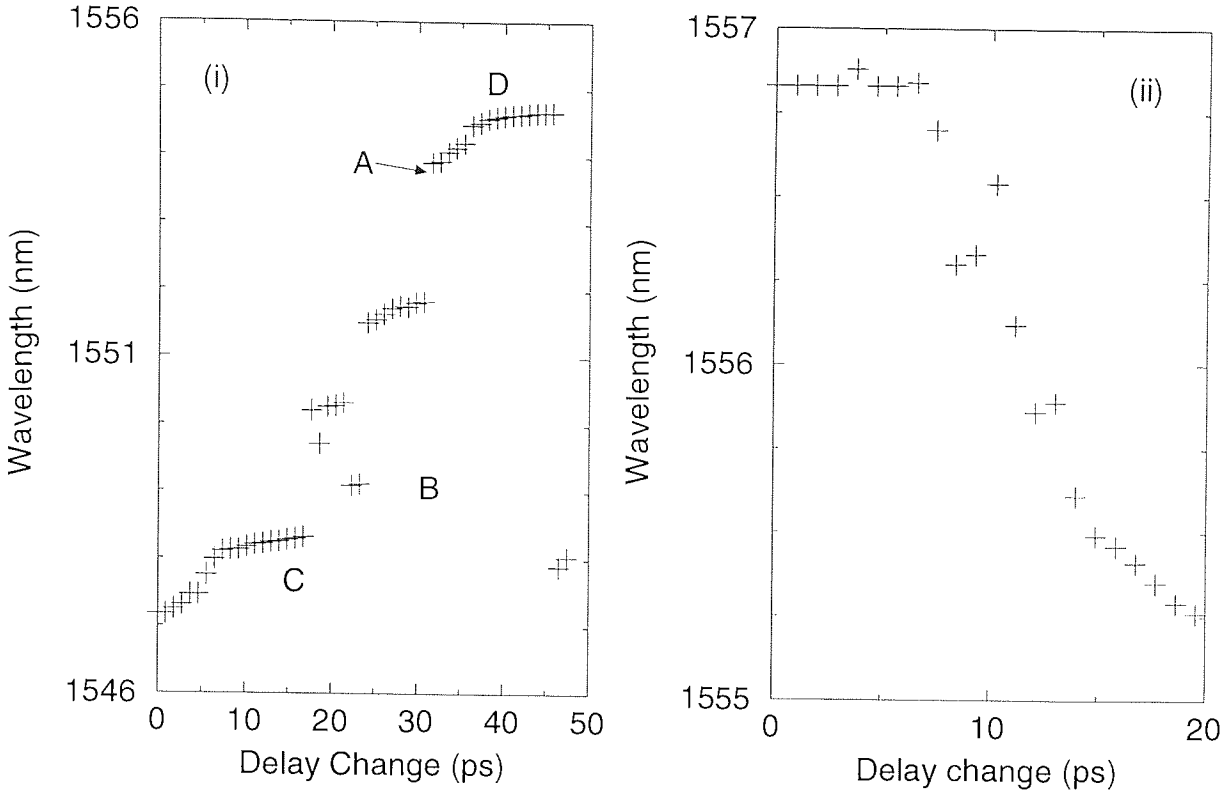

Figure 4.8: Plot of output wavelength against delay change in cavity for two gratings. (i) is L138, (ii) is 115. Points marked are those for which pulse results are given above.

delay change is determined from the fibre stretcher setting and the calibration factor determined in Section 4.1.2 above.

An example of this technique is shown in Figure 4.8. It is clear from this figure that the gratings do not have a continuous, linear relationship between wavelength and delay: this is a function of their manufacture, and disrupts the smooth tuning of the laser. Areas where the slope is steepest correspond to low-dispersion areas, and consequently where the shortest pulses might be expected. As discussed in Section 2.7, the gratings deviate from an ideal profile: there is a periodic reflection and dispersion variation across the grating, visible on the reflectivity and dispersion plots in Figure 4.9.

4.3.2 Soliton sideband measurements

In addition to using the simple dispersion tuning approach described above, it is possible to determine the local dispersion (*i.e.* the dispersion in the wavelength region of the pulse) more effectively from the soliton sidebands present on some

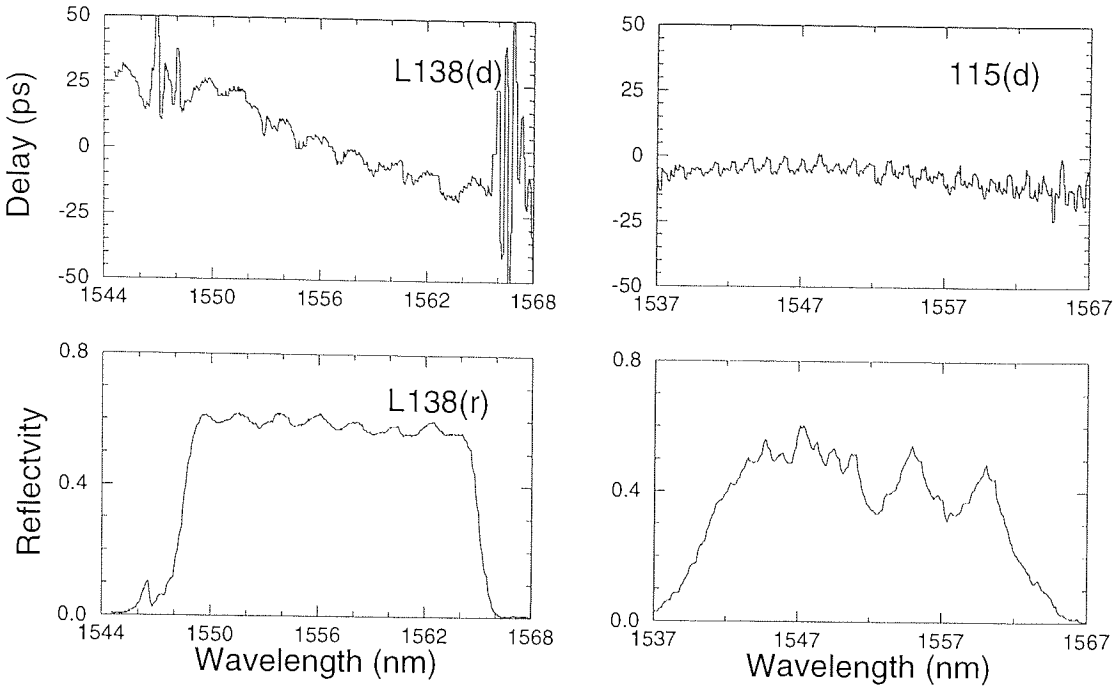

Figure 4.9: Dispersion and Reflectivity plots of two gratings (L138 and 115), measured using a network analyser

pulses. Most of the cases which produced sufficient numbers of sidebands for the application of the technique described in Section 3.6.2 were obtained with a low dispersion grating (estimated average dispersion of 1.9ps/nm). This grating (115) is shown in Figure 4.9(iii) and (iv).

Using the output pulses from the system, however, the local dispersion (*i.e.* at a particular wavelength) of the cavity can be determined from the position of the sidebands on the soliton output pulses of the cavity. A sample autocorrelation (i) and spectrum (ii) are shown in Figure 4.10. The spectral width is 1.36nm and the pulse width is 2.2ps; the time-bandwidth product is 0.37, close to the bandwidth-limit for a sech^2 pulse. This result was obtained using grating 115.

Figure 4.11, by contrast, shows the output from the same grating at a different operating wavelength. The pulse characteristics are similar, however: the spectral width is 1.15nm and the pulse width is 2.3ps. This yields a time-bandwidth product of 0.33, suggesting that the pulse is close to the bandwidth limit for a sech^2 pulse.

Plotting the sideband order against frequency offset, as described in Section 3.6.2 results in the points on Figure 4.12. The solid line is a least-squares fit cubic to

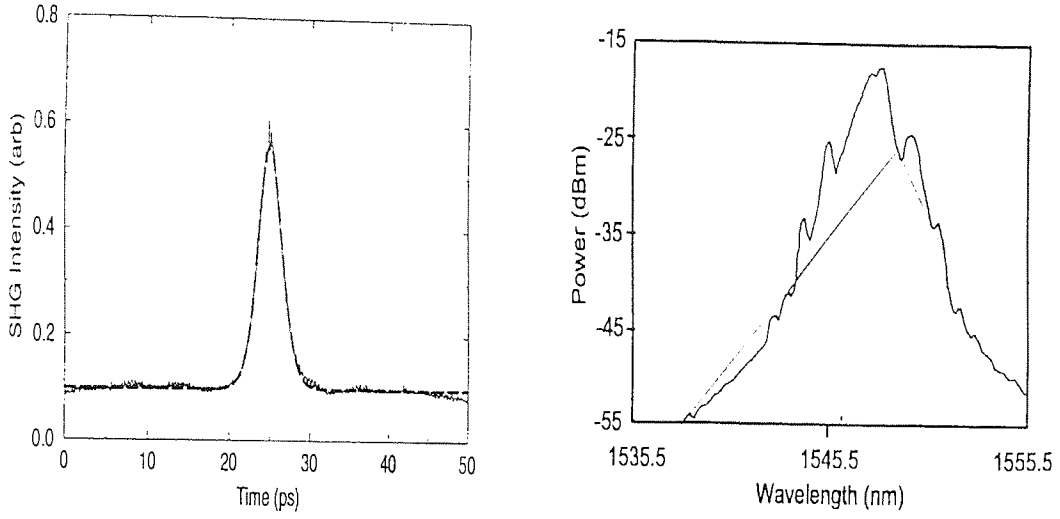

Figure 4.10: Autocorrelation (i) and spectrum (ii) of pulse train, showing clear evidence of soliton sidebands. The dashed line on the autocorrelation is a best-fit sech^2. $\tau(FWHM)$=2.2ps

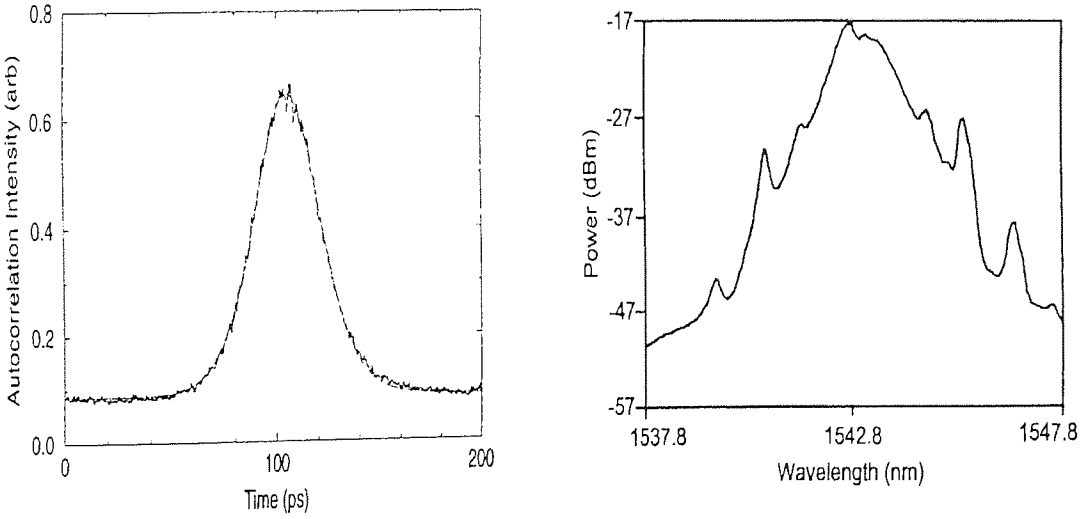

Figure 4.11: Autocorrelation (i) and spectrum (ii) of pulse train, showing soliton sidebands. Solid line on (i) is best-fit to $\mathrm{sech}^2, \tau(FWHM)= 2.3ps$

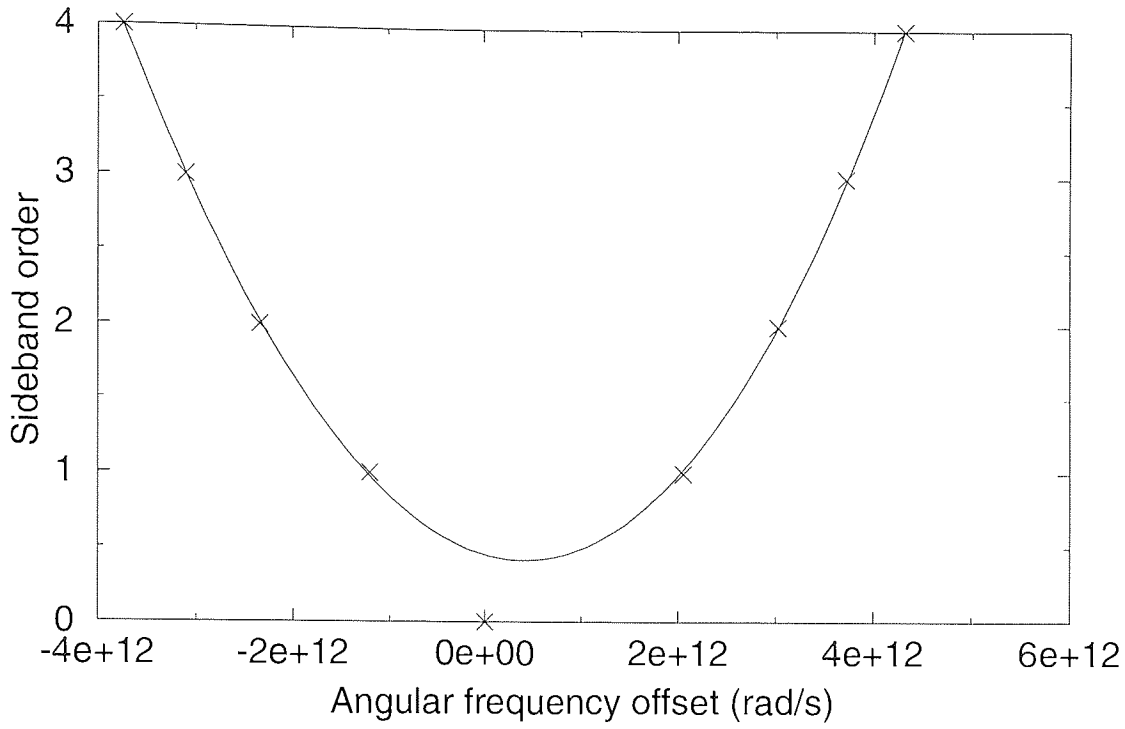

Figure 4.12: Soliton order plotted against angular frequency offset for the output of Figure 4.10. Solid line is a least-squares cubic fit.

the points, and gives dispersion values of $\beta_2 L = -2.978 \times 10^{-24}\text{ps}^2$ and $\beta_3 L = -1.114 \times 10^{-37}\text{ps}^3$. The value of β_2 corresponds to $D = 2.34\text{ps/nm}$; β_3 is sufficiently small in this case to be discounted.

Furthermore, the pulse width equation yields a width (FWHM) of 1.59ps. This compares against a figure of 2.2ps determined from the autocorrelation. These figures are in reasonable agreement, and comparison between the dispersion determined from the sideband positions and that obtained from the simple dispersion tuning work shows a similar agreement.

Performing the same process on the results in Figure 4.11 (plotted in Figure 4.13) yields $\beta_2 L = 2.89\text{ps/nm}$ and $\tau = 1.57\text{ps}$. This result is similar to that obtained above; the two pulse widths measured using sidebands differ from those measured by autocorrelation by the same factor. One possible explanation for this is that the sideband positions reflect the average pulse width, which may be narrower than the output pulses at some points in the cavity.

Notably, both sets of pulses appear to exhibit similar dispersion values and pulse

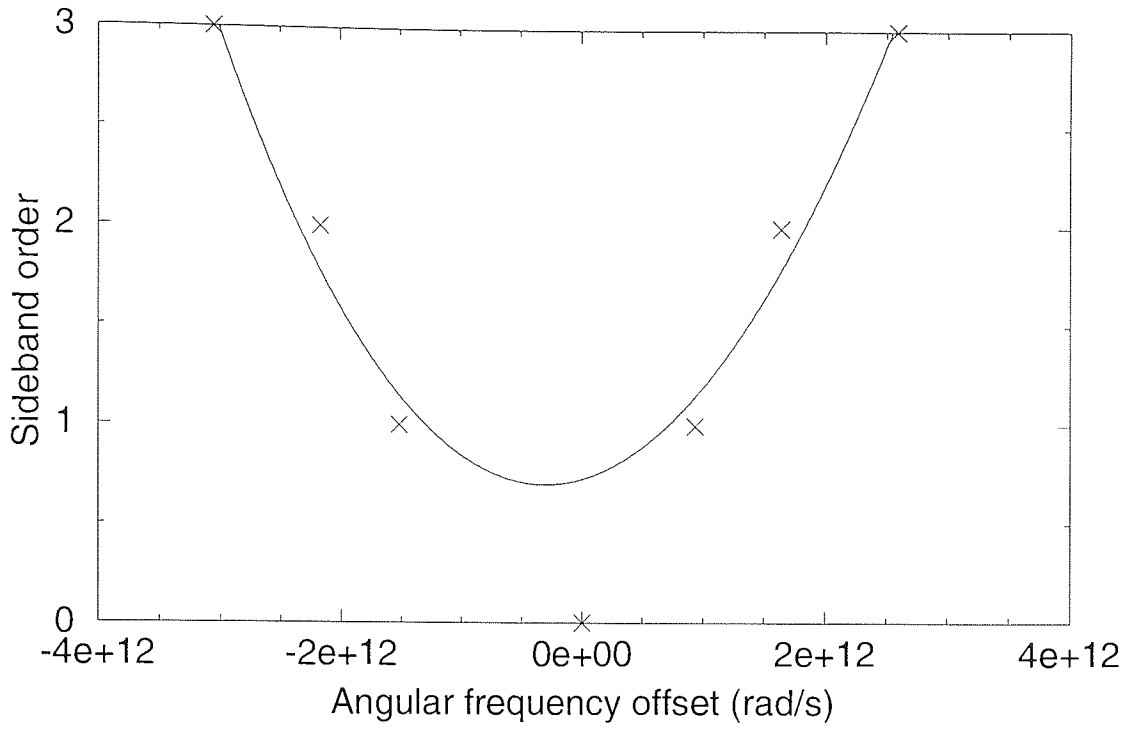

Figure 4.13: Soliton order plotted against angular frequency offset for the output of Figure 4.11. Solid line is a least-squares cubic fit.

widths. As a caution, however, it should be noted that the pulse widths for all the cases obtained were similar, so these cases may all yield similar dispersion values because the laser would only operate for those values of dispersion. However, there still appears to be little effect on the sideband positions of the different local dispersion environments.

4.4 Discussion

It is clear that the different gratings affected the performance of the overall system both in terms of the operating wavelength, and more importantly, by altering the pulse properties. It is also clear that the fabrication of the gratings has an impact upon the system performance. The poor results obtained with grating L160 in the anomalous dispersion regime (compared with the good results obtained in the normal dispersion regime) are further evidence that features of the grating design have an effect.

The situation is complicated somewhat by the use of "non-ideal" gratings: if the gratings had exact linear profiles (as in Figure 2.11, and were free of local aberrations, then it would be more straightforward to compare the performance of gratings. The gratings available, however, while possessing generally flat reflection profiles, had phase profiles which did not monotonically decrease or increase with wavelength, and it is obvious that useful operation of the laser may be due to local, unintentional features in the grating, rather than the deliberate design of the dispersion.

However, these disadvantages of the particular gratings used could be overcome through improvements in grating design, and even with these gratings several points are worth noting.

Firstly, the gratings serve effectively as the wavelength-determining elements in the system. They can be designed to have a flat reflection response which allows approximate wavelength selection without the bandwidth-limiting features of filters. Dispersion tuning ensures a continuous output train even when there are small variations in the cavity length: resistance to external acoustic noise was observed, and the settings of the intracavity polarisation controllers were not critical.

Secondly, the grating clearly influences intracavity dispersion as witnessed from the dispersion-tuning profiles. A general relationship between higher dispersion and longer pulses is suggested though there was insufficient data to determine a form for this relationship.

Finally, dispersion tuning is an effect with many potential applications; it is clear that a variation in the cavity length causes a change in wavelength —this is a simple and effective way to produce a mode-locked laser tunable over a narrow band. Given the good short-term stability of the laser system, this length change could be driven by a feedback system to stabilise the output wavelength. (In normal operation, cavity length adjustments were required every 30–40 minutes to compensate for thermal drift).

Other applications for such a system are discussed in Section 6.6. However, the operation of the current system could clearly be improved. An obvious case would be

the grating manufacturing. Current techniques can produce grating more precisely to a specification and with a profile closer to the ideal than those used for this work.

More significantly, the system could be modified to support higher repetition rates —this is addressed in Chapter 6. The other application which resulted in development was the need for a dual-wavelength laser system to support switching experiments. A modification of the system of this chapter formed the basis for that system, which is described in the next chapter.

Chapter 5

Dual Wavelength Laser System

The increasing use of the dual-wavelength loop mirror for optical switching applications has led to a requirement for appropriate sources of clock pulses. An ideal source for this application would produce pulses at two substantially different wavelengths with no inter-pulse-stream jitter. This chapter will present an ultra-low jitter dual-wavelength fibre laser system, which is capable, in jitter terms, of working with bit rates of up to 130Gb/s. The wavelengths in this case are 20nm apart.

Previous work on multiwavelength modelocked erbium fibre lasers has used both active [140, 141] and passive [142] modelocking. However, in single-amplifier lasers, mode competition in the homogeneously-broadened gain medium requires the use of closely-spaced wavelengths or gain-flattening techniques such as Bragg gratings with tailored reflectivities as end mirrors to provide identical gain at different wavelengths [59]. Even these solutions may not be stable; the balance between the two wavelengths may be very susceptible to external factors, and frequently the amplifier must be cooled in liquid nitrogen to suppress homogeneous broadening[143, 144]. It is also possible to spectrally filter the output of a broadband mode-locked laser, but this can only produce pulses with closely-spaced wavelengths [145]. This process has been used to produce as many as 200 wavelengths [146].

One of the obvious solutions to this problem is to use two laser cavities, which will eliminate gain competition problems but will be less likely to be synchronised. Driving two cavities from the same source involves additional complexity with the

use of two modulators. A compromise approach, where the gain and wavelength selection are separate and the switching is shared, offers a good solution.

The design of this system relies on the availability of the dual-wavelength NOLM and CFBG reflectors on the cavity ends. While it would be possible to use a pair of gratings for each cavity and a single acousto-optic modulator, the use of a NOLM is more effective.

This chapter will describe a dual-wavelength laser system demonstrating ultra-low jitter performance, which is based upon the laser of Chapter 4. The system consists of two linear laser cavities, each using an erbium-doped fibre amplifier and both mode-locked using the same NOLM. The nature of the NOLM as a broadband switchable reflector is ideal for this configuration.

5.1 Design of dual-wavelength laser system

The configuration of the cavity is shown in Figure 5.1. The two cavities are essentially identical in configuration and share the single loop mirror. One cavity has a wavelength range centered around 1540nm (λ_1), and the other around 1557nm (λ_2); the cavities will be referred to by these wavelengths.

The loop mirror is the same two-wavelength design used in Chapter 4. Because the NOLM is a broadband device, the switching characteristics of the two cavities will be similar. Because the loop mirror reflects when switched, it is possible for two signals to be switched simultaneously without the need for wavelength-selective couplers. (These would be required for a system using a solid-state switch; other solutions involving a solid-state switch require additional gratings and are more complex). The ability to use both ports of the NOLM is a key to the simple design of this system.

Obviously, the switching performance may not be identical for both wavelengths, but this is unimportant; in a laser system, only small amplitude modulations are necessary for modelocking. Additionally, the high gain produced by erbium-fibre amplifiers will compensate for considerable intracavity loss. It is, however, important

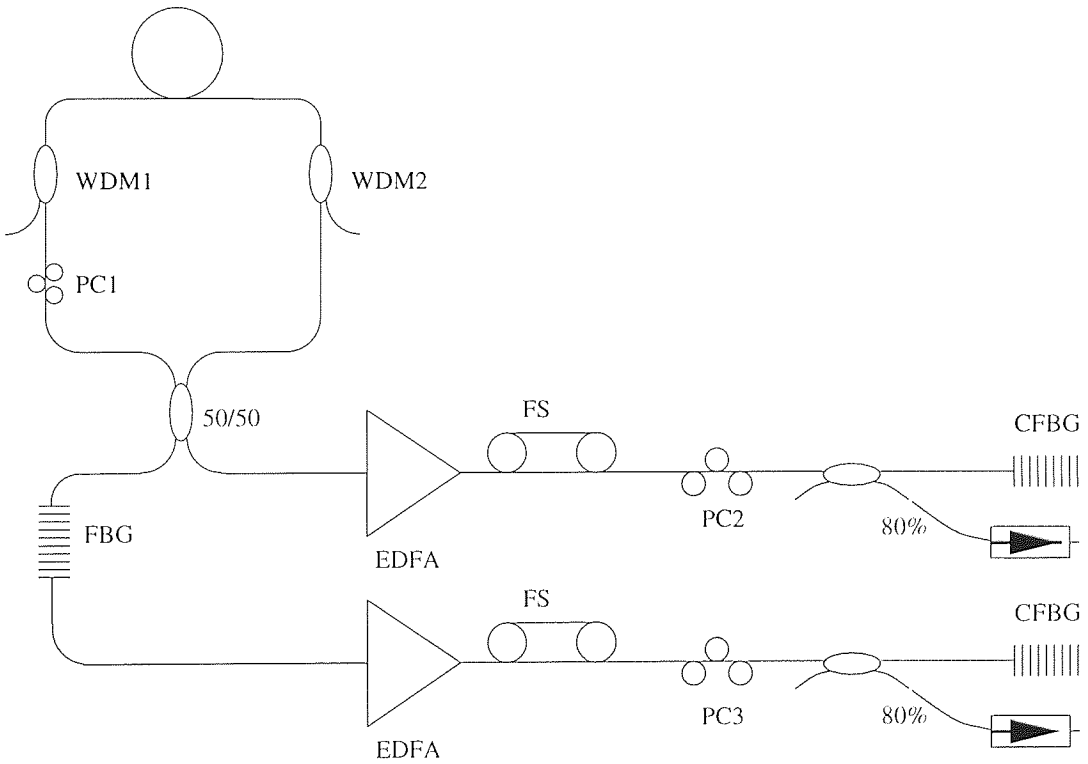

Figure 5.1: Dual-wavelength laser system setup. CFBG: chirped fibre Bragg grating; EDFA: erbium-doped fibre amplifier; FS: fibre stretcher; PC: polarisation controller; WSC: wavelength-selective coupler. FBG: linear fibre Bragg grating with short-wavelength loss

to operate the loop mirror near its maximum transmission point, to avoid amplitude noise from the switching pulses being transferred to the intracavity signal.

Chirped fibre Bragg gratings are used as narrowband mirrors to select the operating wavelengths; as lumped dispersive elements which dominate the cavity dispersion, they also determine the temporal properties of the pulses. This is the same principle as that described in Chapter 4. Furthermore, in conjunction with the shared NOLM described above they are essential: each cavity must exhibit high loss to any pulses from the other cavity. Using Bragg gratings allows the laser operation of each cavity to be confined to a narrow band.

However, any signal through the NOLM from the other cavity will make a single pass through the amplifier. As, in this case, the two amplifiers are similar, the signal from one cavity could deplete the gain in the other. To prevent this, a filter is required. A standard Bragg grating is inappropriate as the signal should not be reflected back into the cavity as this would interfere with normal operation. However, for this application, a Bragg grating exhibiting short-wavelength loss (see Section 2.7.5) is appropriate as it acts a blocking filter. (A standard bandpass filter is inappropriate; unless it has a broad, flat profile, it will both frustrate dispersion tuning and bandwidth-limit the pulses in the cavity.)

This precaution was required because of the gain characteristics of the fibre amplifiers. Although they were both 980nm pumped, one was a diode-pumped, high-power amplifier module and the other was pumped by a Ti:sapphire laser. The low-power cavity required the insertion of a grating as described above to ensure that leakage of the high-power signal did not adversely affect the gain of the amplifier. The spontaneous emission profiles of the fibre amplifiers are shown in Figure 5.2. These give some indication that the 1557nm (λ_2) amplifier will provide gain for a 1540nm (λ_1) signal, but that there is little gain at λ_2 in the (λ_1) amplifier. This difference dictated which amplifier would be used for the λ_1 cavity and which for the λ_2 cavity.

The fibre stretchers were included to provide fine-tuning of the cavity lengths. Each consisted of around 10 metres of standard fibre wrapped around two drums

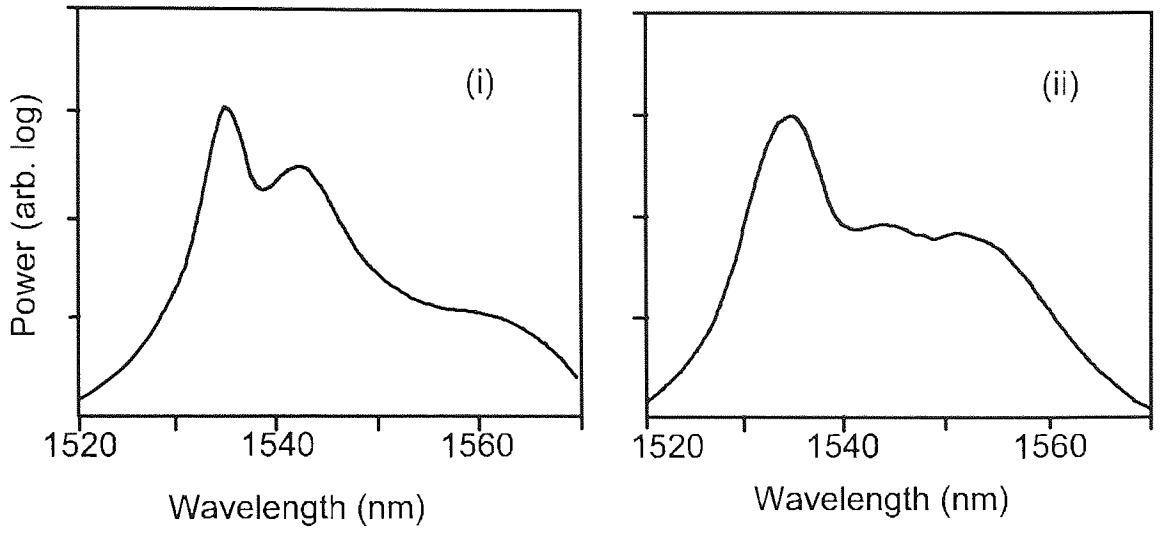

Figure 5.2: Spontaneous emission spectra of erbium-doped fibre amplifiers (i) 1540nm amplifier (ii) 1557nm amplifier.

about 20cm apart, one of which could be moved. The calibration of the displacement controls on these is discussed in Section 4.1.2. For optimum mode-locking the cavity length was adjusted (initially by adding or removing fibre, then using the fibre stretcher) so that the round-trip time was a multiple of the Nd^{3+}:YAG period of $\approx$ 13ns (The exact Nd^{3+}:YAG frequency was measured to be 75.89685MHz: it remained stable over the duration of this work.) As a later development, motorised fibre stretchers were used, which allowed remote control of the laser system. These would also have allowed the use of an electronic feedback system, which is discussed below.

The fibre Bragg grating end mirrors were 4mm long, with a 4nm bandwidth and a linear chirp. One grating had a centre wavelength of $\approx$ 1557nm and the other a centre wavelength of $\approx$ 1540nm The characteristics of the gratings are described further in Section 5.2.1.

The output couplers were used with 70% (1540nm) and 80% (1557nm) of the power coupled out, in order to maximise the output power. After both passes through the coupler, a total of 91% (1540nm) and 96% (1557nm) is coupled out, so that the effective reflectivity of the coupler end of the cavity is only a few percent (The gratings typically had reflectivities of almost 100%). The system still operated,

however, because of the high gain of the amplifiers.

By choosing the orientation of the gratings (*i.e.* short or long wavelength end towards the cavity) either soliton or nonsoliton (Gaussian) pulses could be produced. This is described in more detail below.

The two cavities were of similar length: the "round-trip" length of the long-wavelength (1557nm) cavity was $\approx$ 142m (This is calculated from the noise frequency of 1.449MHz. This frequency also indicates that this cavity when mode-locked was operating at the 52nd harmonic.).

5.2 Characteristics of system components

In this section, some of the data obtained concerning the operation of the system will be presented.

5.2.1 Gratings

The long-wavelength grating was also used in the single cavity work of Chapter 4 and was 4mm long, with a 4nm bandwidth centred on 1557nm. The other grating was of the same length, with a 4nm bandwidth centred at 1540nm. The reflection and phase profiles of the two gratings are shown in Figure 5.3 for comparison.

The gratings had average dispersions of +13.4ps/nm (1540nm) and +9.7ps/nm (1557nm). Although there is a modulation on the delay curve, resulting in local dispersion variations across the grating, the appearance of the soliton sidebands (see Section 5.3.1) is consistent with the average grating dispersion. However, irregularities in the grating profile may inhibit continuous dispersion tuning and lead to poorer environmental stability. The irregularities are consequences of a square reflection profile, and would not be present on an apodised grating.

The features on the delay plots which extend beyond the reflectivity bands of the gratings are edge effects [147] which are not relevant to the determination of the dispersion or the operation of the laser.

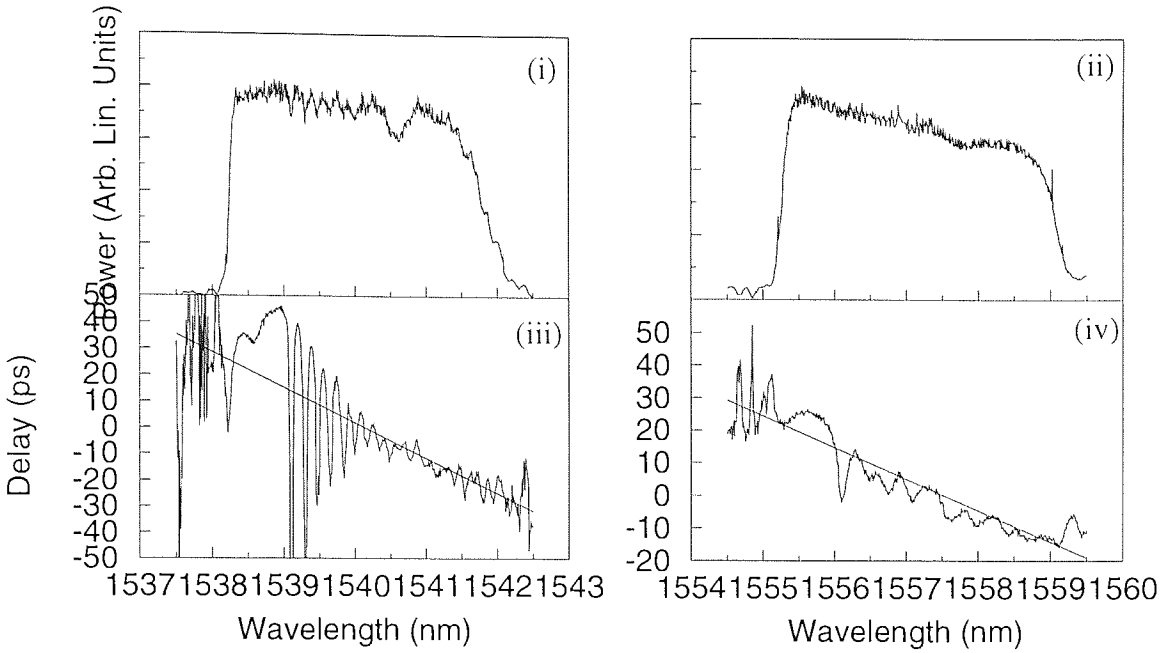

Figure 5.3: Reflection profiles of (i) 1540nm grating, (ii) 1557nm grating. Phase (delay) profiles of (iii) 1540nm grating, (iv) 1557nm grating.

5.2.2 Intrinsic cavity dispersion

Using the simple dispersion tuning approach adopted in Section 3.5 the dispersion of the complete cavity can be measured. For this to be a useful measure of the grating dispersion, the dispersion of the remainder of the cavity must be known. In order to obtain this, the system in Figure 5.4 was used.

A filter was attached to the original output port in place of the isolator, and a mirror was then butted to the other arm of the filter. A tight bend was added to the coupler arm attached to the grating. This ensured that the system lased off the the mirror and not the grating, but avoided disturbing the main part of the cavity which was aligned for modelocking.

The modified cavity was then operated in a continuous wave mode, with an operating wavelength determined by the intracavity filter. A high harmonic of the cavity beat noise signal was then observed. As the filter setting, and therefore the operating wavelength, was changed, the round-trip time of the cavity changed, and this change was clearly visible on a high harmonic of the cavity fundamental

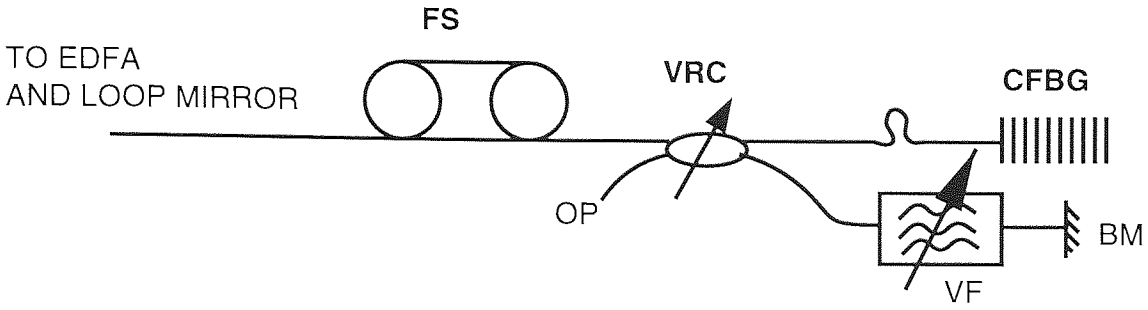

Figure 5.4: Setup used to measure dispersion of laser cavity; VF: tunable filter, BM: butted mirror, OP: output. The bend before the grating introduces a large loss into that arm of the cavity

frequency (The cavity fundamental frequency was approximately 1.5MHz).

Using the long-wavelength cavity, the 6903rd (± 1) harmonic was chosen, was at $\nu_N = 10.0012709$GHz. Values of $\delta\nu_N$ for different wavelengths could be measured. Dividing these by the harmonic number gives $\delta\nu$ which can be converted into a $\delta\tau$ using the expression $\delta\tau = \frac{1}{\nu_0^2}\delta\nu$ These values are plotted alongside $\delta\lambda(\lambda_0 = 1538.8$nm) in Figure 5.5. A straight line fit to this data gives a dispersion value of 2.13ps/nm. This value is consistent with $\approx$ 140m of fibre with a standard dispersion value of 16ps/nm/km.

The dispersion of the short-wavelength cavity was measured using a modification of the standard dispersion-tuning approach. A similar setup to that described above was used, with the butted mirror replaced with another grating. The dispersion tuning of the cavity was measured with the grating in both orientations: as the grating dispersion changes sign when it is reversed, the average of the two "total" dispersions obtained is a measure of the intrinsic dispersion of the cavity. The dispersion tuning plots for the two orientations are shown in Figure 5.6(i)(Normal dispersion orientation) and Figure 5.6(ii)(Anomalous dispersion orientation). The tuning range of the normal dispersion plot is limited because mode-competition from a spurious peak at 1532nm could not be suppressed.

Fitting straight lines to these plots gives dispersion figures of 2.6ps/nm for the normal dispersion regime and -3.11ps/nm for the anomalous dispersion regime. The average of these (which is the intrinsic dispersion) is ≈ -0.25ps/nm. This is clearly

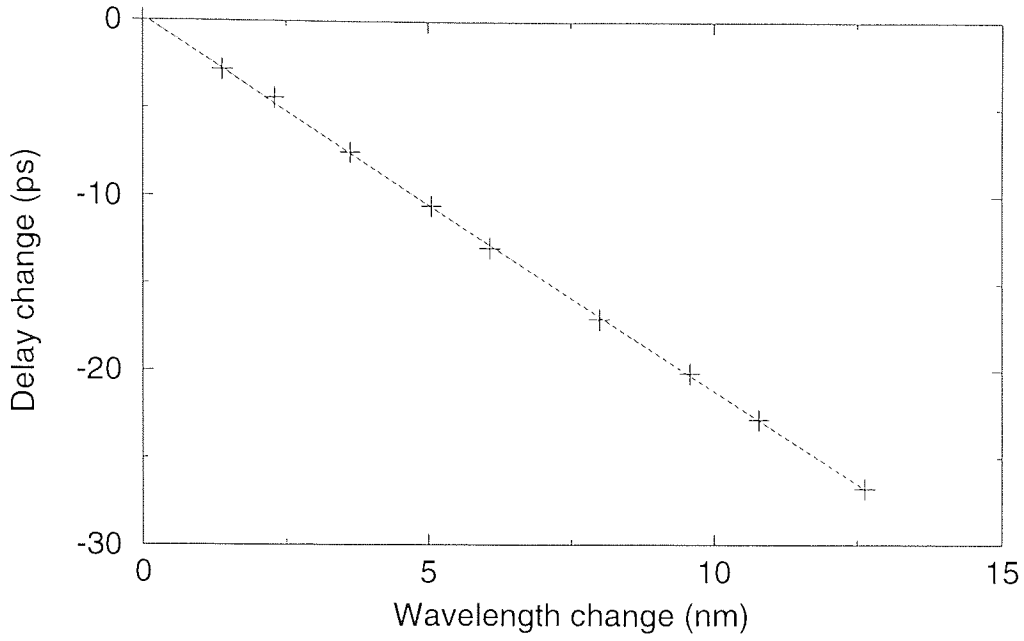

Figure 5.5: Delay vs. wavelength plot for short-wavelength cavity

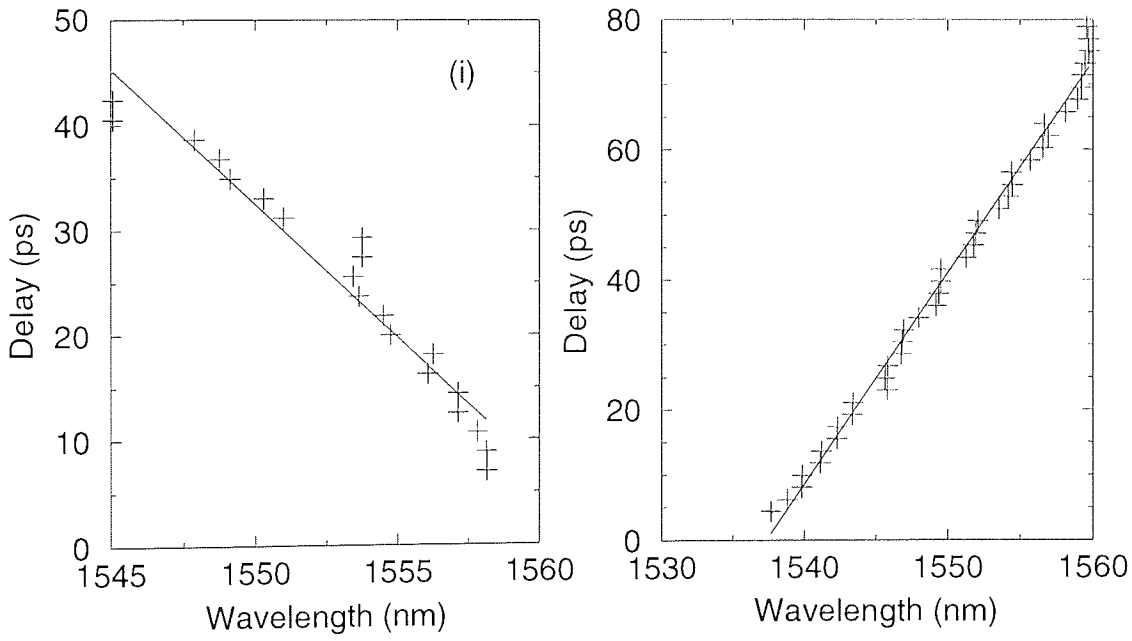

Figure 5.6: Dispersion tuning (wavelength change vs. delay change) of cavity: (i) grating in normal dispersion orientation; (ii) grating in anomalous dispersion orientation

much lower than the other cavity. As the cavities are of approximately the same physical length suggests that there is either a difference in the average fibre dispersion or that there is a significant amount of normal dispersion in the cavity to balance the natural anomalous dispersion of the fibre. As the majority of fibre used in construction of the cavity (on the fibre stretchers, polarisation controllers etc.) was known to be the same type as the other cavity, an element of the cavity must be strongly normally dispersive. In fact, this normal dispersion is introduced by the 13m of erbium-doped fibre.

This fibre is optimised for 980nm pumping, requiring it to be single-mode at 980nm (the pump energy must be closely confined to the doped fibre core for optimum transfer of energy). This significantly affects the dispersion at 1550nm. The fibre amplifier module in the other cavity uses a short length of highly-doped fibre and consequently has less effect on the cavity dispersion.

The value of the whole-cavity dispersion can now be compared with the separate sums of the grating and intrinsic cavity dispersion. For the short-wavelength cavity, the grating dispersion of -13.4ps/nm and the -0.25ps/nm of the cavity give a total dispersion of ≈ -13.6ps/nm. For the long-wavelength cavity, the total dispersion is $-2.13 - 9.7 \simeq -11.8$ps/nm. These values can be compared with the values obtained from dispersion tuning measurements.

A further measurement of dispersion is possible using soliton sidebands: this is discussed later.

5.2.3 NOLM Switching

As in Chapter 4 the NOLM control pulses were provided by a 76MHz pulse train from a Nd^{3+}:YAG laser, and the walk-off in the loop mirror resulted in a switching window of 100ps (FWHM) from the 90ps pulses output by the Nd^{3+}:YAG laser. The broadband nature of the NOLM resulted in approximately equal modulation depths of $\approx 80\%$ for both cavities. The average in-fibre power of the control pulses was ≈ 100mW for maximum modulation, although this was not critical and powers

as low as $\approx$ 60mW could be used, but with increased amplitude jitter. This was due to the increased slope of the loop mirror response. Powers greater than $\approx$ 110mW led to output instability. This may be due to Raman generation, or distortion of the switching window as described in the previous chapter.

The transfer characteristic of the NOLM when the control pulses switch between zero and maximum reflectivity ensures that amplitude variations on the control signal do not result in significant changes in the reflectivity of the loop mirror.

5.3 Pulse output properties

This section will show some of the results obtained from the system, and discuss their significance and possible lines of improvement.

5.3.1 Pulse properties

Each laser cavity produced a full 76MHz pulse train. The temporal properties of the pulses were observed using a background-free autocorrelator, while an optical spectrum analyser was used to observe the pulse spectra.

Figure 5.7(i) shows the autocorrelation and (ii) the spectrum (on a logarithmic scale) of a typical output pulse from the 1557nm laser cavity. The sidebands present on the spectrum are suggestive of soliton pulses [89, 87] in a periodically amplified system (see Section 3.6.2. This is further supported by the good fit of the autocorrelation to an autocorrelated sech^2 profile. The FWHM pulse width is 8ps, and the FWHM spectral width is 0.34nm, giving a time-bandwidth product of 0.34, close to the transform limit of 0.315.

By reversing the grating on the 1557nm cavity, to give a dispersion of -8.2ps/nm, Gaussian pulses were produced, with an autocorrelation (i) and spectrum (ii) (Figure 5.8) indicating a good fit to a Gaussian pulse of $\Delta\tau = 13.5$ps and $\Delta\nu = 0.29$nm. This gives a time-bandwidth product of 0.5, close to the transform limit of 0.44.

This result suggests that the laser could produce Gaussian pulses from one output and sech^2 pulses from the other simultaneously.

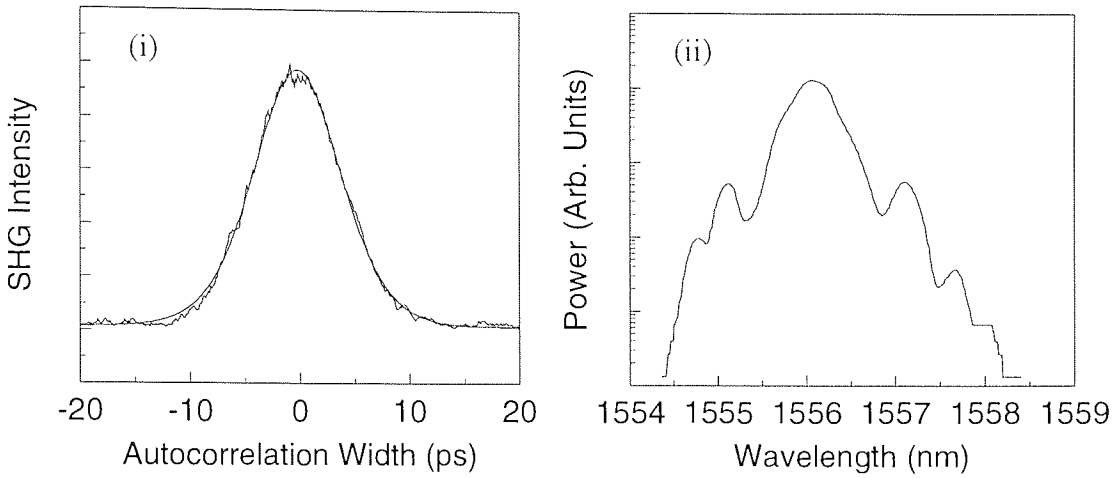

Figure 5.7: Autocorrelation trace of output from dual-wavelength laser system

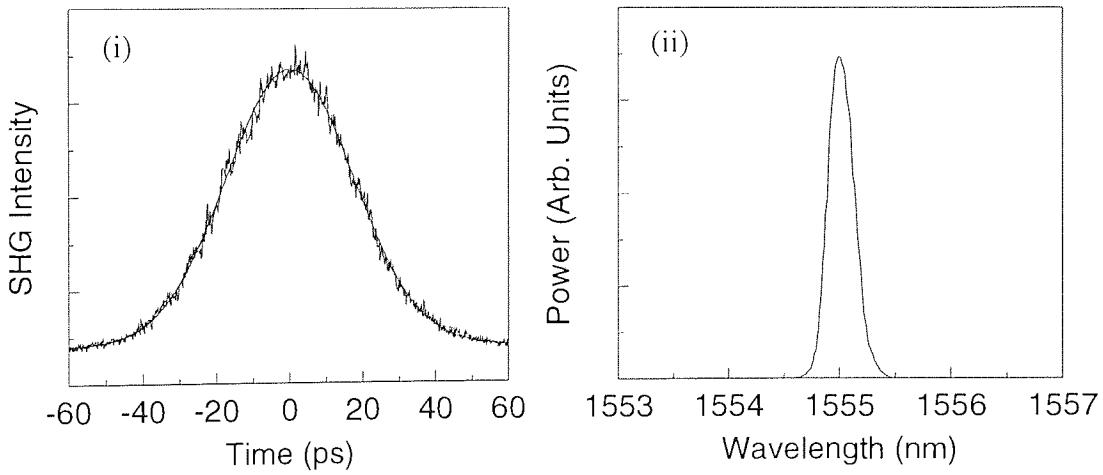

Figure 5.8: Autocorrelation trace of output from dual-wavelength laser system (Gaussian)

5.3.2 Sideband dispersion measurement

As a final method of examining the intracavity dispersion, the positions of the spectral sidebands (see Section 3.6.2) were measured. If there are a sufficient number of visible sidebands, it is possible to determine both second-order (β_2) and third-order (β_3) dispersion, as well as the pulse width, from this information (only second-order dispersion was measured in this case, as $\beta_2 \gg \beta_3$). Using this technique, dispersions of +12.8ps/nm and +17.7ps/nm were measured for the two cavities. These results may differ from the average dispersion values measured above, because the soliton will obviously experience only the local dispersion at a given wavelength. However, it is interesting that the soliton and its sidebands appear to experience a consistent dispersion: there is no skewing of the sidebands (see Figure 5.7) as might be expected from large local variations in dispersion.

5.3.3 Jitter performance

The characterisation of a laser source for both transmission and switching experiments requires that the timing jitter be characterised. In order to measure the jitter of the system, a 50GHz sampling oscilloscope was triggered on the 1557nm pulse train and the 1540nm pulse train was viewed in an infinite persistence display mode. While this yielded a standard deviation jitter of 800 ± 50fs, viewing the 1540nm signal triggered on itself revealed a jitter value of 700 ± 50fs. While it is possible to determine a jitter component contributed by the laser system, the measured value is too close to the resolution limit of the instrument for the value to be accurate; another technique is necessary for accurate measurement.

The examination of a high harmonic of the pulse train's microwave spectrum can provide information on timing jitter [138, 148]; each harmonic contains several noise components caused by pulse amplitude fluctuations, pulse width fluctuations and timing jitter [149]. Because of the soliton nature of the pulses, pulse width fluctuations could be neglected, and the amplitude noise could be minimised by adjusting the intracavity polarisation controller. The timing jitter component could

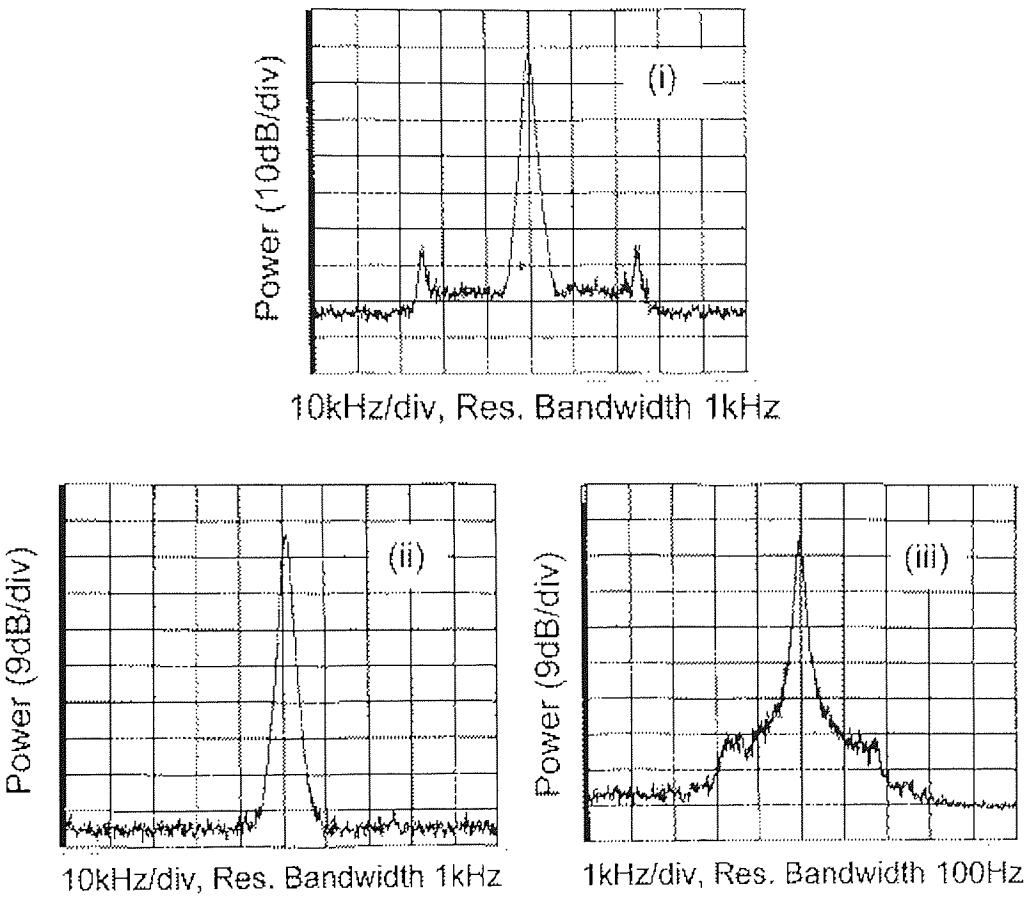

Figure 5.9: Short-wavelength cavity jitter measurement: spectrum of 66th harmonic. (Centre frequency of all plots is approximately 5GHz). (i) spectrum viewed with 100kHz span. (ii) 100kHz span with pulse amplitude fluctuations minimised. (iii) 10kHz span with pulse amplitude fluctuations minimised.

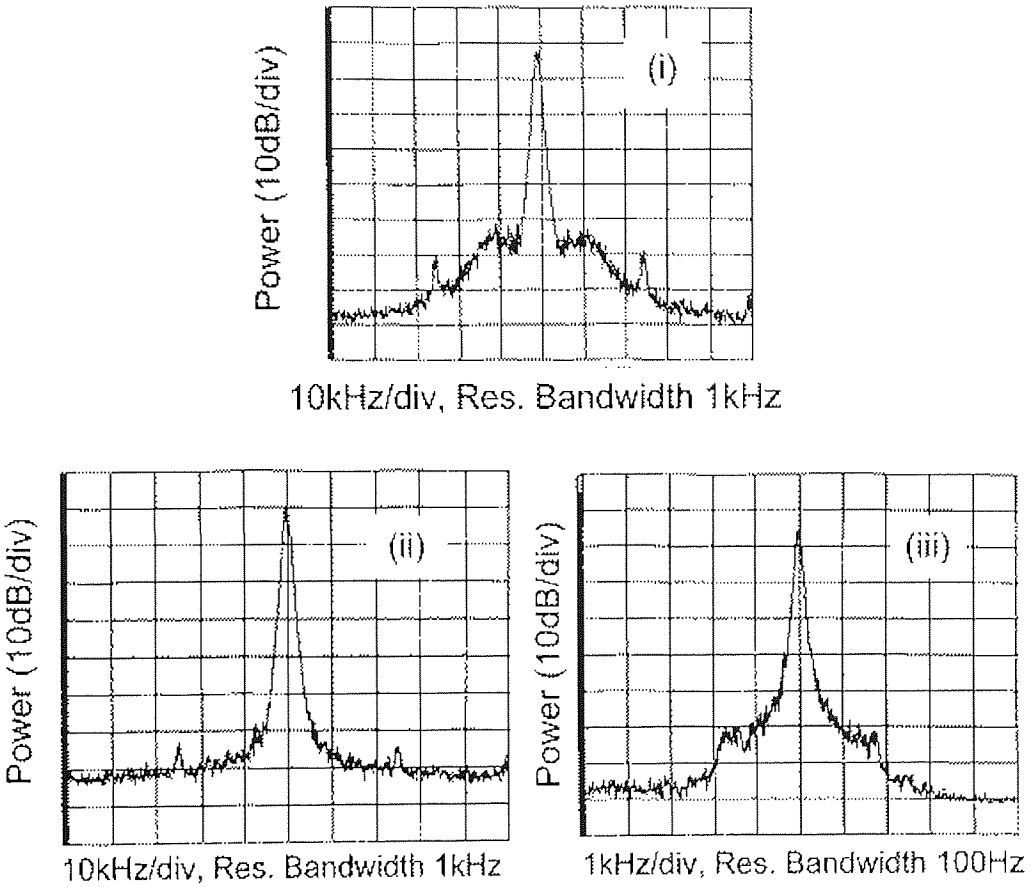

Figure 5.10: Long-wavelength cavity jitter measurement: spectrum of 66th harmonic. (Centre frequency of all plots is approximately 5GHz). (i) spectrum viewed with 100kHz span. (ii) 100kHz span with pulse amplitude fluctuations minimised. (iii) 10kHz span with pulse amplitude fluctuations minimised.

therefore be isolated, and the jitter levels were found to be 390fs (1540nm) and 480fs(1557nm). Combining these gives a figure of 620fs jitter between the two pulse trains.

However, measurement of the jitter (again using microwave spectra) of the Nd^{3+}:YAG laser used to provide the modelocking pulses gave a standard deviation jitter of 430fs. This suggests that the jitter performance of the system is dominated by jitter in the Nd^{3+}:YAG modelocking source.

5.4 Discussion

The laser system presented in this chapter is clearly capable of producing soliton (or Gaussian) pulses with a low level of jitter. This level of jitter compares favourably with other types of source, such as actively modelocked ring lasers with jitter levels of 2.8ps [150] and 3ps [151], as well as results reported for a gain-switched DFB laser of around 500fs [152].

For optical switching applications in which the NOLM is used as an all-optical demultiplexing element, a jitter level of less than $W/12$ (W is the width of the switching window) is required for a BER of 10^{-9} [152]. The maximum bitrate usable with this source can therefore be determined: The jitter levels dictate a switching window of 7.2ps or greater, implying that this laser could successfully demultiplex from a 130Gb/s data rate with 10^{-9} BER. The jitter is limited by the performance of the control pulse source, which is expected for a laser in which the spontaneous decay time ($\approx$10ms in this case) is much longer than the round trip delay ($\approx 0.7\mu$s). The use of a lower-jitter control pulse source would improve the jitter level, but for current practical applications, that appears to be unnecessary.

The dual-wavelength system of this chapter has been shown to be a flexible pulse-generation system. A few comments on future applications and development are worthwhile.

In this example, the wavelengths were only separated by 20nm. However, there is no reason why the two cavities should be at such close wavelengths. Within the

limits of the loop mirror, different amplifiers could be used for the two cavities. This might have applications for *e.g.* 1.3μm (using a Yb^3+-doped fibre laser) to 1.5μm conversion, where a loop mirror is used to switch data between the two wavelengths and a dual-wavelength laser system is used to generate synchronised clock pulses.

As mentioned in the previous chapter, this system should be amenable to higher bitrate operation; it is generally easier to create low-jitter soliton pulsetrains at higher, rather than lower, frequencies. As a switching device, the NOLM does not suffer the inherent bandwidth limitations of some other switching devices. The general problem is the switching power available to switch within the walkoff distance. This aspect will be addressed, in the single wavelength case, in the next chapter.

Chapter 6

High repetition rate system using a semiconductor laser amplifier

The systems so far considered have been low repetition-rate systems designed for use with demonstration systems. This chapter develops the system of Chapter 4 into a high repetition-rate system which operates with gigahertz repetition rates, and considers some of the applications to which this system (and others from this thesis) might be put.

In order to achieve this substantial increase in repetition rate, a high repetition-rate control pulse source must be used. The most obvious choice is a distributed-feedback (DFB) laser diode.

The system of Chapter 4 uses a comparatively short loop mirror, and consequently requires control pulses of $\approx$ 100mW average power to obtain clean switching. The use of a higher repetition-rate source precludes the use of such high control pulse powers and thus another method must be found to enhance the nonlinear phase shift in the loop mirror.

The first approach is to make the loop longer. As the nonlinear phase shift is proportional to the power and the length, operating the loop mirror with 10mW pulses will require a 400m loop mirror and with 1mW pulses a 4km loop mirror. While this option is feasible it has significant drawbacks: the longer length of fibre will be more susceptible to thermal and acoustic fluctuations and its dispersion will

dominate that of the cavity, unless dispersion-shifted fibre is used.

The second approach involves increasing the nonlinearity in the loop mirror. This can be achieved using high nonlinearity fibre[153] (this fibre has $n_2 = 4.0 \times 10^{-10}$, two orders of magnitude greater than standard silica fibre[154], but the high refractive index makes it difficult to integrate this fibre into a system based around standard fibre). However, the method adopted in this chapter is the insertion of a semiconductor laser amplifier (SLA) into the loop mirror.

6.1 Semiconductor laser amplifier

A semiconductor laser amplifier consists of a semiconductor junction whose electronic characteristics support high-efficiency stimulated emission [155]. Such a device, with reflective coatings on its end facets functions as a standing-wave laser, and while operating below threshold behaves as an etalon with gain [156]. It is also possible to use anti-reflection coatings on the device, and this will result in a broadband amplifier (lower reflectivity facets merely reduce the finesse of the etalon —it may be impossible to entirely flatten the gain spectrum). Such a device is often described as a travelling-wave SLA (TWSLA), or simply as a semiconductor optical amplifier (SOA). It has been used in its own right as the gain medium for laser systems [157].

The nonlinear interaction in an SLA is a nonlinear refraction process *i.e.* the refractive index is dependent on the incident power. In the SLA, this process is indirect: the refractive index is dependent on the carrier concentration which in turn is dependent on the incident power. As the carrier concentration is depleted (through stimulated emission) the nonlinear effect is also depleted. This effect (and similarly the gain of the amplifier) has a finite recovery time, which is largely dependent on the electron-hole recombination processes in the semiconductor. The low saturation power of the SLA (often of the order of a few milliwatts or less) results in this effect being significant even for comparatively low incident power levels.

The nonlinear interaction can be used for demultiplexing [158], straightforward

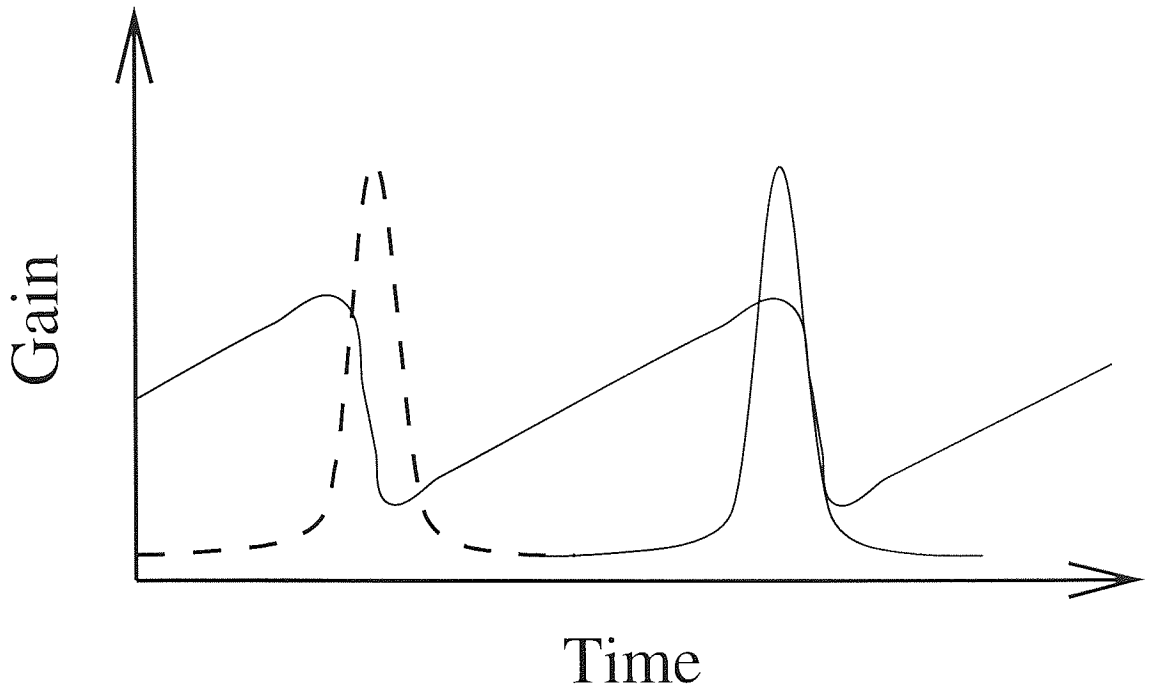

Figure 6.1: Gain modulation of semiconductor laser amplifier. The thin line indicates the change in SLA gain with time, in the presence of a switching pulse (dashed line). If the SLA is the modulator in a laser cavity, then the "signal" pulses in the cavity will occupy the position shown with the thick line with respect to the control pulse. Only one of each pulse is shown, for clarity.

wavelength conversion [159, 160, 161, 162], or as part of a loop mirror [163, 164]. In [165] Adams *et al* describe a figure-of-eight laser containing an SLA in the loop mirror section for 40GHz clock recovery. A passively-modelocked laser incorporating an SLA in a loop mirror is described in [166]. The Terahertz Optical Asynchronous Demultiplexer (TOAD) described in [16, 167] uses an SLA in a loop mirror, and has been used to perform all-optical routing functions[168]. [169] describes the use of a network of TOADs to route ATM packets at 100Gbit/s.

The gain depletion of the SLA, described above, offers another approach to using it as a modulator. The combination of the gain depletion and recovery time results in the modulation curve having a sawtooth shape. This is shown in Figure 6.1. This figure also illustrates the relative positions of the control and signal pulses when the SLA is being used in this way.

The use of a semiconductor laser amplifier in this way is described by Patrick [170]; the SLA is used directly in a ring laser between two wavelength-selective couplersas a simple gain modulator; control pulses passing though it saturate it, resulting in an increase in attenuation for the intracavity signal [171]. The recovery time of the SLA results in the lowest loss through the SLA occurring immediately before the arrival of the control pulse, as shown in Figure 6.1. This system was further extended to perform clock recovery [172]. This required a reverse-pumping arrangement [173, 174, 175] to suppress data-patterning effects caused by the gain variation. This involves injecting a higher power (tens of milliwatts) cw signal into the SLA. This technique can substantially improve recovery time (and therefore increase the operating bandwidth) but it leads to a shortened device lifetime.

The use of the SLA as a nonlinear element in a loop mirror is more complex than its use in a standalone configuration and is described in more detail in [176, 177, 178]. The positioning of the device is important; the placement of the amplifier is a significant factor in determining the switching characteristics of the loop mirror. For the system presented in this chapter, the SLA has to be close to the centre of the loop mirror, as the width of the switching window is proportional to the offset of the SLA from the centre of the loop.

If the SLA is positioned centrally, then both counterpropagating signals will pass through the SLA at the same time, and will acquire identical phase shifts. For the loop mirror to switch, it is necessary that the counterpropagating signals acquire different phase shifts; this can be accomplished by moving the SLA away from the centre of the loop. There will consequently be a time window Δt during which one signal will pass through the SLA before the control pulse, and one will pass through after. This switching window is described by the relationship:

$$\Delta t = \frac{n\Delta x}{2c} \tag{6.1}$$

Accurate positioning of the SLA is therefore important to optimise the width of the switching window.

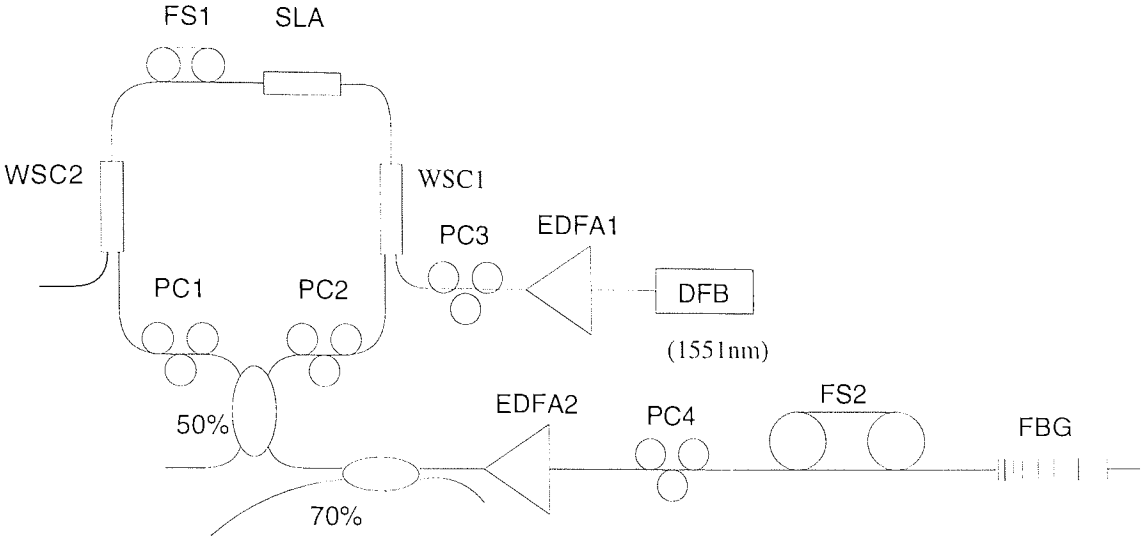

Figure 6.2: Schematic of laser system with SLA in NOLM. PC: polarisation controller, FS: fibre stretcher, EDFA: Erbium-doped fibre amplifiers. WSC1 and WSC2 are a pair of dichroic wavelength-selective couplers.

6.2 Design of laser system

The design of the laser system is shown in Figure 6.2. It is obviously similar to that in Figure 4.1. However, there are clear differences. Firstly, the NOLM has been replaced with a NOLM with a SLA inserted. There is also an additional fibre stretcher (FS1) in the loop mirror, which is used to adjust the position of the SLA with respect to the centre of the loop (it will obviously also alter the overall length of the cavity, which is compensated for by adjusting FS2, the fibre stretcher in the main cavity).

The two polarisation controllers PC1 and PC2 are required because of the polarisation dependence of the SLA, as is PC3 which allows the polarisation state of the switching pulses to be adjusted to match that of the signal, to enhance the nonlinear interaction. The wavelength-selective couplers are a matched pair with a narrow reflection band designed for use with nominal wavelengths of 1537 and 1557nm. In practice, they performed acceptably with wavelengths of $\approx$ 1540nm and 1551nm.

The second major difference is the source of control pulses —these are provided by a 10GHz gain-switched DFB, amplified to an average power of $\approx$1mW by EDFA1. (There are isolators on both the input and output of EDFA1 which are not shown

in the diagram for reasons of clarity). The DFB was capable, when suitably biased, of producing output pulses as short as $\approx$ 15ps.

One of the consequences of using a DFB was the tunability of the control pulse repetition rate. This meant that the cavity length adjustment required in Chapter 4 was not required with this system. (The length adjustment process for the loop mirror was only performed once. Replacement of intracavity components did not require any length adjustment —the control pulse frequency could be modified for optimum modelocking).

The ability to tune the control pulse to an arbitrary repetition rate allowed the investigation of harmonic generation in this system. The theory of this is discussed in Section 3.8.

Generation of harmonics up to the 4^{th} was observed, though there was a deterioration in the quality of the pulse train for higher harmonics. The gain modulation of the SLA by the control pulses also resulted in different amplitudes for adjacent pulses, an effect which is visible on the autocorrelation traces of the output.

6.3 Loop mirror performance

As the switching window is critical to the performance of the system, it was important to determine its width. This was achieved by disconnecting the laser cavity from the loop mirror, and using a second DFB to produce pulses to transmit through the loop mirror. The relative delay between these pulses and the control pulses was varied, and the transmitted power (as measured on a slow detector) was plotted. The results (for one setting of FS1) are shown in Figure 6.3.

This graph suggests a FWHM switching window of 54ps, and the difference in transmission before and after the window is apparent; this is a consequence of the gain depletion of the SLA and the slow recovery time. This is also a possible explanation for the asymmetry of the window.

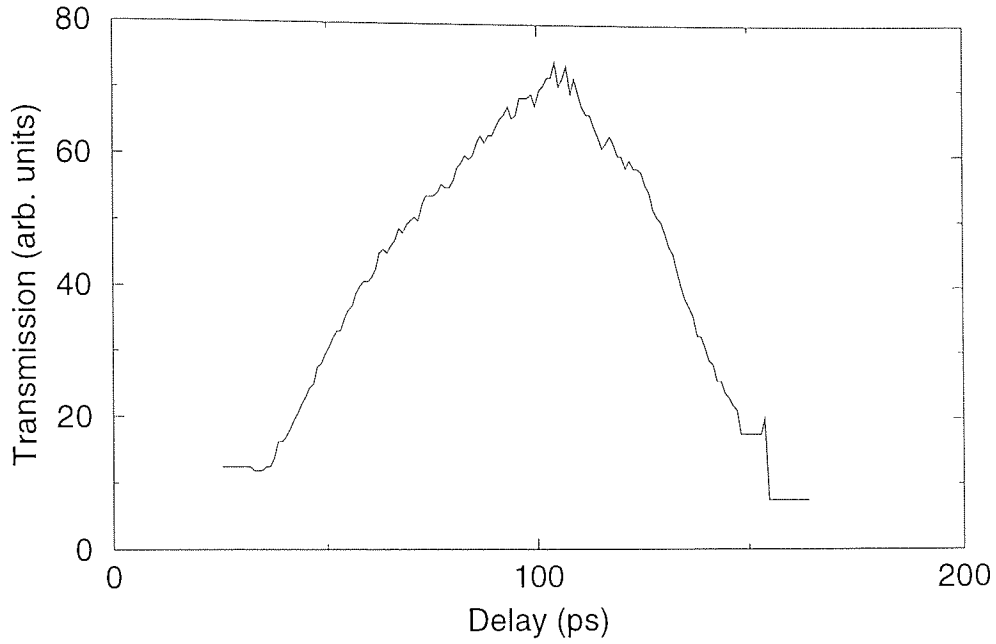

Figure 6.3: Transmission profile of switching window of loop mirror. Note the difference in transmission before and after the window, due to depletion of the SLA gain. FWHM of window is 54ps

6.4 Pulse output properties

Using this loop mirror in a linear cavity, soliton output pulses were readily obtained. An example autocorrelation and spectrum is shown in Figure 6.4. In this case, the pulse has a pulse width of 14.5ps, and a FWHM spectral width of 0.48nm. This results in a time-bandwidth product of 0.87, indicating a substantial chirp on the pulse.

By detuning the driving frequency away from an exact multiple of the cavity fundamental frequency, frequency doubling or tripling could be obtained. An autocorrelation and spectrum of a doubled pulse are shown in Figure 6.5. This pulse has a pulsewidth of 11.2ps and a spectral width of 0.28nm; the time-bandwidth product is therefore 0.39; this is only slightly greater than the ideal value of 0.315. Note that the autocorrelations of this figure and the next contain multiple peaks —these are cross-correlations between adjacent pulses, as the interpulse separation is less than the delay range of the autocorrelator for high repetition rates. The

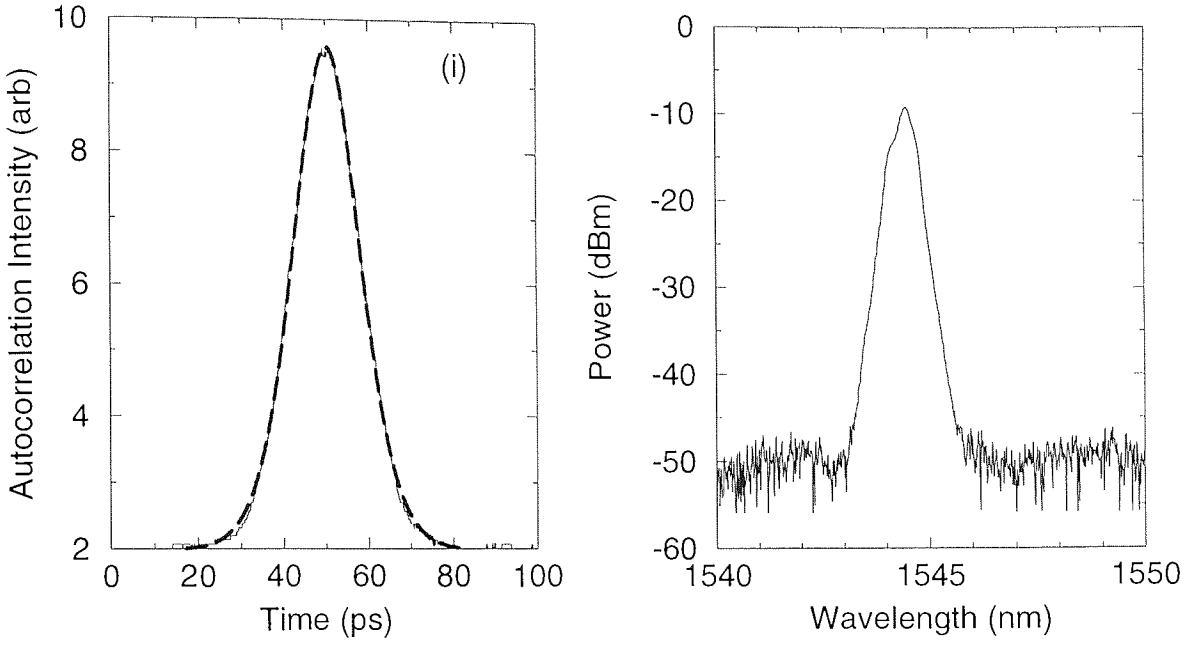

Figure 6.4: Output autocorrelation (i) and spectrum (ii) from laser driven at 10GHz and producing output at 10GHz. The dashed line on the autocorrelation is the best-fit sech^2*;* τ*(FWHM)=14.5ps*

significant difference in amplitude between the outer and central peaks is indicative of an amplitude difference between adjacent pulses, which can be explained by the patterning induced by the SLA recovery time.

Finally, it was possible to obtain frequency tripled output, shown in Figure 6.6. This pulse is again narrower, at 9.2ps, but with a chirp (the time-bandwidth product is 0.53 due to a spectral width of 0.46nm). The amplitude variation of the adjacent peaks is again pronounced.

6.5 Discussion

This chapter has demonstrated that it is possible to use the linear cavity described in Chapter 4 and developed in Chapter 5 at substantially higher repetition rates than the original 76MHz. This is possible because the use of the SLA enables low-power switching pulses to be used —this gives the flexibility to use a high-speed DFB as a source.

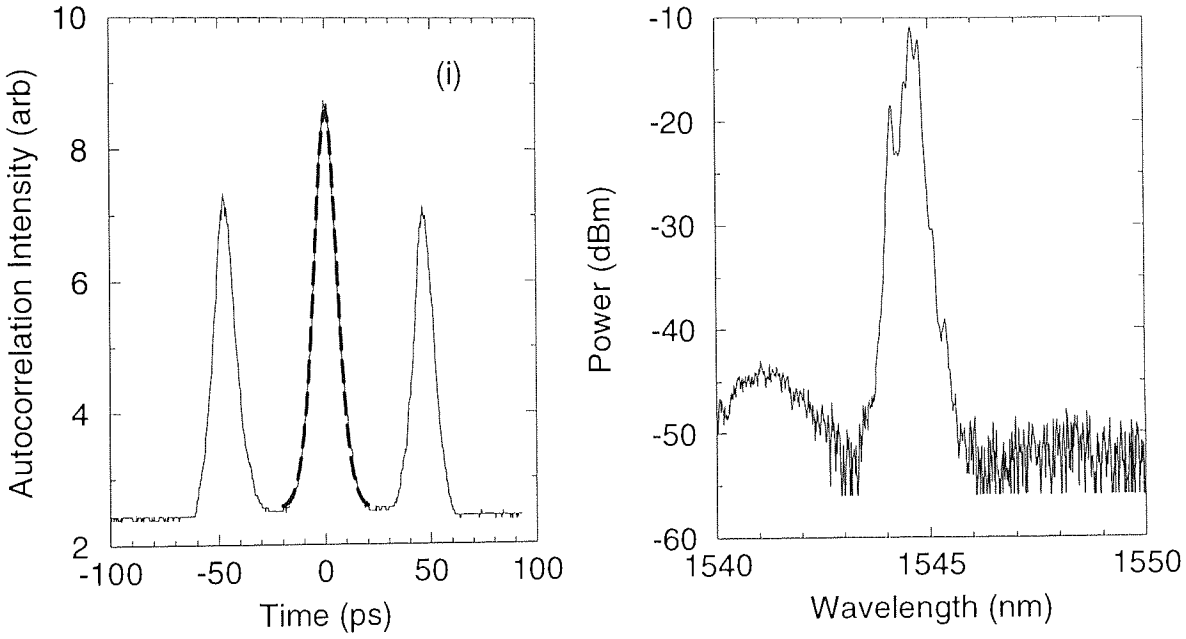

Figure 6.5: Output autocorrelation (i) and spectrum (ii) from laser driven at 10GHz and producing output at 20GHz. The lower intensity peaks on the autocorrelation represent the cross-correlation of adjacent pulses. The dashed curve on the central peak represents the best-fit sech^2*;* τ*(FWHM)=11.2ps*

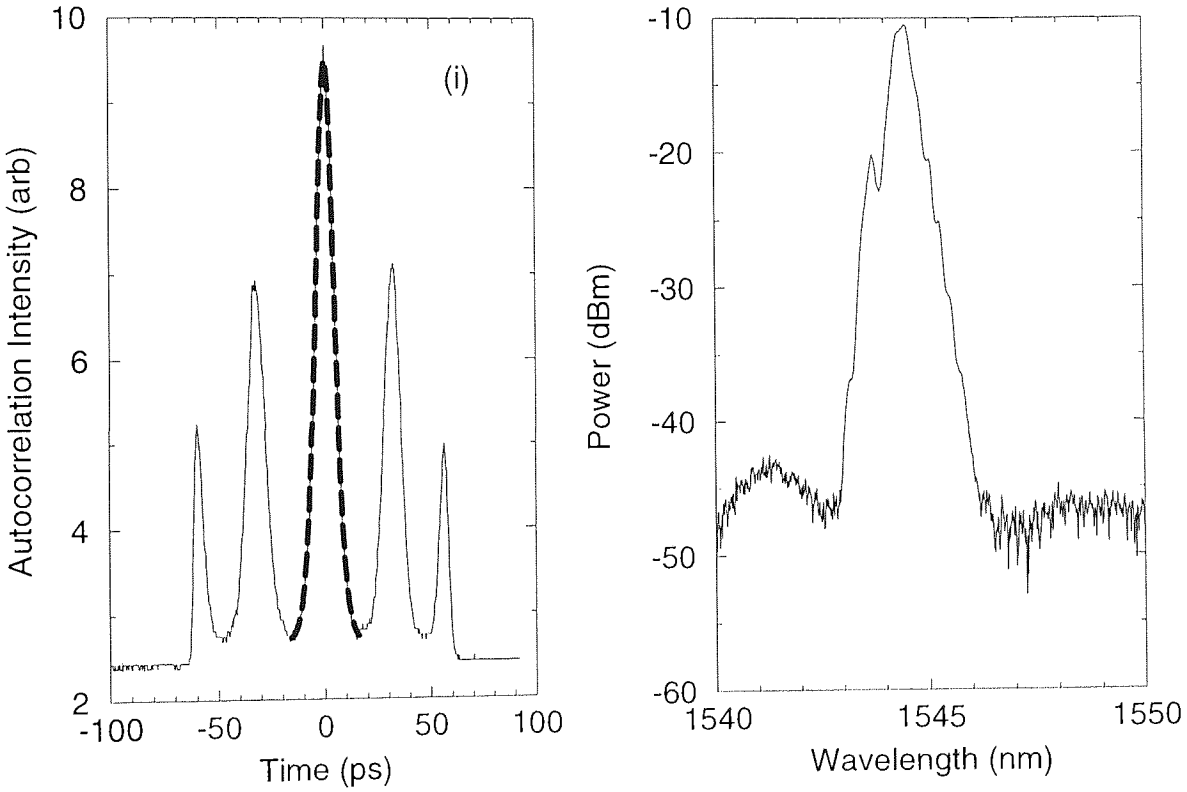

Figure 6.6: Autocorrelation (i) and spectrum (ii) from laser driven at 10GHz and producing output at 30GHz. The dashed line is the best-fit sech^2; $\tau\,(FWHM)$=9.2ps

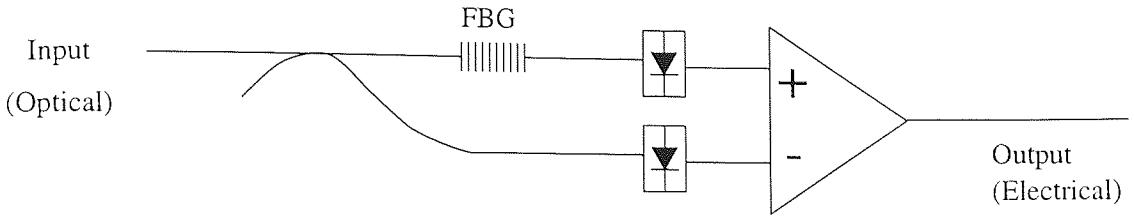

Figure 6.7: Wavelength to voltage converter, using either a chirped grating (for wide bandwidth) or a pair of gratings (as a Fabry-Perot etalon), a pair of (slow) photodiodes and an operational amplifier used in a differential mode

However, the slow recovery time of the SLA introduces a patterning on the output pulse train which has been discussed previously. This can be mitigated using reverse pumping techniques. With attention paid to this issue, the SLA is an essential component in the development of high-speed all-optical switching applications.

6.6 Future development and applications

The work presented in this thesis describes three related laser systems. This section intends to examine some of the possible applications of these systems, and to point to features of their operation which could be developed.

Firstly, it is interesting to note that may of the more recent laser applications rely on ring or figure-8 cavities; while there are disadvantages to a linear cavity (spatial hole burning, for example) there are several advantages which have already been described.

One of the most useful features from an application viewpoint is dispersion tuning. It is convenient to be able to shift the output wavelength of a laser cavity by a small length change. If the output wavelength could be measured, a simple feedback loop could be used for several possible applications.

The system shown in Figure 6.7 is an example of a simple wavelength to voltage converter.

The input to this converter is coupled to the output of the laser system described in Chapter 4 and the output voltage will vary with the change in wavelength. It

can thus provide an error signal for stabilisation of the laser cavity if the wavelength change is a consequence of long-term thermal drift. (The error signal can be amplified and used to drive a piezo-electric element or simple motorised fibre stretcher which will stretch the fibre. Similar approaches has been used to stabilise other kinds of laser system [116, 119]). Obviously, higher-frequency acoustic noise is difficult to suppress using this method.

However, using the output of this converter device, without a stabilising loop allows the use of the laser in several novel applications. These rely on the dependence of output wavelength on input frequency and cavity length.

6.6.1 Tunable source for WDM

It is clear that the feedback system need not have only one defined setpoint; it may have several, calibrated to different wavelengths. A change in the setpoint will therefore result in a change of wavelength. While this change will be limited by the mechanical stretching, and will not be appropriate for data switching, it may be useful for a source which is required to provide one of (for example) four wavelengths as required. This can be achieved with the convenience of having only to push a button. Suitable applications may be as data sources for trialling WDM or all-optical switching applications.

6.6.2 Optical tachometer

It is possible to use a single linear system to perform precise measurements of repetition rate. A calibrated grating is used, and the output wavelength is measured, either using a calibrated wavelength meter or the system of Figure 6.7. This has the virtue of measuring a high-frequency signal and producing a low-bandwidth value, avoiding the requirement for any high-frequency electronics. Obviously the tuning range of the grating is a limiting factor, but this system may be more useful when based around standard telecommunications rates.

6.6.3 Adaptable lasers

For the purposes of clock recovery or wavelength conversion, it is desirable that the operating range (in terms of repetition rate) of the input is not unnecessarily limited. As described above, the dispersion is the proportional factor between the input repetition rate change and the output wavelength. These are related by the expression:

$$\Delta\lambda = -\frac{\Delta\nu}{DL\nu^2} \tag{6.2}$$

In all the systems covered in this thesis, the fundamental frequency of the cavity is substantially less than the operating frequency of the laser; as described in Chapter 4 the cavity length is adjusted so that the modelocking frequency coincides with a harmonic of the cavity fundamental frequency. Once centred around that frequency, the optical tuning range determines the allowable tolerance in the input repetition rate. If this tuning range is sufficiently broad that it overlaps with the tuning range of the adjacent harmonics, the laser will be continuously tunable in terms of repetition rate.

The cavity fundamental frequency (and thus the spacing between harmonics) is defined as

$$\Delta\nu = \frac{c}{2nL} \tag{6.3}$$

Substituting this in the expression above, to find the tuning range required, we obtain:

$$\Delta\lambda = -\frac{c}{2nDL^2\nu^2} \tag{6.4}$$

However, it can be assumed that the grating dispersion dominates the cavity and is the major contribution to the term DL. We obtain the simple result

$$\Delta L = \frac{L}{N} \tag{6.5}$$

In a typical example, a cavity of length $\approx$ 130m intended to be used at 1GHz requires an available length change of 20cm. At 10GHz this change need only be 2cm, which is readily fabricated (this is a round-trip length, so the physical length of the grating needs to be 1cm). Note also that this relationship is independent of

the grating dispersion (on the assumption that it is dominant). Consequently, the dispersion can still be chosen to satisfy other system requirements.

It is clear, however, that such a system is only useful for very high repetition rates. A further drawback is that operation with a low dispersion will require a grating with a large bandwidth. For example, the 10GHz system described above will require a 20nm grating bandwidth to obtain a dispersion of 5ps/nm. Obviously, lower dispersion will require a broader grating. Such a grating may not be feasible for use with an EDFA because of the large peak in the amplifier gain —the laser may not dispersion tune at all if laser action occurs at this peak.

One solution to this problem is the use of longer gratings —gratings over a metre long have been fabricated [47]. However, these gratings are produced from several shorter gratings adjacent to one another and consequently have features in the reflection profile and a higher loss than a short grating.

The challenge is therefore to produce a grating with both low dispersion and low bandwidth, and a short length. Although these two requirements may seem irreconcilable, a nonlinear grating will provide an appropriate solution. An example of the delay *vs.* wavelength profile is shown in Figure 6.8. The grating consists of three distinct regions

1. At the short wavelength end, a high-dispersion region

2. A central, low dispersion region

3. At the long wavelength end, another high-dispersion region

The overall bandwidth of the grating is kept low, but it will still dispersion-tune over the whole delay range required for continuous tuning. However, outside of the central region, the dispersion will be higher but the laser will remain modelocked; the output wavelength can be used to drive a cavity length change to bring the operating wavelength back into the central range. This can be accomplished using the system described above.

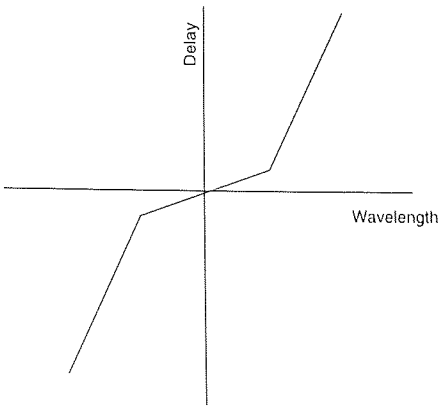

Figure 6.8: Illustration of delay vs. *wavelength curve for chirped grating intended for continuously-tunable laser*

6.6.4 Dual wavelength applications

The flexibility of the schemes described above is increased with the use of the dual wavelength configuration described in Chapter 5. Obviously, the stabilisation and wavelength selection functions are equally useful for such a system, which could be readily packaged to provide a convenient source for WDM and switching experiments.

One further possibility is the prospect of using radically different amplifiers in the two arms of the dual-wavelength system. For example, one cavity could contain a standard EDFA, while the other might use a Praseodymium-doped fluoride fibre amplifier operating at 1.3μm. As the loop mirror is a broadband device, it will switch both wavelengths. Such a system might form part of an all-optical, bidirectional 1.5μm to 1.3μm wavelength conversion system.

Chapter 7

Summary and Conclusions

This thesis has presented several erbium-doped fibre laser systems centred around the use of chirped in-fibre Bragg gratings and loop mirrors.

The simple linear system proposed in Chapter 4 was an effective way of generating short pulses whose parameters could be controlled through the properties of the grating used as a cavity end mirror. The system was straightforward to set up and run, and had the potential to be a useful laboratory source.

In Chapter 5, to satisfy a requirement for a dual-wavelength source, a second cavity was added to the other side of the loop mirror; this was a novel addition and had not previously been described. This system effectively produced two closely synchronised pulsetrains; the jitter performance was fundamentally limited by the jitter performance of the Nd^{3+}:YAG source which provided the modelocking control signal. The stability of this system made it a useful laboratory tool for switching experiments with dual-wavelength loop mirrors.

There is a continuing trend towards higher-bitrate systems. This was addressed in Chapter 6 with the modification of the original linear cavity system to operate at substantially higher bitrates. This system had poorer jitter performance than those previously described, but the output jitter was less than the jitter of the modelocking source, which suggests that a lower jitter source might contribute a further reduction in jitter.

The systems described in this thesis have shared several features —the NOLM,

chirped gratings and linear cavities. These components have fitted into a flexible framework, and the major significance of the lasers described is that they are readily adapted to different applications. The previous section considered some of the practical uses to which they could be put.

Obviously, some of these features depend on component performance (particularly in the case of the gratings and SLAs) and an improvement in the quality and versatility of these components will simplify even further the specification of these systems. A few years ago, erbium-doped fibre amplifiers were specialist devices constructed in laboratories. Now they are available "off the shelf" as packaged products, and are installed in real systems on land and under sea. In-fibre Bragg gratings have also been making a transition from laboratory device to commercial product, and recently fibre lasers have become available in packaged form commercially. All these trends contribute to increased reliability and tighter specifications.

The improvement of component performance will always be significant in improving system performance, and these technologies are maturing over time. At the same time, of course, the demands for communications bandwidth are also increasing; modern applications are exploiting networked information to an ever greater extent, and old assumptions about the kind of material transmitted and the network topologies for doing so, are continually being challenged. The world is now networked by an incredible web of communications infrastructure, and it is sobering to reflect on the impact of this on society.

The lasers described here are more fundamental components of communications systems, but are nonetheless important: the increases in the capacity of communications links have not been delivered through development of new network protocols! The availability of bandwidth for new, network-intensive applications ultimately depends on solid building blocks. The lasers described in this thesis may not find active service in commercial communications systems, but as an exposition of the utility of fibre gratings, and in research environment, I believe that they have a useful role to play in the development of future communications systems.

References

[1] K. C. Kao and G. A. Hockham. Dielectric fiber surface waveguides for optical frequencies. *Proc. IEE*, 113(7):1151–1158, 1966.

[2] A. Werts. Propagation de la lumière cohérente dans les fibres optiques. *L'Onde Electrique*, 46:967–980, 1966.

[3] T. H. Maiman. Stimulated optical radiation in ruby. *Nature, London*, 187:493–494, 1960.

[4] A. D. Ellis, T. Widdowson, X. Shan, G. E. Wickens, and D. M. Spirit. Transmission of a true single polarisation 40 Gbit/s soliton data signal over 205km using a stabilised erbium fibre ring laser and 40 GHz electronic timing recovery. *Electron. Lett.*, 29(11):990–992, 1993.

[5] A. D. Ellis and D. M. Spirit. Unrepeatered transmission over 80km standard fibre at 40Gbit/s. *Electron. Lett.*, 30(1):72–74, 1994.

[6] X. Shan, T. Widdowson, D. J. Malyon, A. D. Ellis, and D. M. Spirit. Comparison of soliton sources for communication applications. In *Colloquium on High Capacity Optical Communications*, pages 6/1–6/6, 1994.

[7] J. M. Senior. *Optical Fiber Commmunications: Principles and Practice*. Prentice Hall, 2nd edition, 1992.

[8] G. P. Agrawal. *Nonlinear Fiber Optics*. Academic Press, second edition, 1995.

[9] M. L. Dennis and I.N. Duling III. Third-order dispersion in femtosecond fiber lasers. *Opt. Lett.*, 19(21):1750–1752, 1994.

[10] H. C. Lefevre. Single-mode fiber fractional wave devices and polarisation controllers. *Electron. Lett.*, 16(20):778–780, 1980.

[11] J. S. Russell. *Reports of the Meetings of the British Association for the Advancement of Science*, chapter 311,417. John Murray, 1838,1844.

[12] A. Hasegawa and F. Tappert. Transmission of stationary nonlinear optical pulses in dispersive dielectric fibers. anomalous dispersion. *Appl. Phys. Lett.*, 23(3):142–144, 1973.

[13] K. J. Blow and N. J. Doran. Soliton phenomena in optical fibres. In C. G. Someda and G. Stegeman, editors, *Anisotropic and Nonlinear Optical Waveguides*, pages 159–183. Elsevier Science Publishers BV, 1992.

[14] K. J. Blow and N. J. Doran. Average soliton dynamics and the operation of soliton systems with lumped amplifiers. *IEEE Photon. Technol. Lett.*, 3(4):369–371, 1991.

[15] N. J. Doran and D. Wood. Nonlinear-optical loop mirror. *Opt. Lett.*, 13(1):56–58, 1988.

[16] J. P. Sokoloff, P. R. Prucnal, I. Glesk, and M. Kane. A terahertz optical asymmetric demultiplexer (TOAD). *IEEE Photon. Technol. Lett.*, 5(7):787–790, 1993.

[17] K. Mori, T. Morioka, and M. Saruwatari. Optical parametric loop mirror. *Opt. Lett.*, 20(12):1424–1426, 1995.

[18] K. Mori, K. Uchiyama, T. Morioka, and M. Saruwatari. Wavelength conversion with an optical parametric loop mirror. *Electron. Lett.*, 32(23):2171–2172, 1996.

[19] I. N. Duling III, C.-J. Chen, P. K. A. Wai, and C. R. Menyuk. Operation of a nonlinear loop mirror in a laser cavity. *IEEE J. Quantum Electron.*, 30(1):194–199, 1994.

[20] M. E. Fermann, F. Haberl, M. Hofer, and H. Hochreiter. Nonlinear amplifying loop mirror. *Opt. Lett.*, 15:752–754, 1990.

[21] Y. T. Chieng, G. J. Cowle, and R. A. Minasian. Optically amplitude-stabilised tunable erbium-doped fibre laser with $< 20\mu$s tuning speed. *Electron. Lett.*, 31(17):1450–1451, 1995.

[22] K. J. Blow, N. J. Doran, B. K. Nayar, and B. P. Nelson. Two-wavelength operation of the nonlinear fibre loop mirror. *Opt. Lett.*, 15(4):248–250, 1990.

[23] M. Jinno. All optical signal regeneration using a nonlinear fiber sagnac interferometer switch with signal-clock walk-off. *IEEE J. Lightwave Technol.*, 12(9):1648–1659, 1994.

[24] H. K. Lee, K. H. Kim, S. Y. Park, and E.-H. Lee. A walk-off balanced nonlinear fiber loop mirror switch. *IEEE Photon. Technol. Lett.*, 7(12):1441–1443, 1995.

[25] K. Uchiyama, T. Morioka, and M. Saruwatari. Polarisation-independent wavelength conversion using nonlinear optical loop mirror. *Electron. Lett.*, 31(21):1862–1863, 1995.

[26] A. J. Poustie, R. J. Manning, and K. J. Blow. All-optical circulating shift register using a semiconductor optical amplifier in a fiber loop mirror. *Electron. Lett.*, 32(13):1215–1216, 1996.

[27] K. L. Hall and K. A. Rauschenbach. All-optical bit pattern generation and matching. *Electron. Lett.*, 32(13):1214–1215, 1996.

[28] D. L. Williams, M. J. Holmes, J. Devaney, R. J. Manning, J. Lucek, K. Smith, and B. J. Ainslie. Optical modelocking at 10GHz using a highly-nonlinear germanosilicate optical fibre. *Electron. Lett.*, 31(15):1256–1257, 1995.

[29] D. K. W. Lam and B. K. Garside. Characterisation of single-mode optical fibre filters. *Appl. Opt.*, 20(3):440–445, 1991.

[30] R. R. A. Syms and J. R. Cozens. *Optical Guided Waves and Devices.* McGraw-Hill, 1992.

[31] M. G. Sceats, G. R. Atkins, and S. B. Poole. Photolytic index changes in optical fibers. *Annu. Rev. Mater. Sci.*, 23:381–410, 1993.

[32] K. O. Hill, B. Malo, F. Bilodeau, and D. C. Johnson. Photosensitivity in optical fibers. *Annu. Rev. Mater. Sci*, 23:125–157, 1993.

[33] I. Bennion, J. A. R. Williams, L. Zhang, K. Sugden, and N. J. Doran. UV-written in-fibre Bragg gratings. *Opt. and Quant. Elect.*, 28(2):93–135, 1996.

[34] D. L. Williams, B. J. Ainslie, J. R. Armitage, R. Kashyap, and R. Campbell. Enhanced UV photosensitivity in boron codoped germanosilicate fibres. *Electron. Lett.*, 29(1):45–47, 1993.

[35] P. J. Lemaire, R. M. Atkins, V. Mizrahi, and W. A. Reed. High pressure h_2 loading as a technique for acheiving ultrahigh UV photosensitivity. *Electron. Lett.*, pages 1191–1193, 1993.

[36] R. M. Atkins, P. J. Lemaire, T. Erdogan, and V. Mizrahi. Mechanisms of enhannced UV photosensitivity via hydrogen loading in germanosilicate glasses. *Electron. Lett.*, 29:1234–1235, 1993.

[37] B. Malo, J. Albert, K. O. Hill, F. Bilodeau, and D. C. Johnson. Effective index drift from molecular hydrogen diffusion in hydrogen-loaded optical fibres and its affect on Bragg grating fabrication. *Electron. Lett.*, 30:442–444, 1994.

[38] K. O. Hill, Y. Fujii, D. C. Johnson, and B. S. Kawasaki. Photosensitivity in optical fibre waveguides: application to reflection filter fabrication. *Appl. Phys. Lett.*, 32:647–649, 1978.

[39] B. S. Kawasaki, K. O. Hill, D. C. Johnson, and Y. Fujii. Narrow-band Bragg reflectors in optical fibres. *Opt. Lett.*, 3(1):66–68, 1978.

[40] G. Meltz, W. W. Morey, and W. H. Glenn. Formation of Bragg gratings in optical fibre by a transverse holographic method. *Opt. Lett.*, 14:823–825, 1989.

[41] Q. Zhang, D. A. Brown, L. Reinhart, T. F. Morse, J. Q. Wang, and G. Xiao. Tuning Bragg wavelength by writing gratings on prestrained fibres. *IEEE Photon. Technol. Lett.*, 6:839–841, 1994.

[42] B.-G. Kim and E. Garmire. Comparison between the matrix method and the coupled-wave method in the analysis of Bragg reflector structures. *J. Opt. Soc. Amer. A*, 9:132–136, 1992.

[43] K. Sugden, I. Bennion, A. Molony, and N. J. Copner. Chirped gratings produced in photosensitive optical fibre by fibre deformation during exposure. *Electron. Lett.*, 30(5):440–442, 1994.

[44] M. C. Farries, C. M. Ragdale, and D. C. J. Reid. Broadband chirped fibre Bragg filters for pump rejection and recycling in erbium doped fibre amplifiers. *Electron. Lett.*, 28:487–489, 1992.

[45] M. C. Farries, K. Sugden, D. C. J. Reid, I. Bennion, A. Molony, and M. J. Goodwin. Very broad reflection bandwidth (44nm) chirped fibre gratings and narrow bandpass filters produced by the use of an amplitude mask. *Electron. Lett.*, 30(11):891–892, 1994.

[46] R. Kashyap, H.-G. Froehlich, A. Swanton, and D. J. Armes. Super-step-chirped fibre Bragg gratings. *Electron. Lett.*, 32(15):1394–1396, 1996.

[47] R. Kashyap, H.-G. Froehlich, A. Swanton, and D. J. Armes. 1.3m long super-step-chirped fibre Bragg grating with a continuous delay of 13.5ns and bandwidth 10nm for broadband dispersion compensation. *Electron. Lett.*, 32(19):1807–1809, 1996.

[48] J. A. R. Williams, L. A. Everall, I. Bennion, and N. J. Doran. Fiber Bragg grating fabrication for dispersion slope compensation. *IEEE Photon. Technol. Lett.*, 8(9):1187–1189, 1996.

[49] V. Mizrahi and J. E. Sipe. Optical properties of photosensitive fiber phase gratings. *IEEE J. Lightwave Technol.*, 11(10):1513–1517, 1993.

[50] T. Erdogan, V. Mizrahi, P. J. Lemaire, and D. Monroe. Decay of ultraviolet-induced Bragg gratings. *J. Appl. Phys.*, 76:73–80, 1994.

[51] M. Douay, E. Fertein, W. X. Xie, P. Bernage, P. Niay, J. F. Bayon, and T. Georges. Thermal hysteresis of Bragg wavelengths of intra-core fibre gratings. *IEEE Photon. Technol. Lett.*, 5:1331–1334, 1993.

[52] P. C. Hill and B. J. Eggleton. Strain gradient chirp of fibre Bragg gratings. *Electron. Lett.*, 30(14):1172–1174, 1994.

[53] G. A. Ball and W. W. Morey. Compression-tuned single-frequency Bragg grating fiber laser. *Opt. Lett.*, 19(23):1979–1981, 1994.

[54] J. Lauzon, S. Thibault, J. Martin, and F. Ouellete. Implementation and characterisation of fibre Bragg gratings linearly chirped by a temperature gradient. *Opt. Lett.*, 19(23):2027–2029, 1994.

[55] E. J. Friebele, C. G. Askins, M. A. Putnam, A. A. Fosha Jr., J. Florio Jr., R. P. Donti, and R. G. Blosser. Distributed strain sensing with fibre Bragg grating arrays embedded in CRTM composites. *Electron. Lett.*, 30(21):1783–1784, 1994.

[56] U. Eriksson, P. Blixt, and J. A. Tellefsen Jr. Design of fiber gratings for total dispersion compensation. *Opt. Lett.*, 19(14):1028–1030, 1994.

[57] K. Tamura, T. Komukai, T. Yamamota, T. Imai, E. Yoshida, and M. Nakazawa. High energy, sub-picosecond pulse compression at 10GHz using a fibre/fibre-grating pulse compressor. *Electron. Lett.*, 31(25):2194–2195, 1995.

[58] D. Taverner, D. J. Richardson, M. N. Zervas, L. Reekie, L. Dong, and J. L. Cruz. Investigation of fiber grating-based performance limits in pulse stretch-

ing and recompression schemes using bidirectional reflection from a linearly chirped fiber grating. *IEEE Photon. Technol. Lett.*, 7(12):1436–1438, 1995.

[59] E. Delevaque, T. Georges, B. Landouises, and E. Taufflieb. Multichannel equalised and stabilised gain amplifier for WDM transmissions. *Electron. Lett.*, 31(25):2149–2150, 1995.

[60] J. A. R. Williams, I. Bennion, and L. Zhang. The compression of optical pulses using self-phase modulation and linearly chirped Bragg-gratings in fibers. *IEEE Photon. Technol. Lett.*, 7(5):491–493, 1995.

[61] B. J. Eggleton, K. A. Ahmed, F. Ouellette, P. A. Krug, and H.-F. Liu. Recompression of pulses broadened by transmission through 10km of non-dispersion-shifted fiber at 1.55μm using 40-mm-long optical fiber Bragg gratings with tunable chirp and central wavelength. *IEEE Photon. Technol. Lett.*, 7(5):494–496, 1995.

[62] F. Ouellette. All-fibre filter for efficient dispersion compensation. *Opt. Lett.*, 16(5):303–305, 1991.

[63] J. A. R. Williams, I. Bennion, and N. J. Doran. The design of in-fiber Bragg grating systems for cubic and quadratic dispersion compensation. *Opt. Comm.*, 116:62–66, 1995.

[64] A. Molony, L. Zhang, J. A. R. Williams, I. Bennion, C. Edge, and J. Fells. Fibre Bragg grating time delay control of phased array antennae. *J. Mod. Opt.*, 43(5):1017–1024, 1996.

[65] G. F. Levy. Raman amplification of solitons in a fiber optic ring. *IEEE J. Lightwave Technol.*, 14(1):72–76, 1996.

[66] W.-Y. Oh, B. Y. Kim, and H.-W. Lee. Passive mode locking of a neodymium-doped fiber laser with a nonlinear optical loop mirror. *IEEE J. Quantum Electron.*, 32(2):333–339, 1996.

[67] R. M. Percival and J. R. Williams. Highly efficient 1.064μm upconversion pumped 1.47μm thulium doped fluroide fibre amplifier. *Electron. Lett.*, 30(20):1684–1685, 1994.

[68] D. U. Noske and J. R. Taylor. Spectral and temporal stabilisation of a diode-pumped ytterbium-erbium fibre soliton laser. *Electron. Lett.*, 29(25):2200–2202, 1993.

[69] W. H. Loh, A. B. Grudinin, and D. N. Payne. Optically controlled wavelength-adjustable passively modelocked erbium-doped fibre ring laser. *Electron. Lett.*, 30(5):413–415, 1994.

[70] R. I. Laming, M. C. Farries, P. R. Morkel, L. Reekie, and D. N. Payne. Efficient pump wavelengths of erbium-doped fibre optical amplifier. *Electron. Lett.*, 25(1):12–14, 1989.

[71] J. R. Armitage. Spectral dependence of the small-signal gain around 1.5μm in erbium doped silica fiber amplifiers. *IEEE J. Quantum Electron.*, 26(3):423–425, 1990.

[72] K. Kannan, S. Frisken, and P. S. Atherton. Characteristics of an erbium-doped fiber amplifier pumped by a frequency doubled diode-pumped Nd:YAG laser. *IEEE Photon. Technol. Lett.*, 3(2):124–126, 1991.

[73] M. C. Farries, P. R. Morkel, R. I. Laming, T. A. Birks, D. N. Payne, and E. J. Tarbox. Operation of erbium-doped fiber amplifiers and lasers pumped with frequency-doubled Nd:YAG lasers. *IEEE J. Lightwave Technol.*, 7(10):1473–1477, 1989.

[74] J.-M. P. Delavaux, C. F. Flores, R. E. Tench, T. C. Pleiss, T. W. Cline, D. J. DiGiovanni, J. Federici, C. R. Giles, H. Presby, J. S. Major, and W. J. Gignac. Hybrid Er-doped fibre amplifiers at 980-1480nm for long distance optical communications. *Electron. Lett.*, 28(17):1642–1643, 1992.

[75] A. Bjarklev. *Optical Fiber Amplifiers: Design and System Applications.* Artech House, 1993.

[76] V. J. Mazurczyk and J. L. Zyskind. Polarization dependent gain in erbium doped-fiber amplifiers. *IEEE Photon. Technol. Lett.*, 6(5):616–618, 1994.

[77] M. N. Islam, L. Rahman, and J. R. Simpson. Special erbium fiber amplifiers for short pulse switching, lasers and propagation. *IEEE J. Lightwave Technol.*, 12(11):1952–1962, 1994.

[78] C.-K. Liu, J.-J. Jou, and F.-S. Lai. Second-order harmonic distortion and optimal fiber length in erbium-doped fiber amplifiers. *IEEE Photon. Technol. Lett.*, 7(12):1412–1414, 1995.

[79] B. Pedersen, J. Chirravuri, and W. J. Miniscalco. Gain and noise penalty for detuned 980-nm pumping of erbium-doped fiber power amplifiers. *IEEE Photon. Technol. Lett.*, 4(4):351–353, 1992.

[80] A. E. Siegman and D. J. Kuizenga. Active mode-coupling phenomena in pulsed and continuous lasers. *Opto-electronics*, 6:43–66, 1974.

[81] M. Hofer, M. H. Ober, R. Hofer, M. E. Fermann, G. Sucha, D. Harter, K. Sugden, I. Bennion, C. A. C. Mendonca, and T. H. Chiu. High-power neodymium soliton fiber laser that uses a chirped fiber grating. *Opt. Lett.*, 20(16):1701–1703, 1995.

[82] M. Zirngibl, L. W. Stulz, J. Stone, J. Hugi, D. DiGiovanni, and P. B. Hansen. 1.2ps pulses from passively mode-locked laser diode pumped Er-doped fibre ring laser. *Electron. Lett.*, 27(19):1734–1735, 1991.

[83] F. Krausz, T. Brabec, and C. Spielmann. Self-starting passive mode-locking. *Opt. Lett.*, 16(4):235–237, 1991.

[84] H. A. Haus and E. P. Ippen. Self-starting of passively mode-locked lasers. *Opt. Lett.*, 16(17):1331–1333, 1991.

[85] G. Town, J. Chow, and M. Romagnoli. Sliding-frequency figure-eight optical fibre laser. *Electron. Lett.*, 31(17):1452–1453, 1995.

[86] M. L. Stock, L. M. Yang, M. J. Andrejco, and M. E. Fermann. Synchronous mode locking using pump-induced phase modulation. *Opt. Lett.*, 18(18):1529–1531, 1993.

[87] N. J. Smith, K. J. Blow, and I. Andonovic. Sideband generation through perturbations to the average soliton model. *IEEE J. Lightwave Technol.*, 10(10):1329–1333, 1992.

[88] D. U. Noske, N. Pandit, and J. R. Taylor. Source of spectral and temporal instability in soliton fiber lasers. *Opt. Lett.*, 17(21):1515–1517, 1992.

[89] M. L. Dennis and I. N. Duling III. Experimental study of sideband generation in femtosecond fiber lasers. *IEEE J. Quantum Electron.*, 30(6):1469–1477, 1994.

[90] M. Y. Frankel, R. D. Esman, and J. F. Weller. Rapid continuous tuning of a single-polarization fiber ring laser. *IEEE Photon. Technol. Lett.*, 6(5):591–593, 1994.

[91] T. F. Carruthers, I. N. Duling III, and M. L. Dennis. Active-passive mode-locking in a single-polarisation erbium fibre laser. *Electron. Lett.*, 30(13):1051–1053, 1994.

[92] L. F. Mollenauer and R. H. Stolen. The soliton laser. *Opt. Lett.*, 9(1):13–15, 1984.

[93] J. Mark, L. Y. Liu, K. L. Hall, H. A. Haus, and E. P. Ippen. Femtosecond pulse generation in a laser with a nonlinear external resonator. *Opt. Lett.*, 14(1):48–50, 1989.

[94] P. K. Cheo, L. Wang, and M. Ding. Low-threshold, self-tuned and passively mode-locked coupled-cavity all-fiber lasers. *IEEE Photon. Technol. Lett.*, 8(1):66–68, 1996.

[95] M. P. Sørensen, K. A. Shore, T. Geisler, P. L. Christiansen, J. Mork, and J. Mark. Dynamics of additive-pulse mode-locked fibre lasers. *Opt. Comm.*, 90(1):65–69, 1992.

[96] K. Smith, J. R. Armitage, R. Wyatt, N. J. Doran, and S. M. J. Kelly. Erbium fibre soliton laser. *Electron. Lett.*, 26(15):1149–1151, 1990.

[97] M. E. Fermann, M. J. Andrejco, Y. Silverberg, and A. M. Weiner. Generation of pulses shorter than 200fs from a passively mode-locked Er fiber laser. *Opt. Lett.*, 18(1):48–50, 1993.

[98] S. K. Kim, H. K. Kim, and B. Y. Kim. Er^{3+}-doped fiber ring laser for gyroscope applications. *Opt. Lett.*, 19(22):1810–1812, 1994.

[99] P. R. Morked, G. J. Cowle, and D. N. Payne. Travelling-wave erbium fiber ring laser with 60kHz linewidth. *Electron. Lett.*, 26:632–634, 1990.

[100] J. L. Zyskind, J. W. Sulhoff, Y. Sun, J. Stone, L. W. Stulz, G. T. Harvey, D. J. DiGiovanni, H. M. Presby, A. Piccirill, U. Koren, and R. M. Jopson. Singlemode diode-pumped tunable erbium-doped fiber laser with linewidth less than 5.5 kHz. *Electron. Lett.*, 27(23):2148–2149, 1991.

[101] H. Schmuck, Th. Pfeiffer, and G. Veith. Widely tunable narrow linewidth erbium doped fibre ring laser. *Electron. Lett.*, 27:2117–2119, 1991.

[102] R. H. Stolen, J. Botineau, and A. Ashkin. Intensity discrimination of optical pulses with birefringent fibres. *Opt. Lett.*, 7:512–514, 1982.

[103] V. J. Matsas, T. P. Newson, and M. N. Zervas. Self-starting passively mode-locked fibre ring laser exploiting nonlinear polarisation switching. *Opt. Comm.*, 92(1):61–66, 1992.

[104] C. R. Doerr, H. H. Haus, and E. P. Ippen. Asynchronous soliton mode locking. *Opt. Lett.*, 19(23):1958–1960, 1994.

[105] M. Nakazawa, E. Yoshida, T. Sugawa, and Y. Kimura. Continuum-suppressed uniformly repetitive 136fs pulse generation from an erbium-doped fibre laser with nonlinear polarisation rotation. *Electron. Lett.*, 29(15):1327–1329, 1993.

[106] K. Tamura, E. P. Ippen, H. A. Haus, and L. E. Nelson. 77-fs pulse generation from a stretched-pulse mode-locked all-fiber ring laser. *Opt. Lett.*, 18(13):1080–1082, 1993.

[107] K. Tamura, Y. Kimura, and M. Nakazawa. Femtosecond pulse generation over 82nm wavelength span from passively modelocked erbium-doped fibre laser. *Electron. Lett.*, 31(13):1062–1063, 1995.

[108] K. Tamura, C. R. Doerr, H. A. Haus, and E. P. Ippen. Soliton fiber ring laser stabilization and tuning with a broad intracavity filter. *IEEE Photon. Technol. Lett.*, 6(6):697–699, 1994.

[109] J. Zhang and J. W. Y. Lit. Erbium-doped fiber compound-ring laser with a ring filter. *IEEE Photon. Technol. Lett.*, 6(5):588–590, 1994.

[110] J. Zhang, C.-Y. Yue amd G. W. Schinn, W. R. L. Clements, and J. W. Y. Lit. Stable single-mode compound-ring erbium-doped fiber laser. *IEEE J. Lightwave Technol.*, 14(1):104–109, 1996.

[111] T. Pfeiffer and G. Veith. Tuneable fibre source for picosecond pulses around 1.55μm with repetition rates up to 20Ghz. *Optical and Quantum Electronics*, 26:S547–S557, 1994.

[112] K. Smith, E. J. Greer, R. Wyatt, P. Wheatley, N. J. Doran, and M. Lawrence. Totally integrated erbium fibre soliton laser pumped by laser diode. *Electron. Lett.*, 27(3):244–246, 1991.

[113] E. J. Greer, Y. Kimura, K. Suzuki, E. Yoshida, and M. Nakazawa. Generation of 1.2ps, 10GHz pulse train from all-optically modelocked, erbium fibre ring laser with active nonlinear polarisation rortation. *Electron. Lett.*, 30(21):1764–1765, 1994.

[114] W. A. Pender, T. Widowson, and A. D. Ellis. Error free operation of a 40 Gbit/s all-optical regenerator. *Electron. Lett.*, 32(6):567–569, 1996.

[115] M. J. W. Rodwell, D. W. Bloom, and K. J. Weingarten. Subpicosecond laser timing stabilisation. *IEEE J. Quantum Electron.*, 25(4):817–827, 1989.

[116] T. Widdowson, D. J. Malyon, X. Shan, and P. J. Watkinson. Soliton propagation without transmission conntrol using a phase-locked erbium fibre ring laser. *Electron. Lett.*, 30(8):661–663, 1994.

[117] M. Nakazawa, E. Yoshida, and K. Tamura. 10GHz, 2ps regeneratively and harmonically FM mode-locked erbium fibre ring laser. *Electron. Lett.*, 32(14):1285–1287, 1996.

[118] M. Nakazawa, E. Yoshida, and Y. Kimura. Ultrastable harmonically and regeneratively modelocked polarisation-maintaining erbium fibre ring laser. *Electron. Lett.*, 30(19):1603–1605, 1994.

[119] X. Shan, T. Widdowson, A. D. Ellis, and A. S. Siddiqui. Very simple method to stabilise mode-locked erbium fibre lasers. *Electron. Lett.*, 32(11):1015–1016, 1996.

[120] M. Romagnoli, S. Wabnitz, P. Franco, M. Midrio, F. Fontana, and G. E. Town. Tunable erbium-ytterbium fiber sliding-frequency soliton laser. *J. Optical Society of America, B*, 12(1):72–76, 1995.

[121] S. J. Frisken, C. A. Telford, R. A. Betts, and P. S. Atherton. Passively mode-locked erbium-doped fibre laser with nonlinear fibre mirror. *Electron. Lett.*, 27(10):887–889, 1991.

[122] D. J. Richardson, R. I. Laming, D. N. Payne, M. W. Phillips, and V. J. Matsas. 320fs soliton generation with passively mode-locked erbium fibre laser. *Electron. Lett.*, 27(9):730–732, 1991.

[123] W. Margulis, K. Rottwitt, and J. R. Taylor. High-power figure-of-eight laser for soliton transmission experiments. *Electron. Lett.*, 31(8):645–646, 1995.

[124] A. J. Stenz and R. W. Boyd. Figure-eight fibre laser with largely unbalanced central coupler. *Electron. Lett.*, 30(16):1302–1303, 1994.

[125] A. Boskovic, S. V. Chernikov, and J. R. Taylor. Femtosecond fibure of eight Yb:Er fibre laser incorporating a dispersion decreasing fibre. *Electron. Lett.*, 31(17):1446–1448, 1995.

[126] S. Bigo and E. Desurvire. 20GHz all-optical clock recovery based on fibre laser mode-locking with fibre nonlinear loop mirror as variable intensity/phase modulator. *Electron. Lett.*, 31(21):1855–1856, 1995.

[127] Z. Ahmed and N. Onodera. High repetition rate optical pulse generation by frequency multiplication in actively modelocked fibre ring lasers. *Electron. Lett.*, 32(5):455–457, 1996.

[128] E. Yoshida and M. Nakazawa. 80–200GHz erbium doped fibre laser using a rational harmonic modelocking technique. *Electron. Lett.*, 32(15):1370–1372, 1996.

[129] R. J. Manning, A. J. Poustie, and K. J. Blow. All-optical clock division using a semiconductor optical amplifier loop mirror with feedback. *Electron. Lett.*, 32(16):1504–1506, 1996.

[130] P. V. Mamyshev, S. V. Chernikov, and E. M. Dianov. Generation of fundamental soliton trains for high-bit-rate optical fiber communication lines. *IEEE J. Quantum Electron.*, 27(10):2347–2355, 1991.

[131] D. J. Richardson, R. P. Chamberlain, L. Dong, D. N. Payne, A. D. Ellis, T. Widdowson, and D. M. Spirit. Demonstration of 205km transmission of 35GHz, 5ps pulses generated from a diode driven, low jitter, beat signal to soliton conversion source. *Electron. Lett.*, 31(6):470–472, 1995.

[132] A. D. Ellis, W. A. Pender, T. Widdowson, D. J. Richardson, R. P. Chamberlain, and L. Dong. All-optical modulation of 40GHz beat frequency conversion soliton source. *Electron. Lett.*, 31(16):1362–1364, 1995.

[133] B. P. Nelson, K. Smith, and K. J. Blow. Mode-locked erbium fibre laser using all-optical nonlinear loop modulator. *Electron. Lett.*, 28(7):656–658, 1992.

[134] M. E. Fermann, K. Sugden, and I. Bennion. Generation of 10nJ picosecond pulses from a modelocked fibre laser. *Electron. Lett.*, 31(3):194–195, 1995.

[135] M. E. Fermann, K. Sugden, and I. Bennion. High-power soliton fiber laser based on pulse width control with chirped fibre Bragg gratings. *Opt. Lett.*, 20(2):172–174, 1995.

[136] M. J. Guy, J. R. Taylor, and R. Kashyap. Single-frequency erbium fibre ring laser with intracavity phase-shifted fibre Bragg grating narrowband filter. *Electron. Lett.*, 31(22):1924–1925, 1995.

[137] J. J. Pan and Y. Shi. Tunable Er^{3+}-doped fibre ring laser using fibre grating incorporated by optical circulator or fibre coupler. *Electron. Lett.*, 31(14):1164–1165, 1995.

[138] D. von der Linde. Characterization of the noise in continuously mode-locked lasers. *Appl. Phys. B*, 39:201–217, 1986.

[139] M. L. Dennis and I. N. Duling III. Role of dispersion in limiting pulse width in lasers. *Appl. Phys. Lett.*, 62(23):2911–2913, 1993.

[140] J.B. Schlager, S. Kawanishi, and M. Saruwatari. Dual wavelength pulse generation using mode-locked erbium-doped fibre ring laser. *Electron. Lett.*, 27(22):2072–2073, 1991.

[141] H. Takara, S. Kawanishi, M. Saruwatari, and J.B. Schlager. Multiwavelength birefringent-cavity mode-locked fibre laser. *Electron. Lett.*, 28(25):2274–2275, 1992.

[142] D. U. Noske, M. J. Guy, K. Rottwitt, R. Kashyap, and J. R. Taylor. Dual-wavelength operation of a passively mode-locked figure-of-8 ytterbium-erbium fiber soliton laser. *Opt. Comm.*, 108(4-6):297–301, 1994.

[143] J. Chow, G. Town, B. Eggleton, M. Ibsen, K. Sugden, and I. Bennion. Multiwavelength generation in an erbium-doped fiber laser using in-fiber comb filters. *IEEE Photon. Technol. Lett.*, 8(1):60–62, 1996.

[144] S. Yamashita and K. Hotate. Multiwavelength erbium-doped fibre laser using intracavity etalon and cooled by liquid nitrogen. *Electron. Lett.*, 32(14):1298–1299, 1996.

[145] K. Tamura, E. Yoshida, and M. Nakazawa. Generation of 10GHz pulse trains at 16 wavelengths by spectrally slicing a high power femtosecond source. *Electron. Lett.*, 32(18):1691–1693, 1996.

[146] T. Morioka, K. Uchiyama, S. Kawanishi, S. Suzuki, and M. Saruwatari. Multiwavelength picosecond pulse source with low jitter and high optical frequency stability based on 200nm supercontinuum filtering. *Electron. Lett.*, 31(13):1064–1066, 1995.

[147] K. O. Hill, F. Bilodeau, B. Malo, T. Kitagawa, S. Thériault, D. C. Johnson, J. Albert, and J. Takiguchi. Chirped in-fiber Bragg gratings for compensation of optical-fiber dispersion. *Opt. Lett.*, 19(17):1314–1316, 1994.

[148] D. Henderson and A.G. Roddie. A comparison of spectral and temporal techniques for the measurement of timing jitter and their application in a mode-locked argon ion and dye laser system. *Opt. Comm.*, 100(5,6):456–460, 1993.

[149] I.G. Fuss. An interpretation of the spectral measurement of optical pulse train noise. *IEEE J. Quantum Electron.*, 30(11):2707–2710, 1994.

[150] J. K. Lucek and K. Smith. All-optical signal regenerator. *Opt. Lett.*, 18(15):1226–1228, 1993.

[151] R. P. Davey, K. Smith, and A. McGuire. High-speed, mode-locked, tunable, integrated erbium fibre laser. *Electron. Lett.*, 28(5):482–484, 1992.

[152] M. Jinno. Effect of timing jitter on an optically controlled picosecond optical switch. *Opt. Lett.*, 18(17):1409–1411, 1993.

[153] M. Asobe, T. Ohara, I. Yokohama, and T. Kaino. Low power all-optical switching in a nonlinear optical loop mirror using chalcogenide glass fibre. *Electron. Lett.*, 32(15):1396–1397, 1996.

[154] M. Asobe, T. Kanamori, and K. Kubodera. Applications of highly nonlinear chalcogenide glass fibres in ultrafast all-optical switches. *IEEE J. Quantum Electron.*, 29(8):2325–2333, 1993.

[155] A. Yariv. *Optical Electronics.* Saunders College Publishing, 4th edition, 1991.

[156] P. Brosson. Analytical model of a semiconductor optical amplifier. *IEEE J. Lightwave Technol.*, 12(1):49–54, 1994.

[157] M. J. Guy, J. R. Taylor, D. G. Moodie, and A. E. Kelly. 10GHz 3ps actively mode-locked ring laser incorporating a semiconductor laser amplifier and an electroabsorption modulator. *Electron. Lett.*, 32(24):2240–2241, 1996.

[158] D. M. Patrick, A. D. Ellis, D. A. O. Davies, M. C. Tatham, and G. Sherlock. Demultiplexing using polarization rotation in a semiconductor- laser amplifier. *Electron. Lett.*, 30(4):341–342, 1994.

[159] B. Mikkelson, T. Durhuus, C. R. J. Joergenson, S. Pedersen, C. Braagraard, and K. E. Stubkjaer. Polarisation-insensitive wavelength conversion of 10Gbit/s signals with SOAs in Michelson interferometer. *Electron. Lett.*, 30:260–261, 1994.

[160] C. Joergensen, S. L. Danielsen, M. Vaa, B. Mikkelson, K. E. Stubkjaer, P. Doussiere, F. Pommerau, L. Goldstein, and M. Goix. 40Gbit/s all-optical wavelength conversion by semiconductor optical amplifiers. *Electron. Lett.*, 32(4):367–368, 1996.

[161] A. D. Ellis, D. A. O. Davies, A. Kelly, and W. A. Pender. Data driven operation of semiconductor amplifier loop mirror at 40 Gbit/s. *Electron. Lett.*, 31(15):1245–1247, 1995.

[162] B. Mikkelsen, S. L. Danielsen, C. Joergensen, R. J. S. Pedersen, H. N. Poulsen, and K. E. Stubkjaer. All-optical noise reduction capability of interferometric wavelength converters. *Electron. Lett.*, 32(6):566–567, 1996.

[163] A. W. O'Neill and R. P. Webb. All-optical loop mirror switch employing an asymmetric amplifier-attenuator combination. *Electron. Lett.*, 26(24):2008–2009, 1990.

[164] M. Eiselt. Optical loop mirror with semiconductor-laser amplifier. *Electron. Lett.*, 28(16):1505–1507, 1992.

[165] L. E. Adams and E. S. Kintzer. All-optical timing extraction at 40GHz using a mode-locked figure-eight laser with an SLA. *Electron. Lett.*, 31(20):1759–1760, 1995.

[166] H. Ammann, W. Hodel, H. P. Weber, C. Holtmann, and H. Melchior. Passive modelocking of 1.3μm semiconductor laser amplifier in loop mirror configuration. *Electron. Lett.*, 31(15):1257–1258, 1995.

[167] J. P. Sokoloff, I. Glesk, P. R. Prucnal, and R. K. Boncek. Performance of a 50Gbit/s optical time domain multiplexed system using a terahertz optical asymmetric demultiplexer. *IEEE Photon. Technol. Lett.*, 6(1):98–100, 1994.

[168] K. Suzuki, K. Iwatsuki, S. Nishi, and M. Saruwatari. Error-free demultiplexing of 160Gbit/s pulse signal using optical loop mirror including semiconductor laser amplifier. *Electron. Lett.*, 30(18):1501–1503, 1994.

[169] B. Y. Yu, R. Rumen, P. Tolver, K.-L. Deng, D. Zhou, T. Chang, S. W. Sea, K. I. Kang, I. Glesk, and P. R. Prucnal. Network demmonstration of 100Gbit/s optical packet switching with self-routing. *Electron. Lett.*, 33(16):1401–1403, 1997.

[170] D. M. Patrick. Modelocked ring laser using nonlinearity in a semiconductor-laser amplifier. *Electron. Lett.*, 30(1):43–44, 1994.

[171] A. Mecozzi and J. Mork. Saturation induced by picosecond pulses in semiconductor optical amplifiers. *J. Optical Society of America, B*, 14(4):761–770, 1997.

[172] D. M. Patrick and R. J. Manning. 20Gbit/s all-optical clock recovery using semiconductor nonlinearity. *Electron. Lett.*, 30(2):151–152, 1994.

[173] R. J. Manning, D. A. O. Davies, D. Cotter, and J. K. Lucek. Enhanced recovery rates in semiconductor-laser amplifiers using optical-pumping. *Electron. Lett.*, 30(10):787–788, 1994.

[174] R. J. Manning, D. A. O. Davies, and J. K. Lucek. Recovery rates in semiconductor-laser amplifiers —optical and electrical bias dependencies. *Electron. Lett.*, 30(15):1233–1235, 1994.

[175] R. J. Manning and G. Sherlock. Recovery of a π-phase-shift in $\approx$ 12.5ps in a semiconductor-laser amplifier. *Electron. Lett.*, 31(4):307–308, 1995.

[176] M. G. Kane, I. Glesk, J. P. Sokoloff, and P. R. Prucnal. Asymmetric optical loop mirror —analysis of an all-optical switch. *Appl. Opt.*, 33(29):6833–6842, 1994.

[177] K. J. Blow, R. J. Manning, and A. J. Poustie. Nonlinear optical loop mirrors with feedback and a slow nonlinearity. *Opt. Comm.*, 134(1-6):43–48, 1997.

[178] K. L. Deng, I. Glesk, K. I. Kang, and P. R. Prucnal. Unbalanced TOAD for optical data and clock separation in self- clocked transparent OTDM networks. *IEEE Photon. Technol. Lett.*, 9(6):830– 832, 1997.